Universidade Federal de Juiz de Fora

Programa de Pós-Graduação em

Engenharia Elétrica

Juan David Valencia Payán

IN-HOME AND LOW-VOLTAGE CHANNEL CHARACTERIZATION OF
NON-COOPERATIVE AND COOPERATIVE POWER LINE COMMUNICATION

Dissertação de Mestrado

Juiz de Fora

2014

Juan David Valencia Payán

In-Home and Low-Voltage Channel Characterization of Non-Cooperative and
Cooperative Power Line Communication

Dissertação apresentada ao Programa de
Pós–Graduação em Engenharia Elétrica,
área de concentração: Sistemas Eletrônicos,
da Faculdade de Engenharia da Universidade
Federal de Juiz de Fora como requisito par-
cial para obtenção do grau de Mestre.

Orientador: Prof. Moisés Vidal Ribeiro, PhD.

Juiz de Fora

2014

Juan David Valencia Payán

In-Home and Low-Voltage Channel Characterization of Non-Cooperative and Cooperative Power Line Communication

Dissertação apresentada ao Programa de Pós–Graduação em Engenharia Elétrica, área de concentração: Sistemas Eletrônicos, da Faculdade de Engenharia da Universidade Federal de Juiz de Fora como requisito parcial para obtenção do grau de Mestre.

Aprovada em 27 de Fevereiro de 2014.

BANCA EXAMINADORA:

_____

Moisés Vidal Ribeiro, PhD.
Universidade Federal de Juiz de Fora, UFJF
Orientador

_____

Gustavo Fraidenraich
Universidade Estadual de Campinas, UNICAMP

_____

Fabrício Pablo Virgínio de Campos
Universidade Federal de Juiz de Fora, UFJF

_____

Rafael Antunes Nóbrega
Universidade Federal de Juiz de Fora, UFJF

To Amparo, José, Paula, María and my beloved Agnieszka

ACKNOWLEDGEMENTS

I would like to thank first of all my Mother Amparo, my Father José, my Sister Paula, my Grandmother María, and Agnieszka. They are the reason why I am here and the constant support in my life. I also have very special gratefulness for Wander Girardi for letting me be part of a Brazilian family.

I want to thank the members of the LABCOM, LAPTEL, NAEP and NIMO laboratories. Thanks for your understanding and patience. Thanks for solving my doubts whenever I was needing, and thanks for your friendship.

Special thanks to Laryssa Amado, Pedro Machado, Thiago Oliveira and Pablo Furtado. Thank you for your very kind friendship.

I want to also thank Michelle Soares and Darlene Engelender. Many thanks for your help during the measurement campaign, and also to show interest in the topic.

My sincere gratefulness Prof. Álvaro Medeiros, besides my supervisor he is an amazing listener and advisor. Many thanks for your support and understanding.

Tremendously thankful from Prof. Moisés Ribeíro, a very special listener, advisor, boss, and teacher. Thank you so much for the opportunity to participate in this Master program at UFJF, as wells as, in the Power Line Communications modem projects. Many thanks for your contagious dreaming attitude and love for work.

Finally, I want to thank the CNPq, CAPES, FAPEMIG, FINEP, INERGE, CEMIG, P&D ANEEL and SMARTi9.

"If not us, then who? If not now, then when?"

John Lewis

ABSTRACT

This thesis outlines a statistical characterization of the Brazilian In-Home Low-Voltage Electric Power Grid as a communication medium. The discussions are based on estimated channels obtained in a measurement campaign carried out in four different apartments with sizes ranging from 50 up to 90 square meters. The parameters considered for this analysis are the Root Mean Square Delay Spread, the average channel gain, and the channel capacity. For the sake of comparison with the Electric Power Grid in United States, the frequency band ranging from 1.705 up to 30 MHz was set. The reported analysis shows that the Root Mean Square Delay Spread and the average channel gain cannot be modeled as log-normal variables, this cast doubt the current results found in the literature, in which is stated that both the Root Mean Square Delay Spread and the average channel gain follow a log-normal distribution. This was followed by the Power Line Communication access impedance and noise measurements in the In-Home Low-Voltage Electric Power Grid. Additionally, the suitability of cooperation concepts for improving the performance of Power Line Communication systems was analyzed, more specifically in the Brazilian In-Home Low-Voltage Electric Power Grid. For this purpose, the performance of the Amplify-and-Forward and Decode-and-Forward protocols, together with the Equal-Gain Combining, Selection Combining, and Maximal-Ratio Combining techniques were analyzed. The analysis was carried out on the measured data covering a frequency band from 1.705 up to 100 MHz. The measured data addresses four scenarios for possible relay node locations. The attained results show that the Amplify-and-Forward is of limited applicability in the Power Line Communication context and the opposite is valid to the Decode-and-Forward protocol, mainly if the error probability of detecting symbols at the relay node is zero.

Key-words: Power line communications, channel characterization, root mean square-delay spread, average channel gain, channel capacity, access impedance, cooperative communications.

RESUMO

Esta contribuição descreve uma caracterização estatística da rede de baixa tensão Brasileira residencial como meio de comunicação. As discussões são baseadas em canais estimados obtidos em uma campanha de medição realizada em quatro apartamentos diferentes, com tamanhos que variam de 50 até 90 metros quadrados. Os parâmetros considerados para esta análise são o Root Mean Square Delay Spread, o ganho médio do canal e a capacidade do canal. Para efeitos de comparação com a rede de potencia dos Estados Unidos, a banda de frequência utilizada foi de 1.705 até 30 MHz. A análise relatada mostra que o Root Mean Square Delay Spread e o ganho médio do canal não podem ser modelados como variáveis log-normal. Os resultados obtidos geram dúvidas em relação aos atuais encontrados na literatura, em que se afirma que tanto o Root Mean Square Delay Spread quanto o ganho médio do canal seguem uma distribuição log-normal. Foram medidos também a impedância de acesso e o ruído do canal de comunicação via rede elétrica. Além disso, os conceitos de cooperação para melhorar o desempenho dos sistemas de comunicação via rede elétrica foram analisados, mais especificamente na rede de baixa tensão Brasileira residencial. Para isso, foram analisados a performance dos protocolos de Amplify-and-Forward e Decode-and-Forward, em conjunto com as técnicas de combinação Equal-Gain Combining, Selection-Combining e Maximal-Ratio Combining. A análise sobre os dados medidos cobriram uma faixa de frequência de 1.705 a 100 MHz. Os dados medidos abordam quatro cenários para possíveis localizações do nó Relay. Os resultados obtidos mostram que o Amplify-and-Forward é de aplicabilidade limitada no contexto de comunicação via rede elétrica e o oposto é válido para o protocolo de Decode-and-Forward, principalmente se a probabilidade de erro de detecção de símbolos no nó Relay tende a zero.

Palavras-chave: Comunicação via rede elétrica, caracterização do canal, root mean square-delay spread, ganho médio do canal, capacidade do canal, impedância de acesso, comunicação cooperativa.

CONTENTS

LIST OF FIGURES

LIST OF TABLES

ACRONYMS

AF Amplify-and-Forward

BB Broad-Band

BP Band-Pass

CP Cyclic Prefix

DFT Discrete Fourier Transform

DSP Digital Signal Processing

DS Delay Spread

DF Decode-and-Forward

D Destination

EGC Equal-Gain Combining

ECCDF Empirical Complementary Cumulative Distribution Function

EPG Electric Power Grid

HV High-Voltage

IH In-Home

I/O input/output

ISI Inter-Symbol Interference

i.i.d independent and identically distributed

LV Low-Voltage

LTI Linear Time-Invariant

MV Medium-Voltage

MTL Multi-conductor Transmission Line

MIMO Multiple-Input Multiple-Output

MRC Maximal-Ratio Combining

NB Narrow-Band

OFDM Orthogonal Frequency-Division Multiplexing

PLC Power Line Communications

PL Power Line

PLs Power Lines

P2P Point-to-Point

PSD Power Spectral Density

pk-pk peak-to-peak

RF Radio Frequency

RMS Root Mean Square

R Relay

RD Relay-Destination

Rb Rubidium

SC Selection Combining

S Source

SD Source-Destination

SR Source-Relay

SRD Source-Relay-Destination

SMT Surface-Mount Technology

SEE Signal Energy Estimation

SNR Signal-to-noise Ratio

US United States

UPS Uninterruptible Power Supply

1 INTRODUCTION

Communications over Power Lines (PLs) is very discussed nowadays, because it is the shortest path among devices connected to the Electric Power Grid (EPG), and their ubiquitousness facilitate the large scale implementation of smart grid communication infrastructure for several and challenging applications such as smart metering and smart homes. However, they can also be useful for Broad-Band (BB) internet access. And this is the big advantage to other technologies. The PLs are spread almost everywhere (where humans are settled). This makes the PLs a favorite solution for data transmission from the service provider to the customers and this what is widely understood as BB Power Line Communications (PLC). Besides residential services PLC could help communications services wherever you find power line cables, for instance, the automotive, naval and aerospace industries. It is then possible to reduce vehicles or planes costs by reducing the amount of cables that are necessary to connect different devices inside a car, vessel or a plane but then using the already existent Power Line (PL) cables.

In Brazil for instance, there are different initiatives to the PLC use. On the one hand, the motivations to use this technology are clear and very suitable for emergent countries with a lack of telecommunications infrastructure for their populations. On the other hand, the indiscriminate and inaccurate use of the PLC technologies from foreign companies for the Brazilian power grid have been a great deception concerning the PLC systems performance in Brazil.

Therefore, the correct use of the EPG as a medium for data communication demands a deep characterization of this challenging communication medium in Brazil. In this context this thesis aims to complement the PLC understanding by characterizing non-cooperative and cooperative communications PLC channels.

1.1   THESIS OBJECTIVES

This thesis has been developed to achieve the following objectives:

- General Objective

  - To develop a clear methodology and understanding of non-cooperative and cooperative In-Home (IH)-Low-Voltage (LV) PLC channel characterization.

- Specific Objectives

  - To obtain the state of the art of PLC channel characterization methodologies.

  - To study the methodology for PLC channels measurement.

  - To perform a PLC channel measurement campaign for non-cooperative and cooperative IH-LV PLC channels.

  - To perform statistical analysis of PLC non-cooperative channels within the 1.705 to 100 MHz frequency band.

  - To perform statistical analysis of PLC cooperative channels within the 1.705 to 100 MHz frequency band.

1.2   THESIS OUTLINE

This thesis is organized as follows: In Chap. 2, the PLC channels characterization methodologies are reviewed and the proposal methodology for the Brazilian IH-LV case is explained. The measurement configuration, the Digital Signal Processing (DSP) techniques, the statistical analysis and comparisons are presented. In Chap. 3, the cooperative PLC approach is presented with the proposed mathematical expressions. In addition, the most popular cooperative protocols and diversity combining techniques are explored and included together with the channel model proposed. Finally, the conclusions of this thesis are presented in Chap. 4.

2 POWER LINE COMMUNICATION CHANNEL CHARACTERIZATION

The EPG offers an alternative for data communication for Narrow-Band (NB) and BB applications. This makes of paramount importance to correctly understand the PLs behaviour in different environments such as High-Voltage (HV), Medium-Voltage (MV) and LV links, because in these environments the coverage of telecommunication infrastructure is scarce and the EPG is ubiquitous. In order to develop more reliable and robust PLC systems, it is necessary to analyse the channel, which is crucial for telecommunication systems design and prototyping. For this purpose, different investigations are focused on developing a generalized PLC channel model. However, due to different PLs properties such as time-varying behaviour (CANETE et al., 2003), impedance mismatching at the connection and branching points, harmful additive noises (BERT et al., 2011), strong attenuation profiles as the frequency and/or distance increases, and frequency selectivity; it is not possible yet to develop a model that might generalize the PLC channel behaviour in all possible scenarios and locations, because of the lack of information in some places and the huge amount of measurements required to generalized a model.

In this chapter we aim to first show briefly different contributions about PLC channel characterization. This is done in order to give the reader a better perspective of the techniques used for PLC channel characterization, additionally to show that even though the techniques are used for different environments such as indoor and outdoor networks; the techniques are still similar to each other and applicable for all environments. We emphasize the top-down approach, because is the one used during this thesis in order to contribute with the Brazilian efforts to a global understanding of the PLC channel. Therefore, parameters such as the Root Mean Square (RMS)-Delay Spread (DS) and channel gain measured in Brazil were compared to United States (US) results, to identify possible similarities that might help in developing PLC systems. Additionally, the access impedance measurements of Brazilian IH-LV EPG are included, because they show the importance of developing adaptable impedance

matching techniques for minimizing signal reflection at the connection points between the EPG and the PLC transceivers.

This chapter is organized as follows: the PLC channel characterization methodologies are reviewed in Sec. 2.1 and this is followed by the proposed channel characterization methodology for the Brazilian case in Sec. 2.2, in which the channel measurements, channel parameters, statistical results, access impedance, and noise levels are presented.

2.1 CHANNEL CHARACTERIZATION METHODOLOGIES

This section presents an overview of the two most common channel characterization methodologies studied for PLC channel modelling. They are defined as the top-down and bottom-up approaches.

2.1.1 BOTTOM-UP APPROACH

The bottom-up approach implies that the PLC channels are modelled by using transmission line theory, the network topology, PL cable characteristics, and load impedances at the terminal nodes. Commonly, the transmission line theory analysis are focused on voltage ratio calculations and two-port mathematical models such as the scattering parameters (s-parameters), and the ABCD matrix representation.

In (TONELLO; ZHENG, 2009), the PLC channel is estimated by several voltage ratios between the receiver and the transmitter nodes, which are calculated on random network topologies. Additionally, in (TONELLO; VERSOLATTO, 2010), the PLC channels estimations are evaluated statistically by using relevant criteria for PLC channel characterization, such as the path-loss profile, average channel gain, root-mean-square delay spread, and channel capacity. These analyses are followed by (TONELLO; VERSOLATTO, 2011) in which a PLC channel simulator is proposed, where the PLC channels, between two different electrical outlet pairs that are arranged in a circuit topology composed of several nodes, are estimated by calculating the transfer function as the voltage ratio between the input voltages at the receiver and at the transmitter nodes.

Another example of Bottom-up modelling is found in (GALLI; BANWELL, 2006), where the ABCD matrix representation is used to model the EPG. This contribution enhance the PLC channel modelling by adding wiring methodologies investigations. Thus, the power lines are modelled as grounded and ungrounded links through Multi-

conductor Transmission Line (MTL) models.

The MTL theory is also analysed, as the main method for PL links modelling. Therefore, the signal propagation is discussed together with power line analysis of three-conductor, cable terminations, and discontinuity models. For instance , in (GALLI; BANWELL, 2005), the PL channel model developed in (BANWELL; GALLI, 2005) is generalized by means of ABCD matrices representation of a cascade of two-port networks. Additionally, in (VERSOLATTO; TONELLO, 2011), the MTL theory together with Multiple-Input Multiple-Output (MIMO) configuration concepts are explored, in order to develop a PLC channel simulator.

Both the two-conductor and multi-conductor approaches can also be found in (ANATORY; THEETHAYI; THOTTAPPILLIL, 2009a) and (ANATORY; THEETHAYI; THOTTAPPILLIL, 2009b), respectively. The authors investigated for both cases the PLC channel modelling considering the EPG with multiple branches and loads.

Another, modelling case is reported in (BAKHOUM, 2011), where the three-phase EPGs are modelled through a group of three two-port networks. In this specific case, the s-parameters concepts were chosen in order to develop the mathematical formulation.

The majority of works focused their research within indoor environments. However, the bottom-up approach can be followed in different environments. For instance, in (SARTENAER; DELOGNE, 2006) the MTL theory is also applied for underground scenarios.

2.1.2   TOP-DOWN APPROACH

Top-down methodologies do not require to know the network topology (OLIVEIRA, 2010). In general, these methodologies regard the channel as a black box and return an analytical expression of its response, by applying fitting algorithms over the results from measurements accounting for multi-path propagation (ZIMMERMANN; DOSTERT, 2002b) in the time domain or in the frequency domain (TONELLO; VERSOLATTO, 2011). As a result, the PLC channel is accurately estimated by using a reduced amount of parameters. These methodologies offer fast PLC channels estimation but it does lack of generalization. This is mainly because each derived model depends on the measurement location, configuration and frequency band. Therefore, a generalized model requires a large number of measurements (ZHU et al., 2013).

The contribution in (TONELLO et al., 2012), presents a PLC random channel generator, in which a derived multi-path model is fitted to the measured channels. Similarly, the work in (MOHAMED; GAUTIER; AHMED, 2008) classifies the measured PLC channels in different classes related to their capacities, which is of great importance to determine whether the PLC channel might be valuable or not for data communication purposes.

In (VERONESI et al., 2011), a PLC channel model is developed, based on measured data by using a MIMO configuration in the 0 to 100 MHz frequency band. This work, focused its analysis on the statistical extraction from several channel estimations in different locations, provided by the HomePlug Powerline Alliance. The measured data was obtained by using a sounding scheme, where the sounding signals were composed of a synchronization portion and Orthogonal Frequency-Division Multiplexing (OFDM) encoded symbols. Similarly, the investigation in (HASHMAT et al., 2011) presents a statistical PLC channel model using the MIMO configuration in the 2 to 150 MHz frequency band, based on measured data from five different houses.

2.2 CHANNEL CHARACTERIZATION IN BRAZIL

In the previous sections, different PLC channel characterization contributions were reviewed. It is possible to see that in some cases several measurements for the PLC channel estimation were needed to characterize indoor and outdoor EPGs.

Therefore, as a global contribution, this thesis is focused on a top-down-based characterization approach used for Brazilian IH-LV PLC channels. This characterization is made by using a channel estimation technique which is based on OFDM symbols sounding through the EPG, and can lead new investigations towards new EPG characteristics for a generalized PLC channel model.

2.2.1 MEASUREMENT CAMPAIGN OF THE IH-LV PLC CHANNEL

As stated before, for PLC channel characterization, a measurement campaign is essential for further analysis. Therefore, as a first approach in IH-LV PLC channels in Brazil, a campaign was carried out in middle class apartments with areas ranging between 54 to 93 square meters, in Juiz de Fora, Brazil. In this section a detailed description about the measurement configuration used for the PLC channel measurements is presented, which is a derived configuration from the measurement setup discussed in (COLEN et al., 2013).

2.2.1.1   GENERAL DESCRIPTION

For the PLC channel characterization a Point-to-Point (P2P) configuration was chosen, in order to have a direct connection between both the transmitter and the receiver nodes. The PLC channel under study is the path between two different electrical socket-outlets. This configuration can be regarded in Fig. 1. On the transmission side, there is a signal generator computer, a frequency reference device, a coupler to the PL, and an Uninterruptible Power Supply (UPS) which is used to isolate the equipment from the LV-EPG. Similarly, on the receiver side there is a signal acquisition computer, a frequency reference device, a coupler to the PL and an UPS.
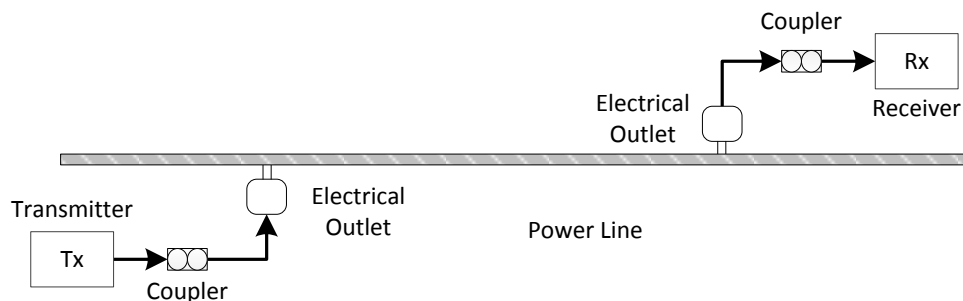
Figure 1: Point-to-point channel measurement setup.

2.2.1.2   EQUIPMENT DESCRIPTION

The equipment used in the measurement setup was carefully chosen to do accurate PLs measurements. In this section the role of each device is explained.

UPS: During the measurements, different configurations were simulated (before field measurements) and it was found that both the transmitter and receiver computers induced a certain noise on the EPG. This noise is harmful for the quality of channel responses. Therefore, the idea to use a power supply source in order to isolate the equipment from the power grid was taken into consideration. This power supply is used to provide with energy for quick measurements the acquisition and the transmission computers, and the rubidium-based frequency reference device. This means that the PLC channel is measured directly using the coupler and without more additive noises yielded by the measurement/transmission devices. However, this topic can be widely discuss since the equipment and the power supply themselves might generate other kind of noises in the Radio Frequency (RF) spectrum. In Fig. 2, two measurements are compared. In (a) a noise measurement using an UPS connected to the EPG generates a more noisy signal than if both UPS are not used. In (b) a transmitted signal is

compared as well, and it is possible to check that the measurement using the UPS devices is more noisy. This justifies the need to unplug the power supplies for every single measurement, or to deploy a blocking filter that can be used at the connection point between the EPG and the UPS.
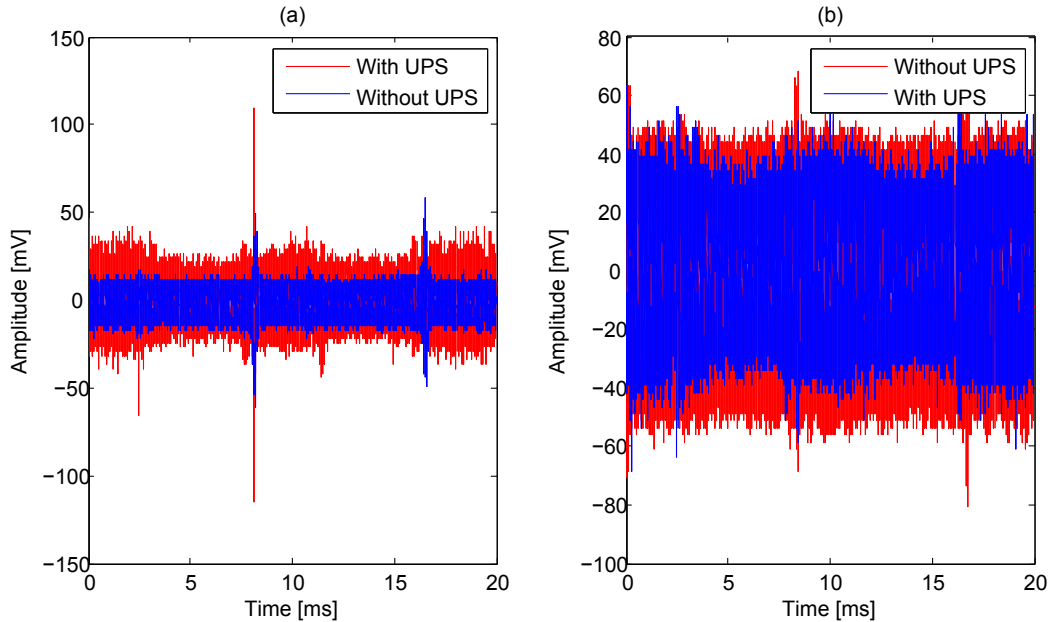
Figure 2: (a) Amplitude of the noise in the EPG with and without UPS, and (b) Amplitude of the signal, used to estimate the PLC channel, plus the noise in the EPG with and without UPS.

Couplers: The connection between the measurement equipment and the power grid is of great importance. On the one hand, it has to protect the equipment input from the main voltage signal (50 or 60 Hz) and its harmonics with high power levels. On the other hand, its frequency response must be as flat as possible, in order to transmit and receive signals with minimum attenuation for all frequency bands or more precisely in the studied frequency band. In this work the frequency band of interest is between 1.705 MHz and 100 MHz. The lowest frequency boundary (1.705 MHz) is due to the Brazilian regulation (ANATEL, 2009).

The coupler circuit used for this work is presented in Fig. 3. It is composed of a Band-Pass (BP) filter (using a Polyester Capacitor with 400 V RMS of maximum voltage) with a cut-off frequency in 1.705 MHz and a Surface-Mount Technology (SMT) RF transformer (with a 3 dB bandwidth between 0.0035 and 125 MHz). This coupler was designed to have a frequency response that can be seen in Fig. 4. In addition, it can be observed that the highest attenuations are allocated in the 80-100 MHz frequency band. This attenuations can be reduced by pre-coding the sounding signal.
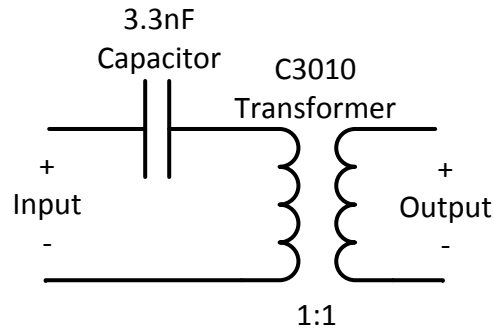
Figure 3: Coupler circuit.
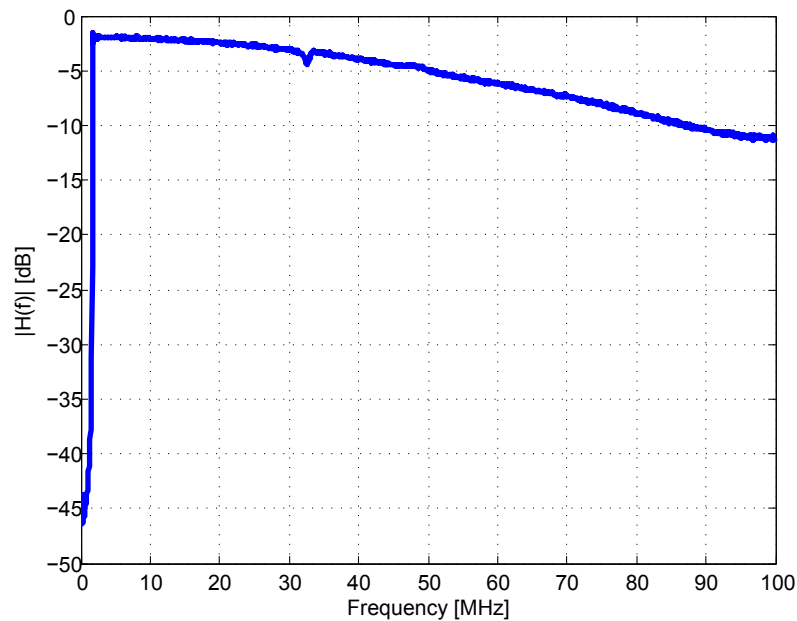
Figure 4: Coupler frequency response.

Signal Generator Computer: The signal generation computer is equipped with two main boards:

- High-speed arbitrary waveform generator card (CompuGen 4302) (GAGE, a): this board has an important capability of generating arbitrary signals. This is a great feature for this work because it allows the transmission of a customized signal that contains multiple OFDM symbols. It also can store up to 16 Mega samples on its own memory, and it has a 12 bit resolution for generated signals. Additionally, it has an external input clock that can be used to generate the arbitrary signal at the external sampling frequency, and also in-board sampling frequency that can reach up to 300 MHz.

- Multi-channel digitizer card (CompuScope 1642) (GAGE, b): this board has spe-

cial features for data acquisition. For instance, maximum sampling frequency of 200 MHz, 16 bits of resolution and very low distortion. Its main utility for the data transmission is the clocking system. It has a frequency correction circuit that corrects an output clock to the desired sampling frequency. Thus, an external clock serves as a reference clock. And finally, the fixed clock (output clock) is used as the external clock for the arbitrary waveform generator board. This guaranties that the generated signal has a very stable sampling frequency.

Signal Acquisition Computer: The signal acquisition computer is also equipped with the same configuration of the signal generator computer. It is composed of an arbitrary waveform generator card and a digitizer card. It also uses the same capabilities for the clock correction and, therefore, data with a negligible sampling error due to clock offset can be acquired, since the sampling frequency at the receiver side is approximately the same as in the transmission side.

Frequency Reference: As mentioned previously, at both the transmitter and receiver sides it is important to have an external clock reference, in order to correct the transmission and reception sampling frequencies to approximately the same values. Therefore, a stable clock is desired to have a better correction. In this work, it was possible to use a Rubidium (Rb)-based frequency reference. This device is a portable atomic clock with 10 MHz sine-wave 50 Ohm output. Besides, it does have a very long ageing of 5×10^{-10} Hz/year and a very high accuracy of $\pm 5 \times 10^{-11}$ Hz. The use of the frequency reference device, considerably reduces the clock offset between the transmitter and the receiver, as a consequence, the PLC channel frequency response estimates are more reliable.

2.2.1.3 *EQUIPMENT CONNECTION*

The equipment previously described has a many input/output (I/O) ports. Therefore, a detailed connection is presented, in order to clarify how the measurement equipment was configured. These connections are divided in two diagrams, transmitter side in Fig. 5, and receiver side in Fig. 6 respectively.
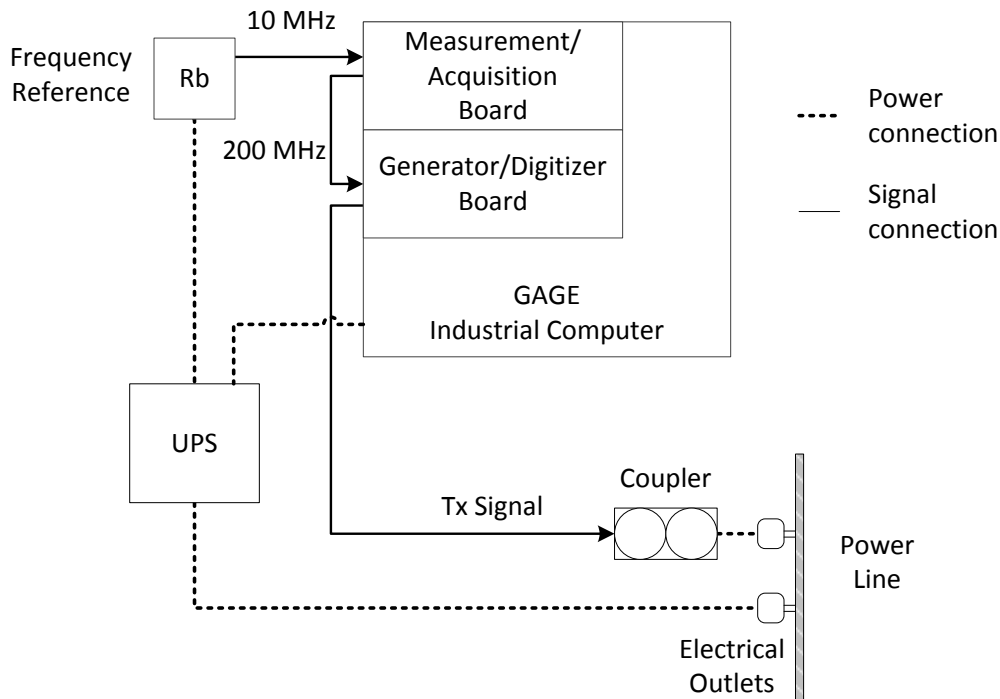
Figure 5: Transmitter side setup.
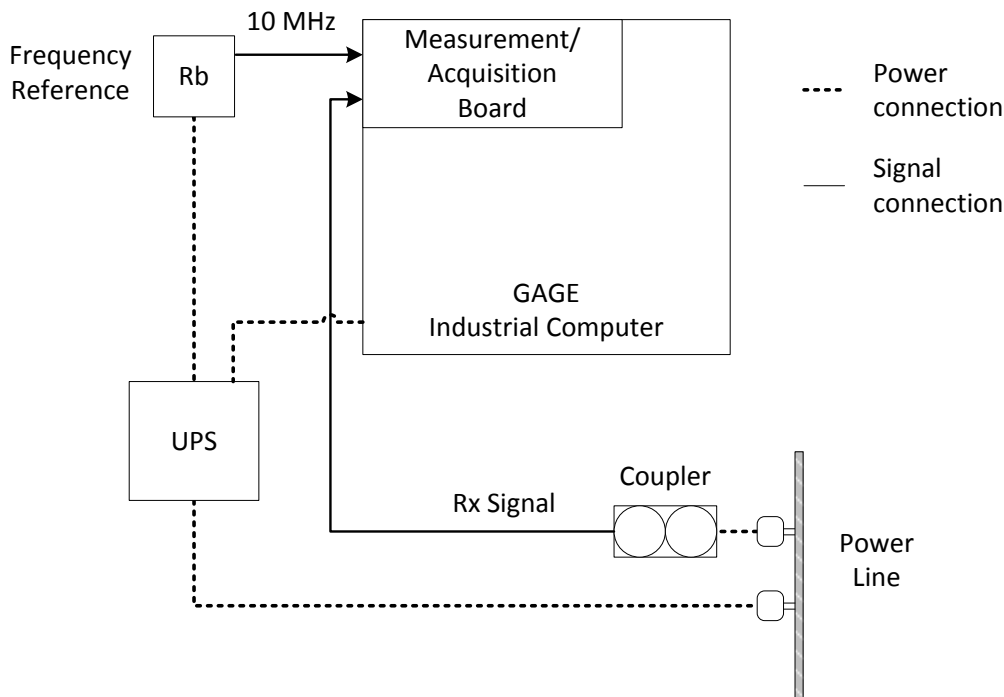
Figure 6: Receiver side setup.

2.2.1.4 MEASUREMENT PROCEDURE

To obtain representative data from the measurement campaign it was necessary to specify a measurement procedure that can be repeated in every house. This is crucial

to avoid inaccurate measurements and accidents. The procedure is as follows:

1st Connect all the cables on each equipment, the clock references and the couplers.

2nd Set the transmitter and receiver equipment on the desired test outlets.

3rd Unplug the UPS from the power grid in both outlets.

4th Check if the arbitrary signal generator board is deactivated from software.

5th Check if the acquisition board is deactivated from software.

6th Plug in the couplers in both outlets.

7th Activate the arbitrary signal generator board with the test signal.

8th Activate the acquisition board.

9th Save the measurement with the desired amount of samples.

In addition to the channel measurement procedure, it is necessary to register general values to understand the behaviour in one house and thus make better comparisons, which are essential for results reports. These general values (O'MAHONY, 2006) are registered in each house:

- Approximated house area $[m^2]$.

- Year of construction.

- Location (city, state).

- House type (single house, apartment, county house, etc.).

- Neighbourhood.

- Service Type (underground, aerial).

- Approximated distance to transformer [m].

- Approximated distance from house central panel to house meter box [m].

- Total house outlets.

To enclose the measurement procedure, a brief report is done in each house. This must include a general transmitter and receiver details (in case they change in a certain location), electrical and floor plan, and highlight the electrical outlet connections in the floor plan that might be suitable for PLC. These details are included in Appendix. A.

2.2.2 SOUNDING TECHNIQUE

The sounding technique is actually a set of DSP techniques that are applied to generate the sounding signal and to process the measured data, in order to estimate the frequency response of the PLC channel (OLIVEIRA; FINAMORE; RIBEIRO, 2013). In this thesis, the sounding makes use of baseband OFDM, as the modulation scheme, to generate the sounding signal that is transmitted through the EPG, depicted with a block diagram in Fig. 7, where it is assumed that the PLC channel model is Linear Time-Invariant (LTI) during the period for transmitting one OFDM symbol, and devices non-linearities are neglected (FERREIRA et al., 2010). The frequency representation of an OFDM symbol is $\mathbf{X} \in \mathbb{C}^{2N \times 1}$, such that $E\{\mathbf{X}\} = 0$ and $E\{\mathbf{X}\mathbf{X}^{\dagger}\} = \sigma_x^2\mathbf{I}$, where $E\{.\}$ and $\dagger$ denote the expectation and Hermitian operators, respectively. Two consecutive OFDM symbols are gathered together in a discrete signal version of $x(t)$, denoted as $x[n]$, where each OFDM symbol has length $2N$, where N is the number of sub-carriers, a Cyclic Prefix (CP) length L_{CP}, and can be regarded as a short frame as depicted in Fig. 8, where the CP is used for timing synchronization and frequency domain estimation at the receiver.
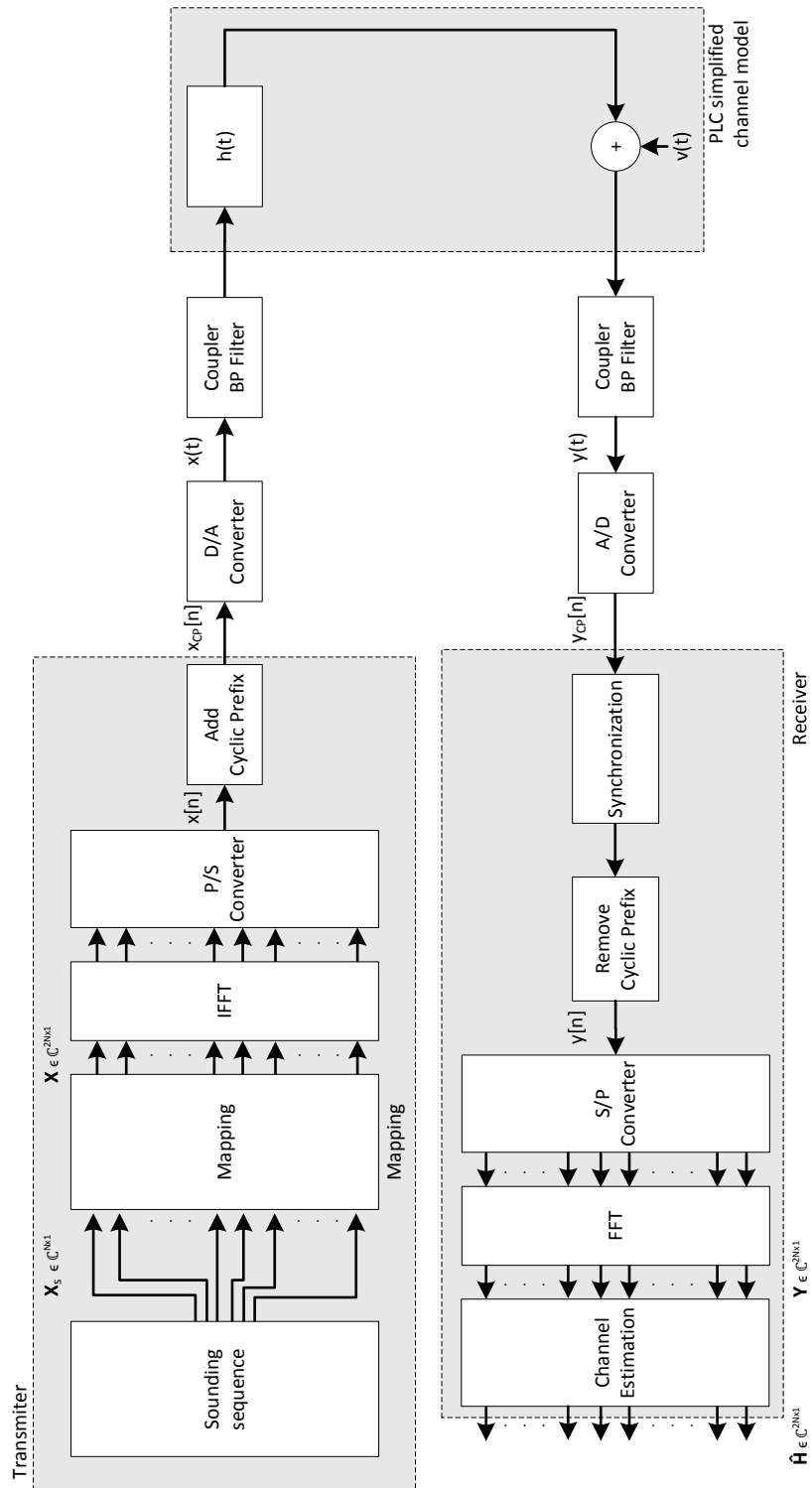
Figure 7: Simplified sounding technique block diagram.
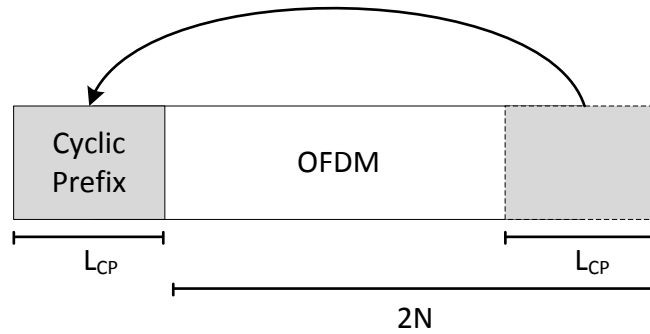
Figure 8: OFDM symbol.

After timing synchronization, the OFDM symbols are extracted from the received sequence. As soon as the OFDM symbols are extracted, it must be identified whether they belonged to one of the two symbols coming from the transmitter. This identification is made also by means of correlation between the transmitted and the received symbols. Then the PLC channel frequency response estimation is given by

$$
\begin{aligned}
\hat{\mathbf{H}} &= \mathrm{diag}^{-1}\{\mathbf{X}\}\mathbf{Y} \\
&= \mathrm{diag}^{-1}\{\mathbf{X}\}[\mathcal{H}\mathbf{X} + \mathbf{V}],
\end{aligned}
\tag{2.1}
$$

where $\mathrm{diag}\{\mathbf{X}\} = \mathrm{diag}\{X[0]\,X[1]\,...\,X[2N-1]\}$,

$$
\mathbf{Y} = \frac{1}{\sqrt{2N}}\mathbf{W}\mathbf{y},
\tag{2.2}
$$

where $\mathbf{y}$ is a vector constituted by samples of the sequence $y[n]$ (see block diagram in Fig. 7); $\mathbf{W} \in \mathbb{C}^{2N \times 2N}$ is the Discrete Fourier Transform (DFT) matrix, and $\mathcal{H} = \mathrm{diag}\{H[0]\,H[1]\,...\,H[2N-1]\}$ can be defined as the diagonal matrix composed of the frequency representation of the channel impulse response $\mathbf{h} = [h[0]\,h[1]\,...\,h[L_h-1]]^T$, which is given by

$$
\mathbf{H} = \frac{1}{\sqrt{2N}}\mathbf{W}\begin{bmatrix} \mathbf{h} \\ \mathbf{0}_{2N-L_h} \end{bmatrix},
\tag{2.3}
$$

where $\mathbf{0}_{2N-L_h}$ is a column vector constituted by $2N - L_h$ zeros.

For the measurement campaign, the number of sub-carriers and the CP length are equal to $N = 2048$ and $L_{CP} = 512$, respectively. The sampling frequency at the transmitter and receiver is equal to $Fs = 200$ MHz, the frequency bandwidth is $B = 100$ MHz, and it is assumed that the channel impulse response is time-invariant for a period shorter than $(2N + L_{CP})/Fs = 23.04$ us.

2.2.3 PARAMETERS FOR POWER LINE CHANNELS ANALYSIS

In this section the widely known parameters that are applied to characterize the PLC channels are described.

Average Channel Gain: The average channel gain parameter represents the average channel capability for signal amplification. This is therefore of great importance when different amplification algorithms need to be implemented in a transmission scheme. For instance, in cooperative communications, this parameter may be used for fixed and variable gain amplification in relaying protocols (DOHLER; LI, 2010). The average channel gain is calculated as in (GALLI, 2011) and (FERREIRA et al., 2010), by using the following expression

$$G = \frac{1}{N} \sum_{k=0}^{N-1} |H[k]|^2, \tag{2.4}$$

where $H[k]$ is the k-th coefficient of the normalized channel frequency response.

Impulse Response Duration: This parameter is essential for the calculation of the RMS-DS (further explained in the next item), and it is defined as the time interval that contains a certain percentage of the total energy of the impulse response, e.g. 99%, 99.9% or 99.99%. However, the estimated impulse response is polluted with additive noise from the measurement process, that does not vanish with time (LI et al., 2000). Therefore, different DSP techniques have been developed, in order to find the effective impulse response trying to mitigate the noisy behaviour. In this work, the Signal Energy Estimation (SEE) technique was used for this purpose. Let us consider the effective channel impulse response composed of M samples and assume the n-th sample of the estimated impulse response given by

$$h[n] = s[n] + e[n], \ n = 0, 1, ..., N - 1, \tag{2.5}$$

where $s[n]$ denotes the n-th sample of the channel impulse response and $e[n]$ denotes the n-th sample of the estimation error, modelled as a zero-mean white Gaussian noise with an unknown variance σ_e^2.

The application of the SEE technique consists in estimate M, where $M < N$, from the channel impulse response sequence $\{h[n]\}_{n=0}^{N-1}$, and requires the calculation of the total and deterministic signal energy, which is expressed by

$$E_s \triangleq \sum_{n=0}^{N-1} |s[n]|^2 = E_h - E_e, \tag{2.6}$$

where E_h and E_e are the energies of the sequences $\{h[n]\}_{n=0}^{N-1}$ and $\{e[n]\}_{n=0}^{N-1}$, respectively. These energies can be calculated by using the expressions

$$E_h \triangleq \sum_{n=0}^{N-1} E\left\{|h[n]|^2\right\} \tag{2.7}$$

and

$$E_e \triangleq \sum_{n=0}^{N-1} E\left\{|e[n]|^2\right\} = \frac{N}{N-L+1}E_{LN}, \tag{2.8}$$

in which the constant value L must be large enough following $M \leq L \leq N$; E_{LN} denotes the total energy of $\{h[n]\}_{n=L}^{N-1}$, expressed by

$$E_{LN} \triangleq \sum_{n=L}^{N-1} E\left\{|h[n]|^2\right\} = (N-L+1)\,\sigma_e^2. \tag{2.9}$$

For practical purposes, E_h and E_{LN} can be calculated, respectively, as $\hat{E}_h = \sum_{n=0}^{N-1}|h[n]|^2$ and $\hat{E}_{LN} = \sum_{n=L}^{N-1}|h[n]|^2$. Therefore, (2.6) can be rewritten as

$$\hat{E}_s = \hat{E}_h - \frac{N}{N-L+1}\hat{E}_{LN}. \tag{2.10}$$

The procedure to estimate the effective channel impulse response duration ($\hat{M}_{SEE}$) is described in Algorithm 1.

Algorithm 1 SEE algorithm

Step 1: Calculate $\hat{E}_s$.
Step 2: Set $\breve{M} = 1$ and $\hat{E}'_s = 0$.
Step 3: Compute $\hat{E}'_s = \hat{E}'_s + |h[\breve{M}]|^2 - \frac{\hat{E}_e}{N}$.
Step 4: If $\hat{E}'_s = k\hat{E}'_s$ $(0.9 \leq k \leq 0.9999)$ or $\breve{M} = L$ then $\hat{M}_{SEE} = \breve{M}$ and stop the algorithm. Otherwise $\breve{M} = \breve{M} + 1$ and go to **Step 3**.

In Fig. 9, it is presented the channel impulse response of one measured PLC channel, and its impulse response duration for three different energy percentages.
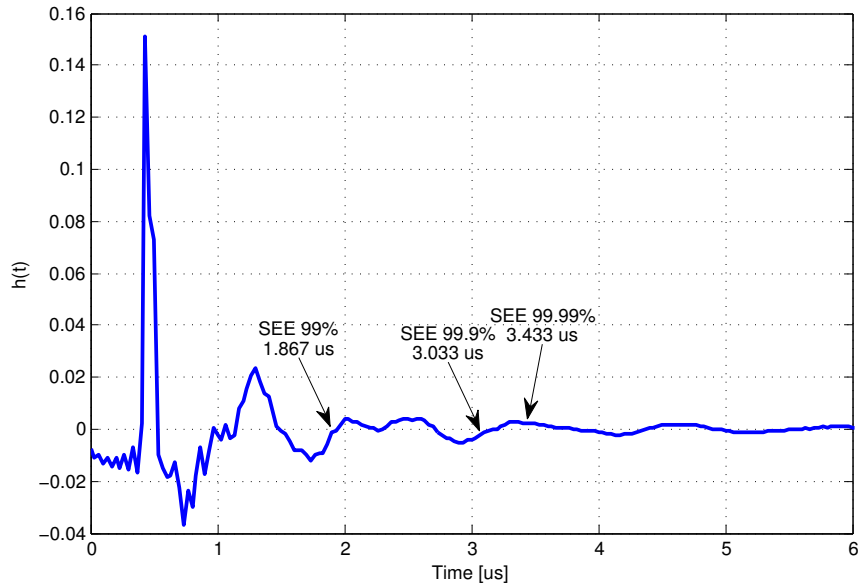
Figure 9: IH power line channel impulse response.

RMS-DS: The root-mean square delay spread (RMS-DS) is the square root of the second central moment of a power-delay profile, which provides an indication of the dispersion or distribution of the transmitted power over various paths in a multipath propagation model (MOHAMED; GAUTIER; AHMED, 2008). The RMS-DS also gives an indication of the nature of the Inter-Symbol Interference (ISI) and it is a value usually smaller than the impulse response duration. If M is the effective number of samples of the channel impulse response and T_s is the sampling period, the RMS-DS (σ_τ) is expressed by

$$\sigma_\tau = T_s \sigma_0, \tag{2.11}$$

in which

$$\sigma_0 = \sqrt{\mu_0' - \mu_0^2}, \tag{2.12}$$

$$\mu_0 = \frac{\sum_{n=0}^{N-1} n |h[n]|^2}{\sum_{i=0}^{N-1} |h[n]|^2} \tag{2.13}$$

and

$$\mu_0' = \frac{\sum_{n=0}^{N-1} n^2 |h[n]|^2}{\sum_{i=0}^{N-1} |h[n]|^2}. \tag{2.14}$$

Note that σ_0 is the RMS-DS normalized to a unitary sampling time and μ_0 is the average delay.

Channel Capacity: One of the important ways of characterizing the achievable performance of communication schemes is through the use of information theory concepts, such as the system capacity (LIU et al., 2009). In this work the system capacity for each evaluated channel (measured channel) is calculated through the expression (2.15), which is discussed in (PENG; HÉRALD; HAESE, 2013) and (LIU et al., 2005). Assuming that each frequency sub-band is flat and the Power Spectral Density (PSD) of the additive noise is also constant in each sub-carrier, then the channel capacity is denoted by

$$C = \frac{B}{N} \sum_{k=1}^{N} \log_2 \left(1 + \mathbf{\Lambda}_{SNR} \left(k, k \right) \right) \tag{2.15}$$

in which B is the frequency bandwidth and $\mathbf{\Lambda}_{SNR}$ is a diagonal matrix constituted by the Signal-to-noise Ratio (SNR) in all sub-carriers. The SNR matrix is given by

$$
\begin{aligned}
\mathbf{\Lambda}_{SNR} &= \frac{E\left\{ (\mathcal{H}\mathbf{X})(\mathcal{H}\mathbf{X})^{\dagger} \right\}}{E\left\{ \mathbf{V}\mathbf{V}^{\dagger} \right\}} \\
&= \frac{\mathcal{H} E\left\{ \mathbf{X}\mathbf{X}^{\dagger} \right\} \mathcal{H}^{\dagger}}{E\left\{ \mathbf{V}\mathbf{V}^{\dagger} \right\}} \\
&= \frac{\mathcal{H} \mathbf{\Lambda}_{\sigma_{\mathbf{X}}^2} \mathcal{H}^{\dagger}}{\mathbf{\Lambda}_{\sigma_{\mathbf{V}}^2}} \\
&= \frac{\mathcal{H}\mathcal{H}^{\dagger} \mathbf{\Lambda}_{\sigma_{\mathbf{X}}^2}}{\mathbf{\Lambda}_{\sigma_{\mathbf{V}}^2}} \\
&= \frac{|\mathcal{H}|^2 \mathbf{\Lambda}_{\sigma_{\mathbf{X}}^2}}{\mathbf{\Lambda}_{\sigma_{\mathbf{V}}^2}},
\end{aligned}
\tag{2.16}
$$

because $\mathbf{X} \in \mathbb{C}^{N \times 1}$ and $\mathbf{V} \in \mathbb{C}^{N \times 1}$ are random vectors such that $E\{\mathbf{X}\} = \mathbf{0}$, $E\{\mathbf{V}\} = \mathbf{0}$, $E\{\mathbf{X} \odot \mathbf{V}\} = E\{\mathbf{X}\} E\{\mathbf{V}\}$. As a result, $E\{\mathbf{X}\mathbf{X}^{\dagger}\} = \mathbf{\Lambda}_{\sigma_{\mathbf{X}}^2} = \mathrm{diag}\{\sigma_{\mathbf{X}}^2[0]\, \sigma_{\mathbf{X}}^2[1] \ldots \sigma_{\mathbf{X}}^2[N-1]\}$, and $E\{\mathbf{V}\mathbf{V}^{\dagger}\} = \mathbf{\Lambda}_{\sigma_{\mathbf{V}}^2} = \mathrm{diag}\{\sigma_{\mathbf{V}}^2[0]\, \sigma_{\mathbf{V}}^2[1] \ldots \sigma_{\mathbf{V}}^2[N-1]\}$. Also $|\mathcal{H}|^2 = \mathrm{diag}\{|H[0]|^2\, |H[1]|^2 \ldots |H[N-1]|^2\}$, and $\odot$ and $E\{.\}$ denote the Hadamard product and stochastic expectation operators, respectively.

2.2.4 ANALYSIS OF PLC CHANNEL PARAMETERS

This section includes the analysis of the PLC channels measured in the Brazilian IH-LV scenarios. For this purpose, four different houses were selected for an initial overview of the PLC measurements and channel characteristic analysis. The RMS-

DS and the average channel gain estimates are compared to US results, presented in (GALLI, 2011), which are focused on the 0-30 MHz frequency band. The log-normality relationship between the RMS-DS and the average channel gain is tested using a normal fitting and through the Jarque-Bera, Lilliefors, and Chi-square normality tests at the 5% of significance level. Additionally, the channel capacity is presented for two analyzed frequency bands: 1.705-30 MHz and 1.705-100 MHz, in which the former is used for comparisons with the US results, and the latter is the maximum frequency band that we were able to use with the laboratory equipment.

RMS-DS Log-normality: The log-normality of the RMS-DS was investigated by testing the logarithm of the RMS-DS against a normal distribution, following the condition: if the random variable $\mathcal{X}$ is log-normally distributed, then $\mathcal{Y} = \log(\mathcal{X})$ is normally distributed. By observing Figs. 10 and 11, it is noticed that the RMS-DS does not exactly follows a normal distribution, and there is a high concentration of this parameter around -70 dB for both frequency bands. Also in the 1.705-100 MHz it can be regarded, that the distribution seems to have four main concentration points: between -73 and -70 dB, around -70 dB, between -70 and -65 dB, and also around -65 dB. This might suggest that for each house there is an RMS-DS associated. Moreover, it was found that 100% of the cases rejected log-normality of RMS-DS at the 5% of significance level for the Brazilian IH-LV PLC channels. These results casts doubt with the results found in (GALLI, 2011). However, due to the amount of data used in this thesis, it is not possible to guarantee that these results will behave similarly when more measurements are taken into account.
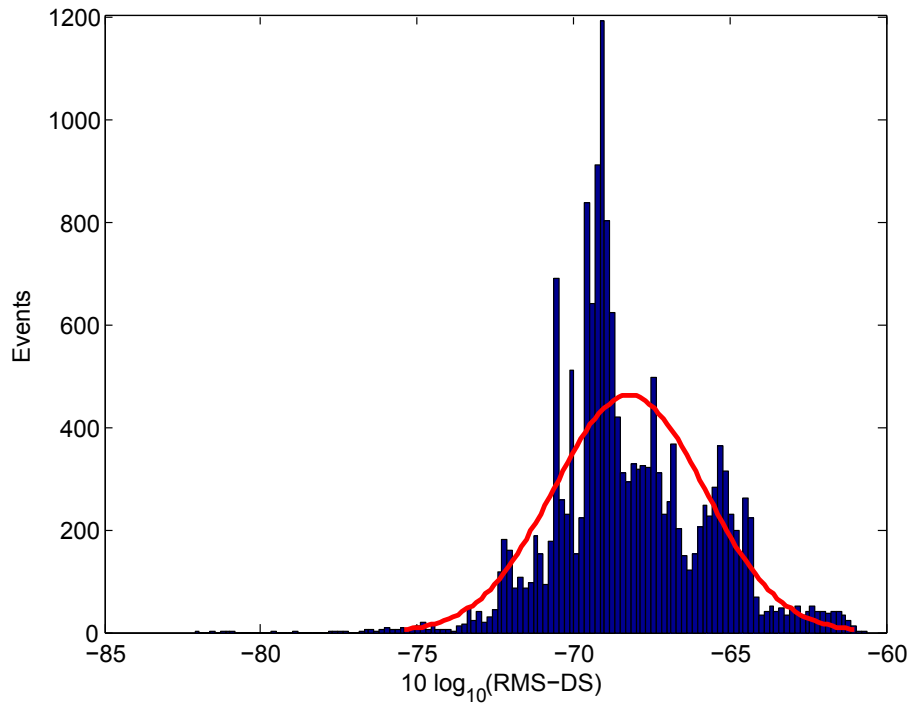
Figure 10: RMS-DS log-normality test for the acquired data in the 1.705-30 MHz frequency band.
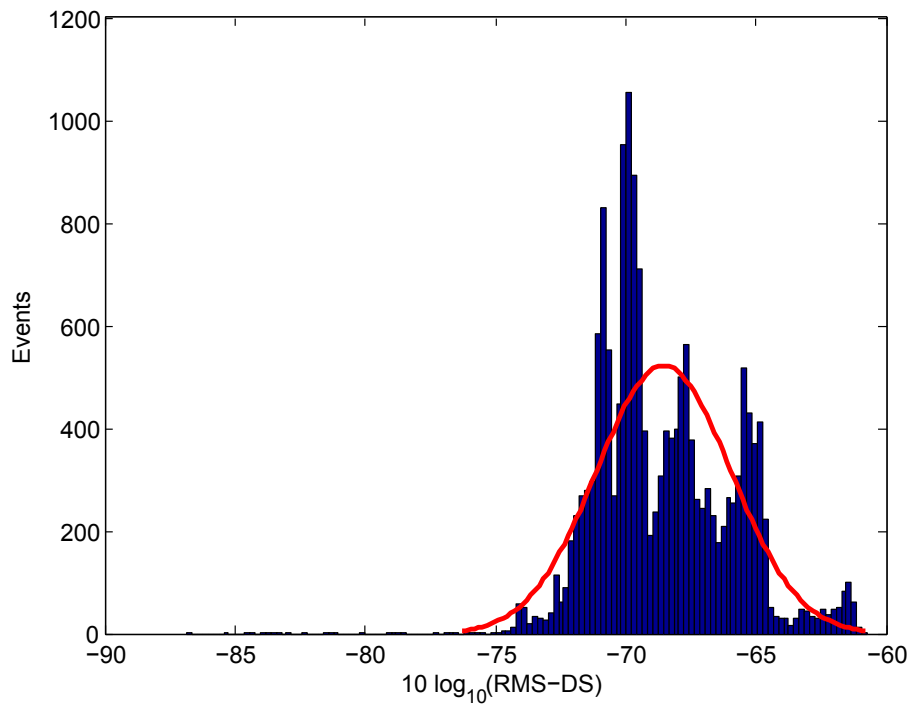
Figure 11: RMS-DS log-normality test for the acquired data in the 1.705-100 MHz frequency band.

Average Channel Gain Log-normality: Similarly to the RMS-DS, the average channel gain was evaluated against normality tests and normal fitting. In Figs. 12

and 13, the distributions of the average channel gain logarithm for the 1.705-30 MHz and 1.705-100 MHz frequency bands are presented, respectively. It can be seen that the channel gain does not follow a normal distribution, and in 100% of the cases, the log-normality was rejected, when the normality tests were applied. For the case of the 1.705-30 MHz frequency band, it is noticed three different kind of concentrations centered around -23 dB, -19 dB, and -13 dB, respectively. Similarly, in the 1.705-100 MHz frequency band, there are two main strong channel gain concentrations around -28 dB, and -17 dB. These results suggest as well that there are different channel gain behaviors in different houses.
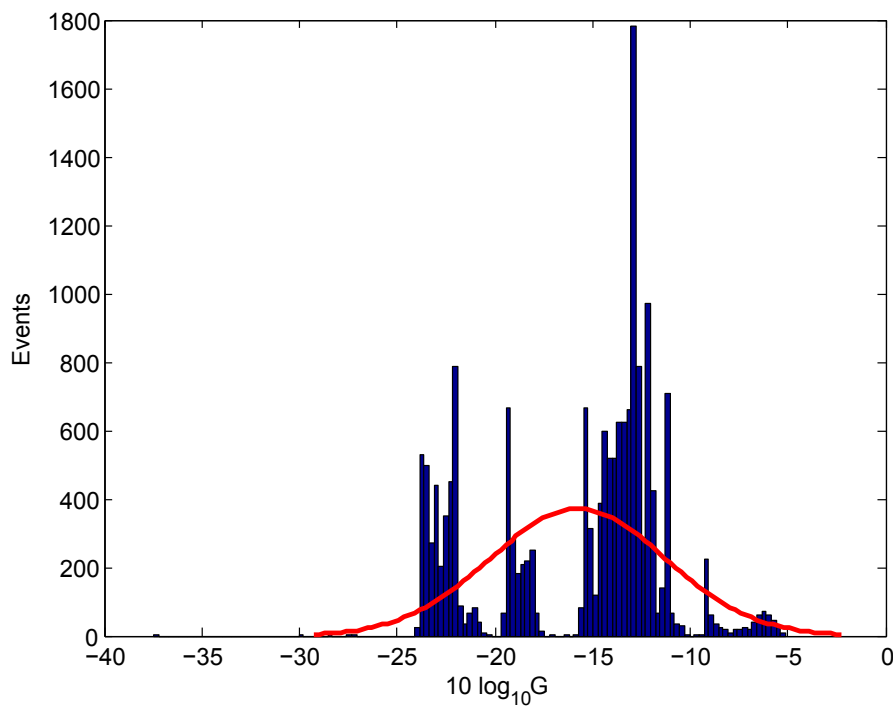
Figure 12: Average channel gain lognormality test for the 1.705-30 MHz frequency band.
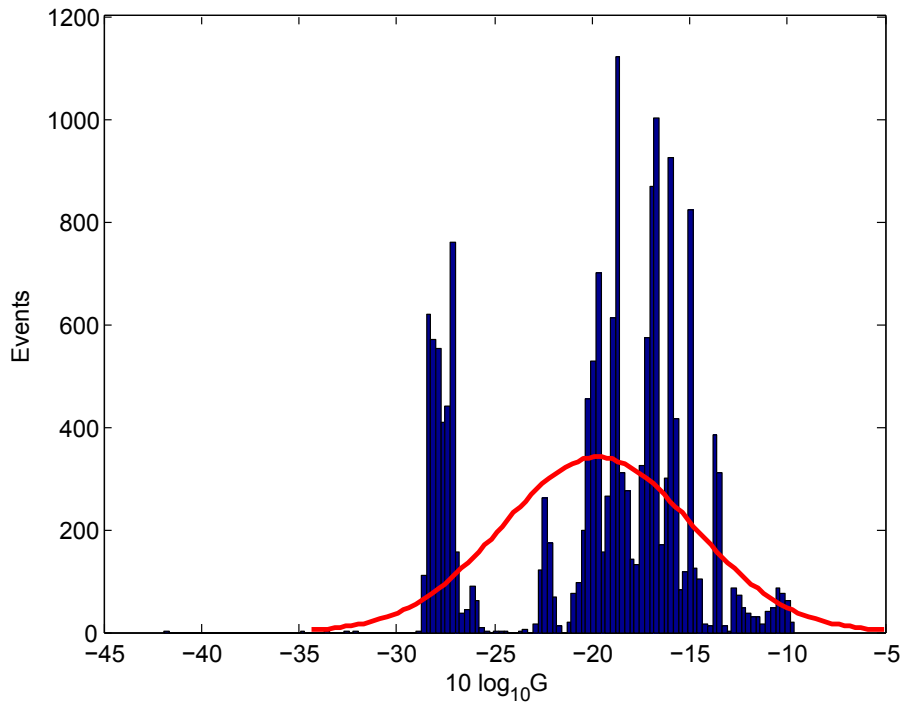
Figure 13: Average channel gain lognormality test for the 1.705-100 MHz frequency band.

The relationship between the RMS-DS and the Average Channel Gain: According to (GALLI, 2011), (GALLI, 2009), and (GALLI, 2010), the RMS-DS and the average channel gain are negatively correlated log-normal random variables, for the LV and MV PLC channels in the US. By analysing the same parameters of the IH-LV PLC channel in Brazil, it was observed the same negative correlation between the RMS-DS and the average channel gain as in the US case. This behaviour is presented using a scatter plot shown in Fig. 14. It can be seen that data is too spread around different RMS-DS values. Therefore, a method to extract a less noisy scatter plot was developed. This method simply makes frequency response averages by taking groups of consecutive estimates of the PLC channel frequency responses. Let consider the measured frequency responses independent and identically distributed (i.i.d) random variables, thus a frequency response average of a group of M frequency responses is given by

$$
\begin{aligned}
\bar{\mathbf{H}} &= E\left\{\hat{\mathbf{H}}_i\right\} \\
&= \frac{1}{M}\sum_{i=0}^{M-1}\hat{\mathbf{H}}_i,
\end{aligned}
\tag{2.17}
$$

where $\hat{\mathbf{H}}_i$ is the i-th estimate of $\mathbf{H}$. This averaging procedure was adopted because the estimates of the PLC channel frequency responses are corrupted by additive noise. As

a consequence, averaging results in estimates less corrupted by additive noise, which are constituted by background and impulsive components.
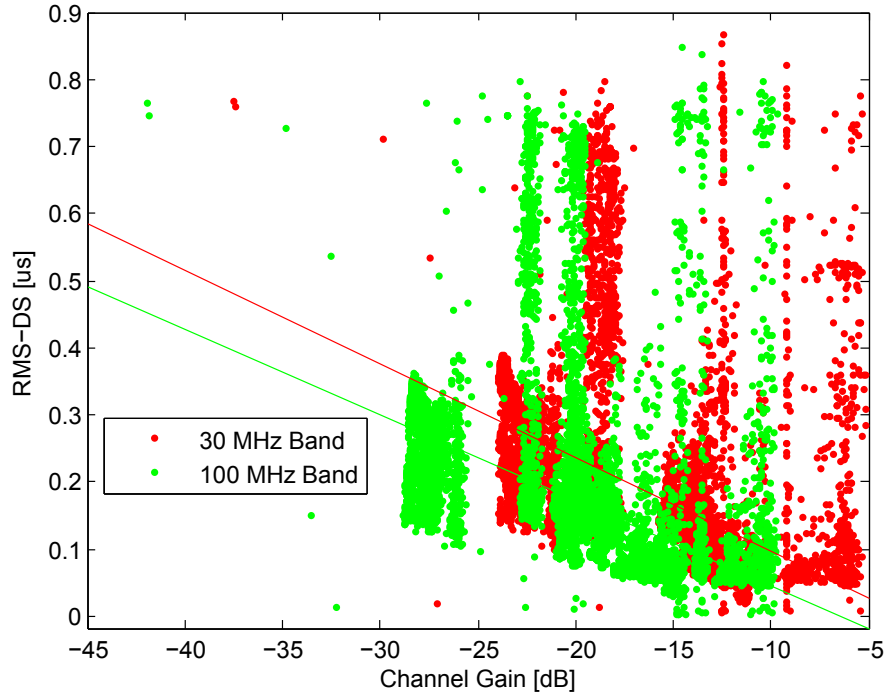
Figure 14: Scatter plot of IH-LV PLC channels measured in Brazil with a least square trend lines for the 1.705-30 MHz and 1.705-100 MHz frequency bands.

The PLC channels were estimated during 15 ms. Then, the number of frequency response estimates is around 646. By setting $M = 20$ we can consider that the averaged frequency response is invariant for about 0.46 ms, which is still lower than the coherence PLC channel time as stated in (CORRIPIO et al., 2006). As a result, this procedure reduces significantly the spread in the scatter plot because the additive noise interference is reduced. Also it shows more clearly that the RMS-DS and the channel gain are negatively correlated as depicted in Fig. 15. This finally, allow us to extract less biased features from the measured data.
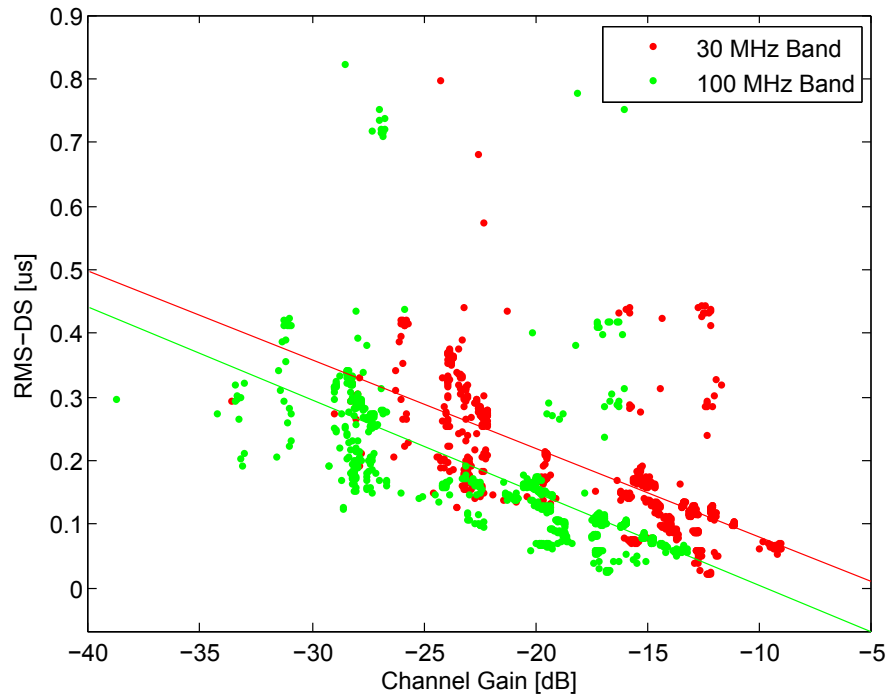
Figure 15: Scatter plot of IH-LV PLC channels measured in Brazil with a least square trend lines for the 1.705-30 MHz and 1.705-100 MHz frequency bands.

The adopted methodology to reduce the noisy influence in the estimates of the PLC channel frequency responses can also be evaluated individually for the RMS-DS (see Figs. 16 and 17) and the average channel gain (see Figs. 18 and 19) respectively. It can be regarded that the behavior of logarithm of the RMS-DS is closer to a normal distribution, and for the specific case of the frequency band between 1.705 and 100 MHz a 33% of the evaluated tests confirms the log-normality of the RMS-DS. However, the average channel gain is still not closer to a normal distribution and the normality tests reject the hypothesis in 100% of the tests.
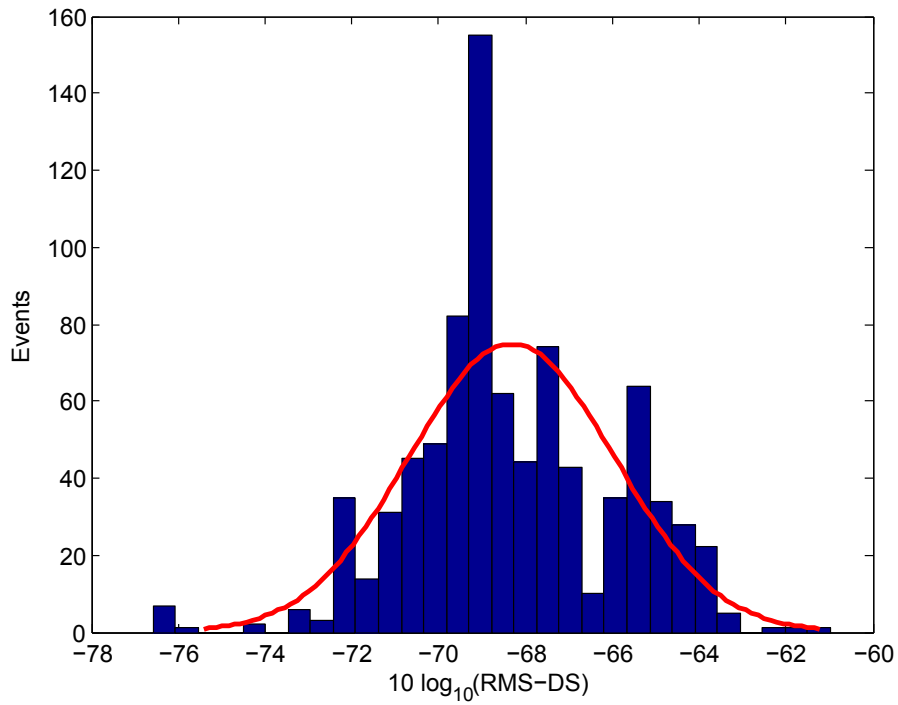
Figure 16: RMS-DS log-normality test for the acquired data in the 1.705-30 MHz frequency band by using frequency response averages ($M = 20$).
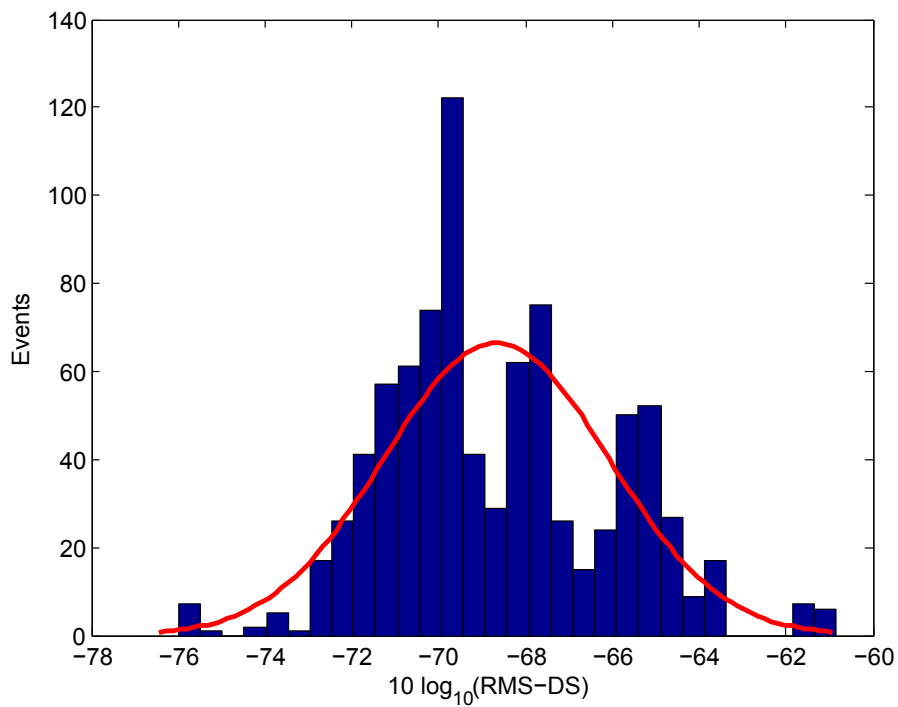
Figure 17: RMS-DS log-normality test for the acquired data in the 1.705-100 MHz frequency band by using frequency response averages ($M = 20$).
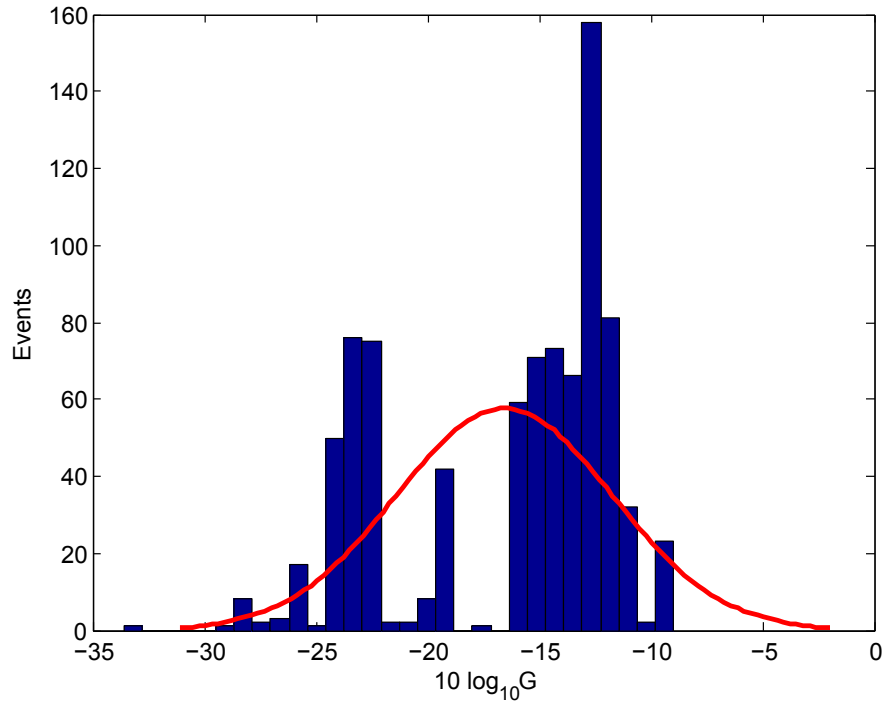
Figure 18: Average channel gain lognormality test for the 1.705-30 MHz frequency band by using frequency response averages ($M = 20$).
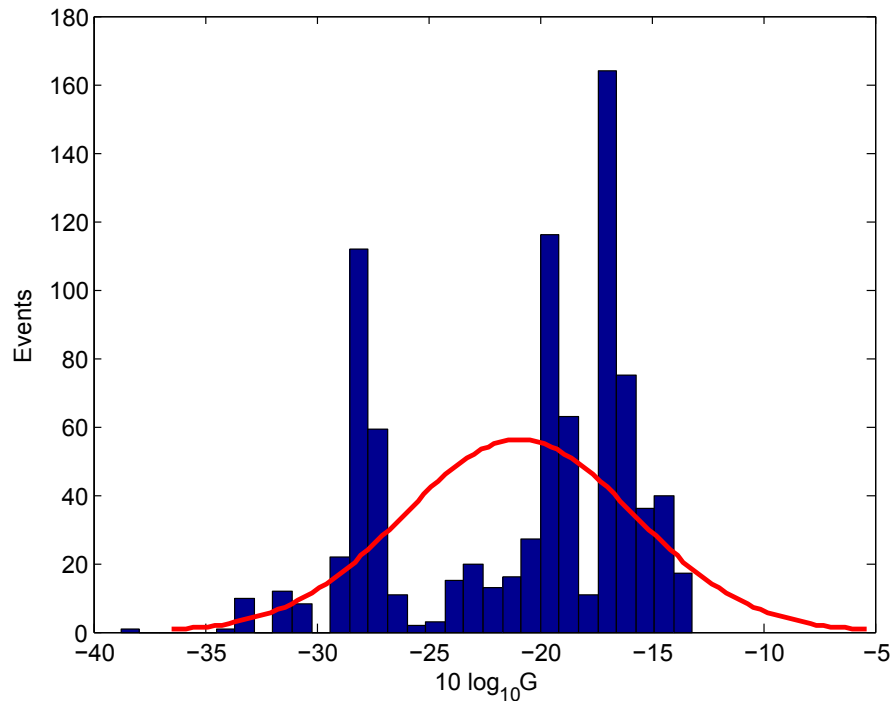
Figure 19: Average channel gain lognormality test for the 1.705-100 MHz frequency band by using frequency response averages ($M = 20$).

The results from the log-normality test applied to the complete database in both analyzed frequency bands are presented in Tab. 1.

	1.705-30 MHz		1.705-100 MHz	
Test\Param.	RMS-DS	Average Channel Gain	RMS-DS	Average Channel Gain
Jarque-Bera	Rejected	Rejected	Rejected	Rejected
Lilliefors	Rejected	Rejected	Rejected	Rejected
Chi-square	Rejected	Rejected	Rejected	Rejected
	100% Rejected		100 % Rejected	

Table 1: Summary of the log-normality tests when the complete dataset is used.

The results from the log-normality test applied to the averaged database in both analyzed frequency bands are presented in Tab. 2.

	1.705-30 MHz		1.705-100 MHz	
Test\Param.	RMS-DS	Average Channel Gain	RMS-DS	Average Channel Gain
Jarque-Bera	Accepted	Rejected	Rejected	Rejected
Lilliefors	Rejected	Rejected	Rejected	Rejected
Chi-square	Rejected	Rejected	Rejected	Rejected
	66.67% Rejected		100 % Rejected	

Table 2: Summary of the log-normality tests when the averaged database is used.

Comparison: The statistical values of the measured channel attenuation and the measured RMS-DS of Brazilian IH-LV PLC channels, are compared to the US MV and IH-LV PLC channels presented in (GALLI, 2011). These comparisons can be regarded in Fig. 20, for the channel attenuation statistics, and in Fig. 21, for the RMS-DS statistics.

For the case of channel attenuation statistics, it is possible to see that the Brazilian PLC channels are characterized with low attenuation values, in which the worst case is even less than 40 dB. Comparing the Brazilian results, it is worth to mention that the channel attenuation does not depend on the bandwidth incremental. It is also possible to see that the attenuation barely increases in about 5 dB (see Fig. 20).
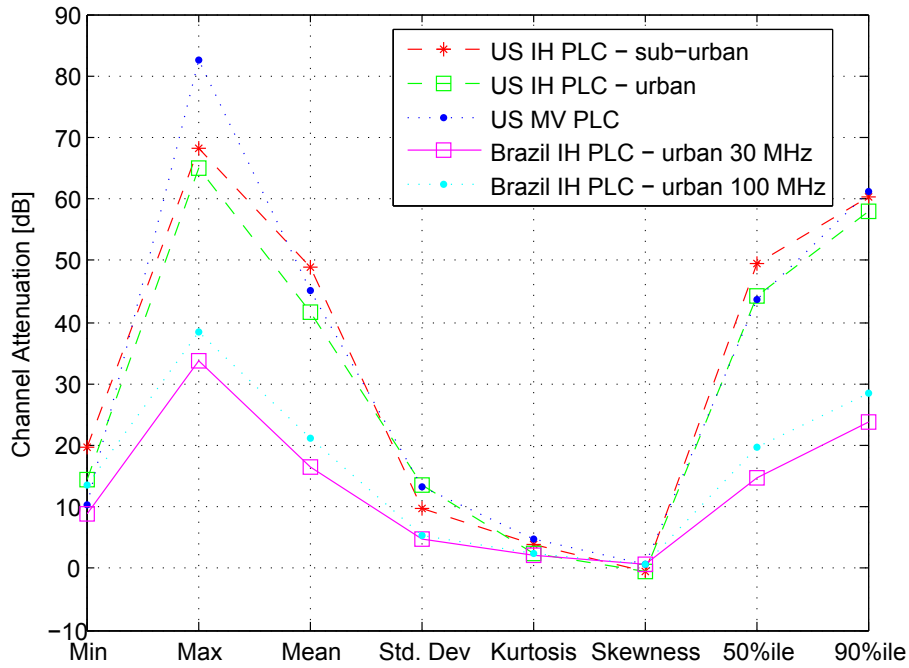
Figure 20: Channel attenuation statistics comparison between the US IH-LV, US MV and Brazilain IH-LV PLC channels. The channel attenuation is calculated as $A_{db} = -G_{dB}$.

The RMS-DS statistics comparison shows a strong similarity between the IH-US and IH-Brazilian cases. Which lead us to think that the RMS-DS does not vary considerably by location. Moreover, the frequency band (either 30 MHz or 100 MHz), does not modify the typical values such as minimum, maximum and mean values. However, for the 100 MHz frequency band, it is possible to see that the RMS-DS values are highly concentrated (high kurtosis) between 0-1 us.
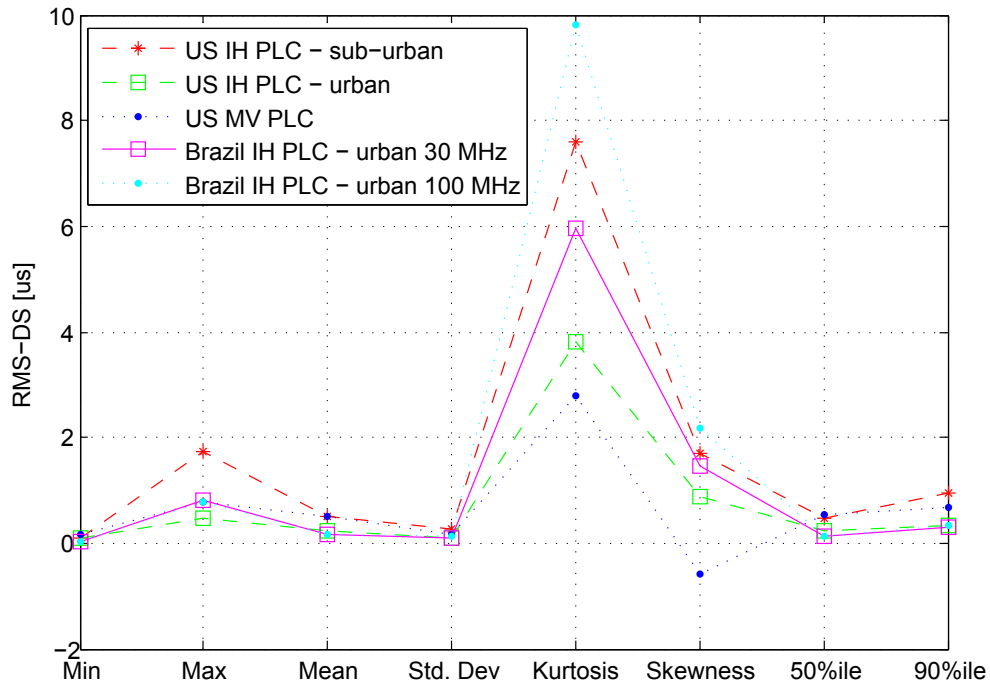
Figure 21: RMS-DS channel statistics comparison between the US IH-LV, US MV and Brazilian IH-LV links.

Channel Capacity: In order to investigate the channel capacity presented in the measured channels, the total transmitted power was simulated to estimate the channel capacity in different PLC channels. This power varied from -10 up to 30 dB. The simulations for the 1.705-30 MHz frequency band are presented in Figs. 22 and 23. It can be noted that the mean capacity ranges from 45 up to 350 Mbps, and it slightly tends to be closer to the maximum values. Additionally, five different curves are presented with the individual Empirical Complementary Cumulative Distribution Function (ECCDF)s of the channel capacity for the specific transmission powers. This curves give the probability that the capacity is larger than a value in the x-axis.
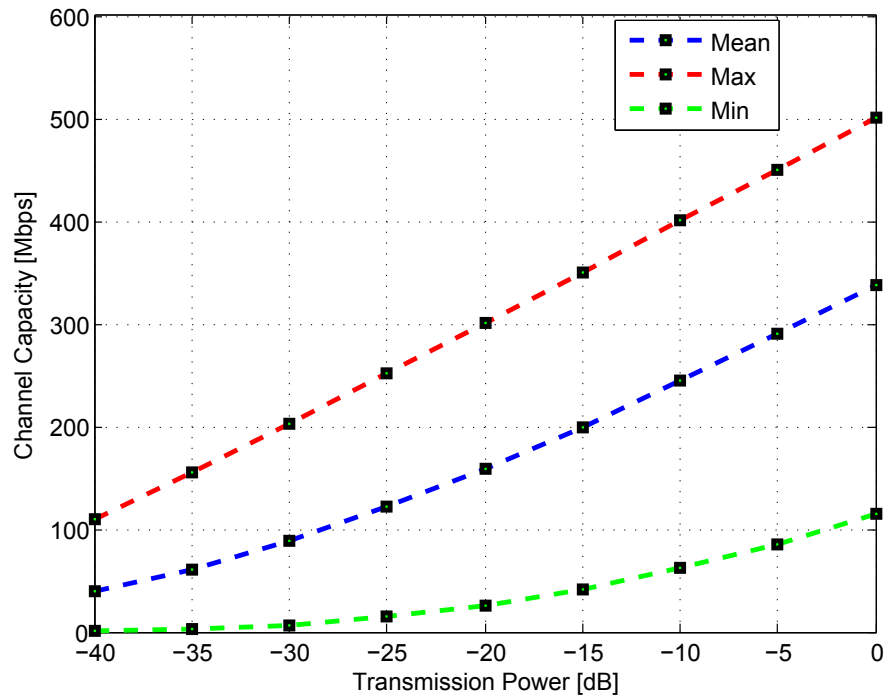
Figure 22: Channel capacity in terms of transmission power for IH-LV PLC channels in the Brazil for the 1.705-30 MHz frequency band.
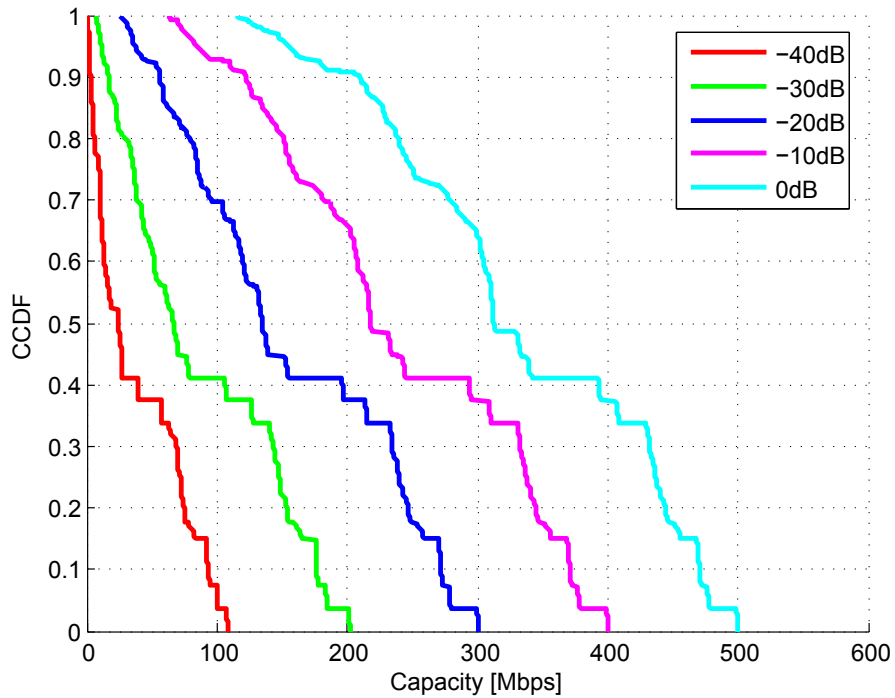
Figure 23: ECCDF of the channel capacity for each simulated power for the 1.705-30 MHz frequency band.

The channel capacity for the 1.705-100 MHz is presented in Figs. 24 and 25. In this case the channel capacities have high data rates (varying in mean from 60 Mbps

to around 900 Mbps), which is expected due to the high channel bandwidth. Also the mean capacity is closer to the maximum values, showing that the minimum values are a reduced amount of events.
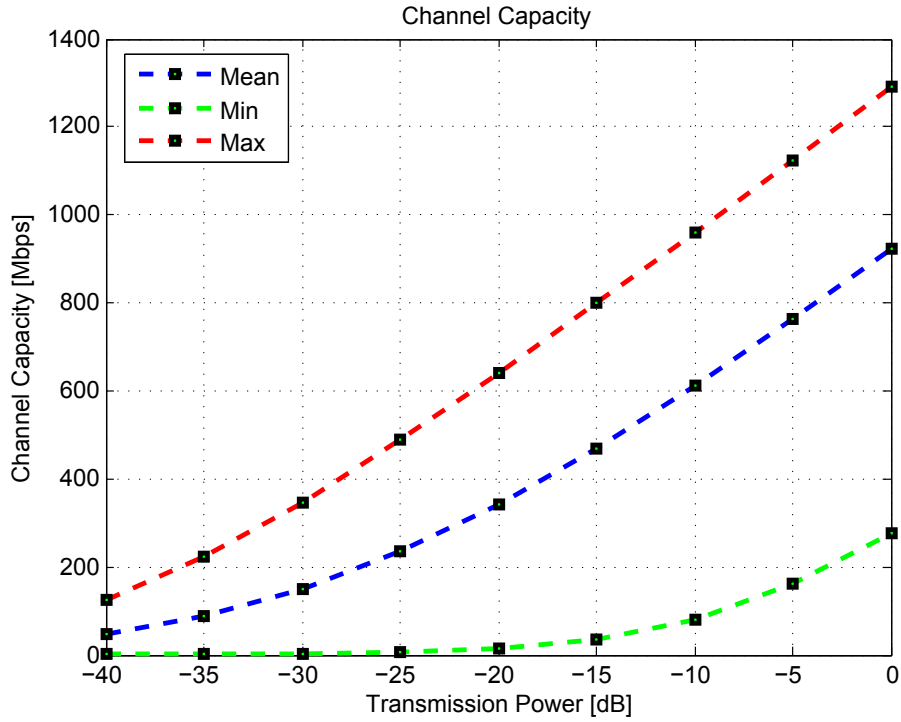
Figure 24: Channel capacity in terms of transmission power for IH-LV PLC channels in the Brazil for the 1.705-100 MHz frequency band.
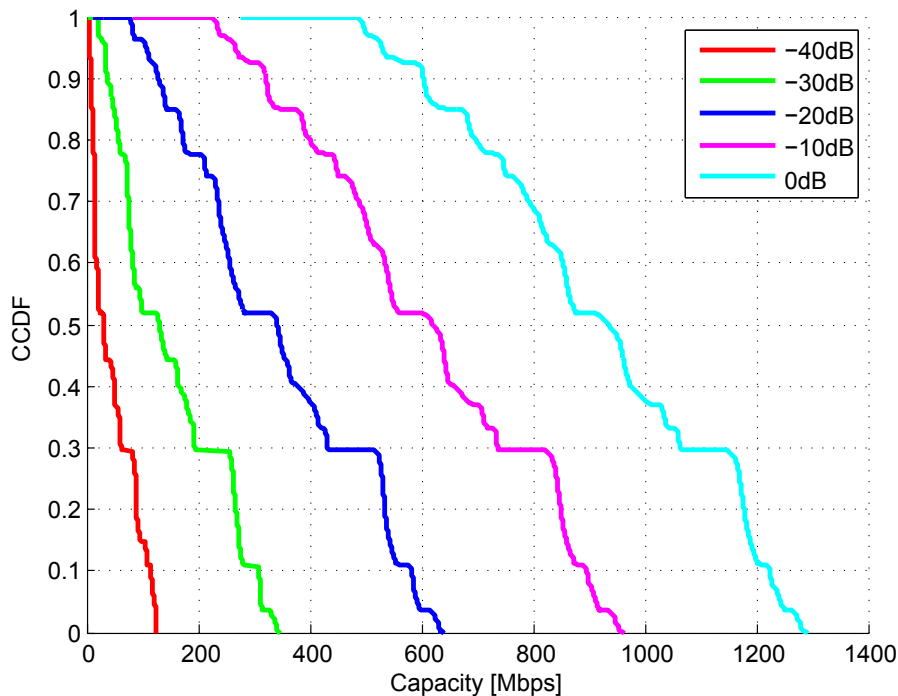
Figure 25: ECCDF of the channel capacity for each simulated power for the 1.705-100 MHz frequency band.

2.2.5 ACCESS IMPEDANCE

The access impedance is another important parameter for the proper understanding of the EPG for data communication purpose. It is of paramount to obtain this parameter in order to develop better couplers to the EPG, that reduce significantly the impedance mismatching existing at the connection points where PLC devices (PLC modems, repeaters, gateways, to name a few.) are connected. The access impedance is also one of the main reasons for high frequency selectivity, and it also varies with location, frequency and time (TAHERINEJAD et al., 2011). Therefore, an additional procedure was used during the measurement campaign. This was a measurement of the scatter parameters of access impedance at the connection points by using a portable RF analyser (Agilent FieldFox N9912A). With this device, it is possible to acquire the frequency spectrum of the S_{11}, S_{12}, S_{21}, and S_{22} parameters. Then the access impedance can be calculated following (ARANEO; CELOZZI; LOVAT, 2009), as

$$Z_{network} = Z_{ref} \left(\frac{1 + S_{11}^{network}}{1 - S_{11}^{network}} \right), \tag{2.18}$$

where $S_{11}^{network}$ is the scattering parameter at the EPG port (outlet) and Z_{ref} is the reference impedance (usually 50 or 75 Ohms), which was considered as 50 Ohms,

because it is the characteristic impedance of the EPG in Brazil.

The real and imaginary parts of the measured impedance at the connection points of the EPG are shown in Figs. 26 and 28, respectively. It can be seen that the resistance might vary from few Ohms (ranging from 4-5 Ohms) up to almost 1700 Ohms. With strong variations in the 20-30 MHz and 70-80 MHz frequency bands. Similarly, the reactance has strong variations within the 20-30 MHz, and 70-80 MHz frequency bands. It is also possible to see from the reactance that the nature of the PLC impedance may be capacitive and inductive, and varying in the frequency domain. Moreover, in Figs. 27 and 29, the variances for both the resistance and the reactance are presented. These results confirm that the frequency bands between 20-30 MHz, and 70-80 MHz have strong variations and cannot be approximated by the mean values. On the contrary, the frequency bands between 1.705-20 MHz, 30-70 MHz, and 80-100 MHz yield less variant resistance and reactance results (see mean values).
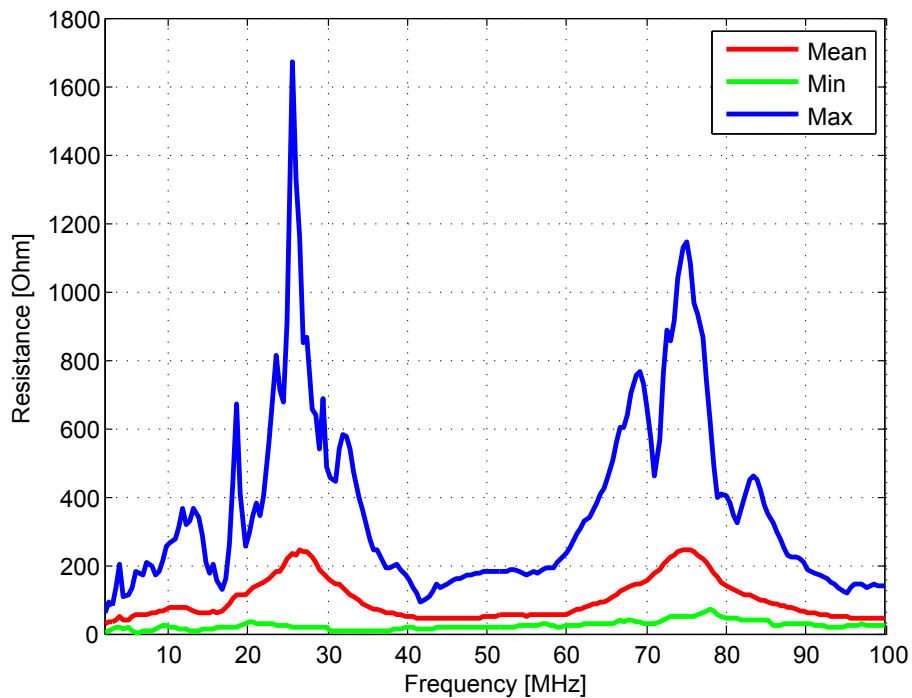
Figure 26: Frequency spectra of the real part of the access impedance of the Brazilian IH-LV EPG.
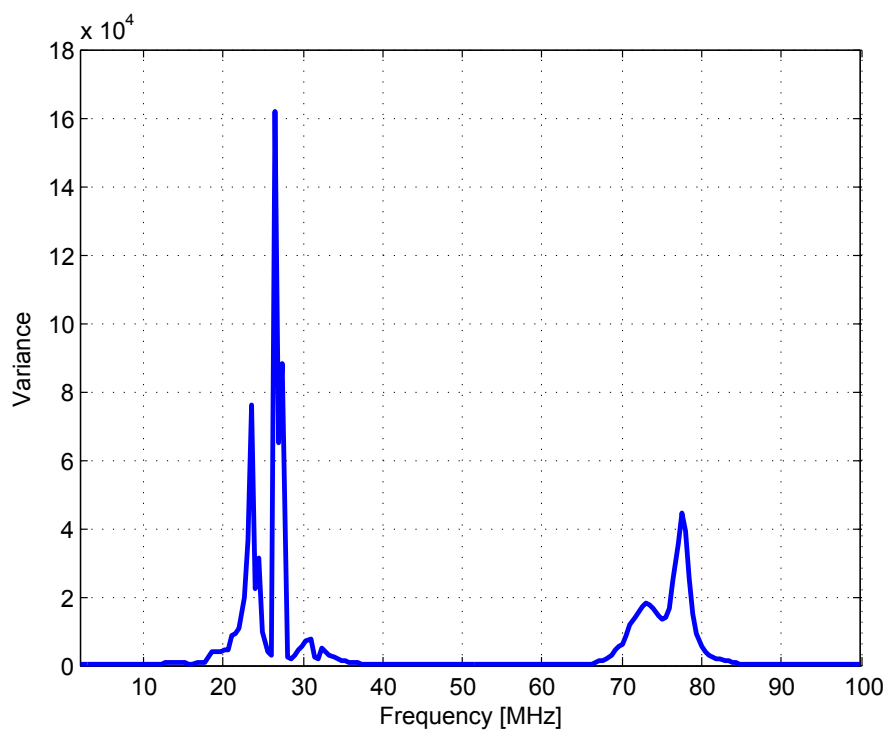
Figure 27: Variance of the frequency spectra of the real part of the access impedance of the Brazilian IH-LV EPG.
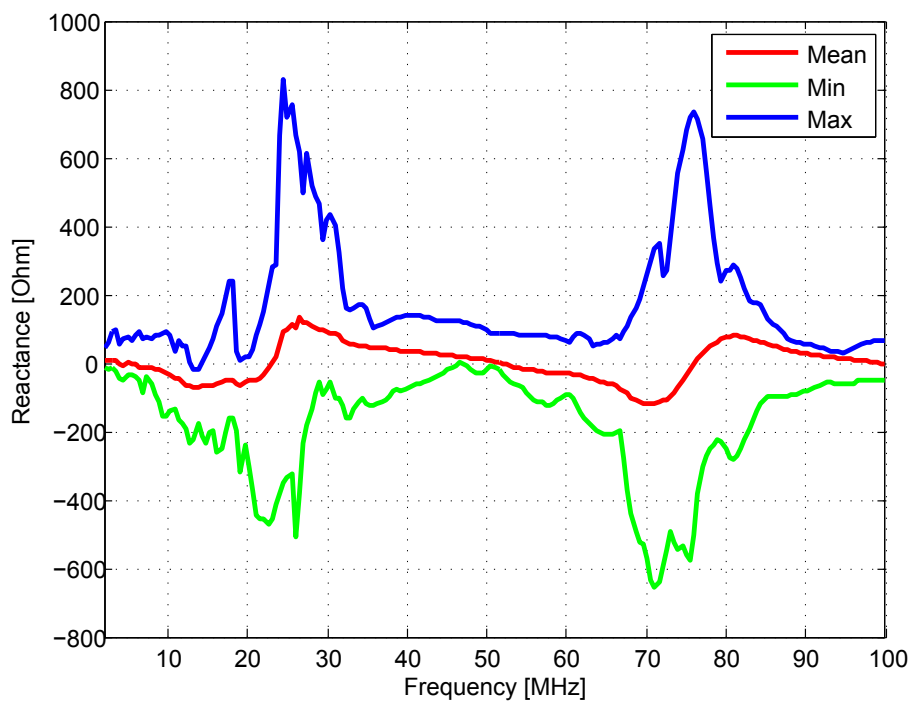
Figure 28: Frequency spectra of the imaginary part of the access impedance of the Brazilian IH-LV EPG.
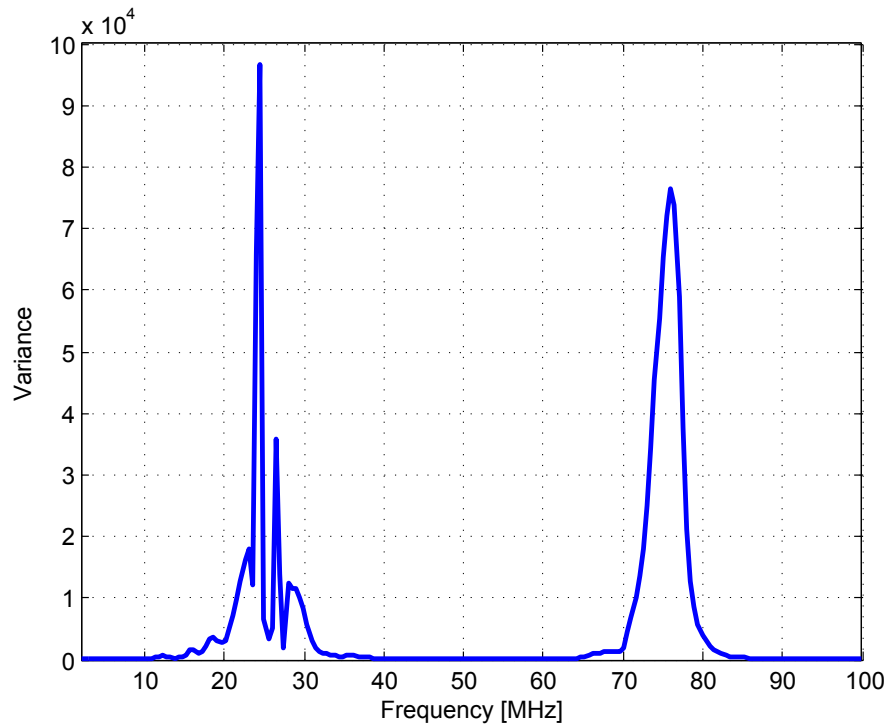
Figure 29: Variance of the frequency spectra of the imaginary part of the access impedance of the Brazilian IH-LV EPG.

2.2.6 IH-LV NOISE

PLC noise is usually presented as the addition of background noise and impulsive noise (ZIMMERMANN; DOSTERT, 2002a) in the PLC channel. It is widely discussed that the background noises are composed of NB and colored noises. Additionally, the impulsive noise has different variations such as: periodic impulse noise synchronous to the mains frequency, periodic impulsive noise asynchronous to the mains frequency, and asynchronous impulsive noise. In order to offer an initial characterization of the IH-LV noise behavior in the Brazilian EPG, the PLC noise was measured right after every PLC channel was measured. These results are briefed by means of PSD (Welch's power spectral density estimate, see technical report in (SCHMID, 2012)) as can be seen in Fig. 30, where the noise PSD levels vary from -60 dB to -125 dB. Also, some time sequences are presented, as relevant examples of the types of noises stated above (see Figs. 31, 32, 33, 34, and 35). It is possible to notice that the noise levels vary from 5 mV peak-to-peak (pk-pk) to about 1200 mV pk-pk.
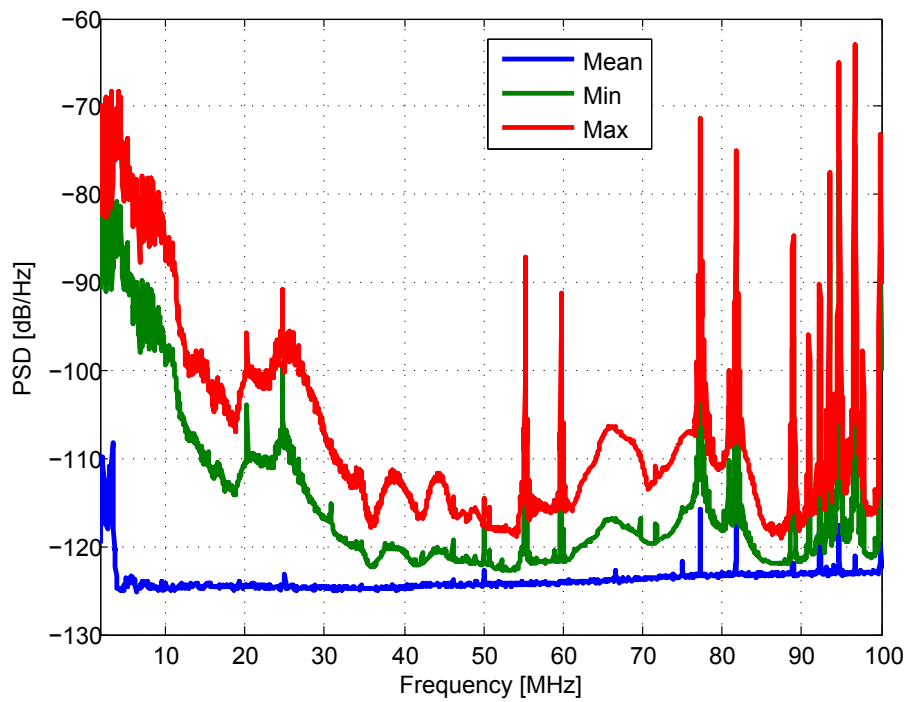
Figure 30: Characteristic of the PSD of the noise in the Brazilian IH-LV EPG.
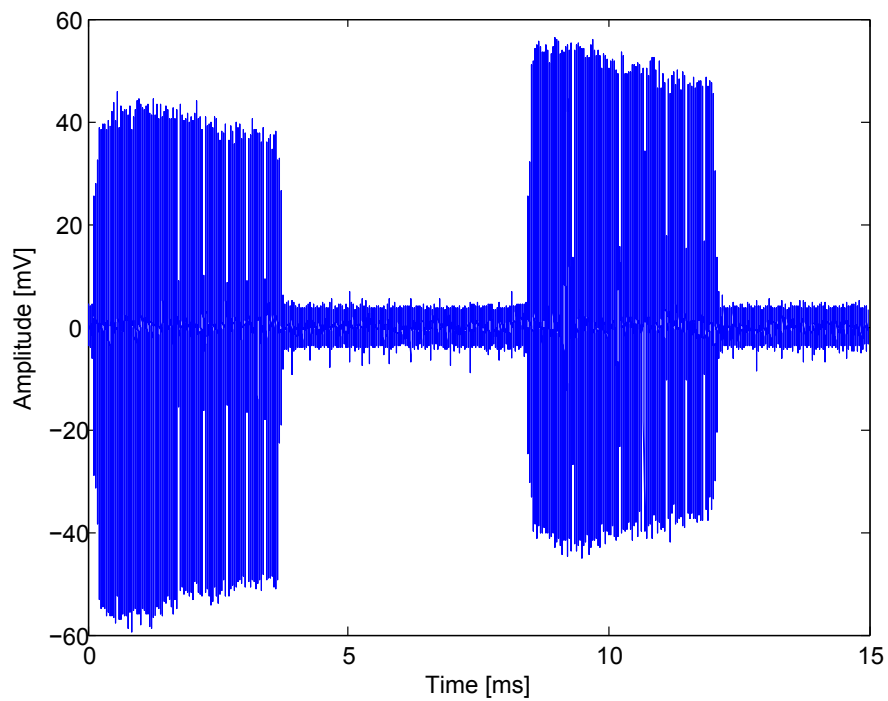
Figure 31: Sample of the measured noise.
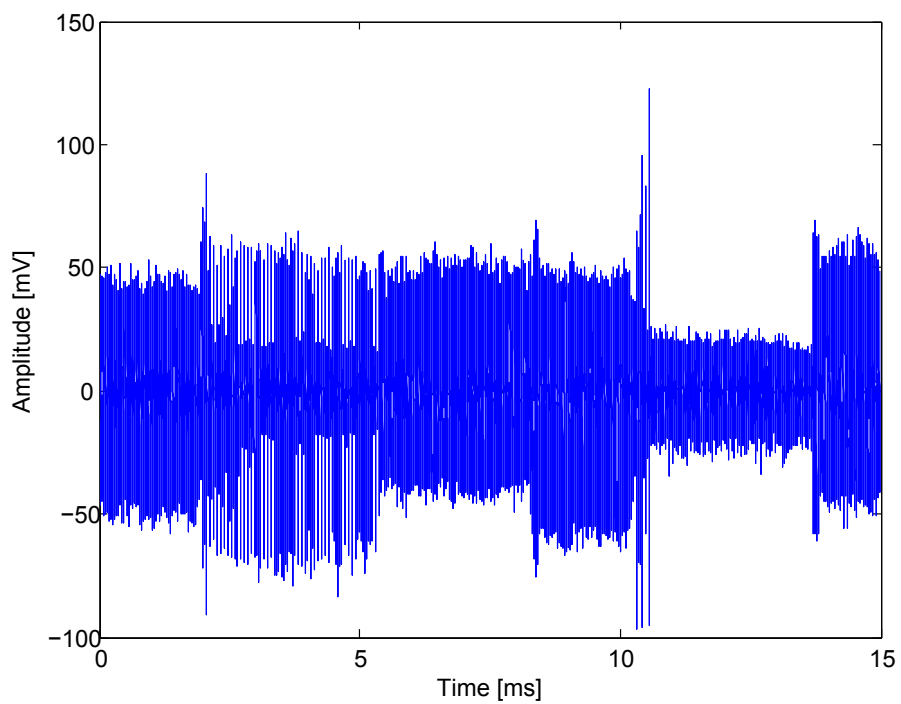
Figure 32: Sample of the measured noise.
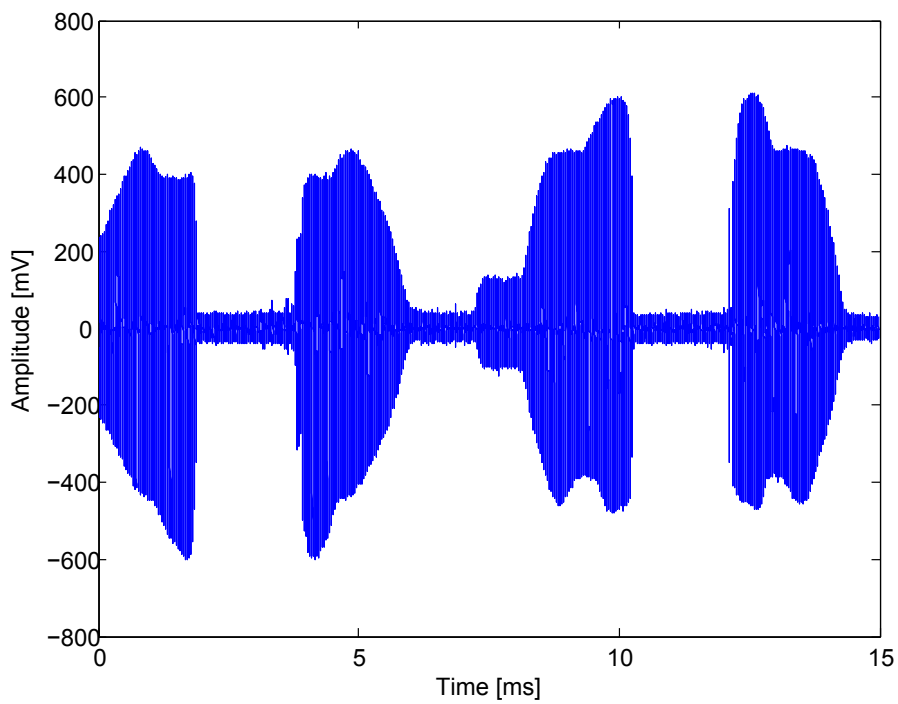
Figure 33: Sample of the measured noise.
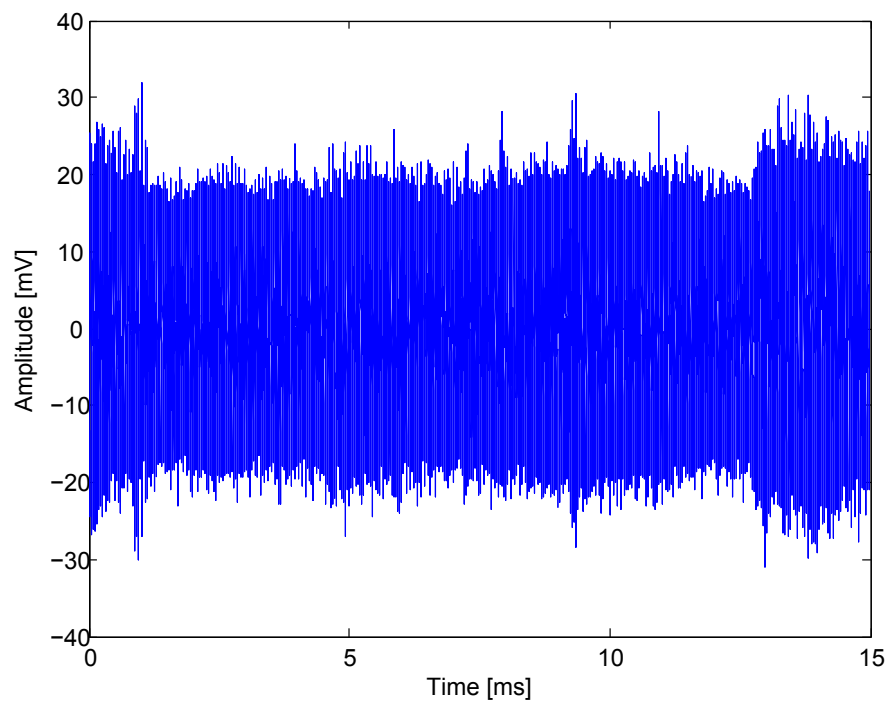
Figure 34: Sample of the measured noise.
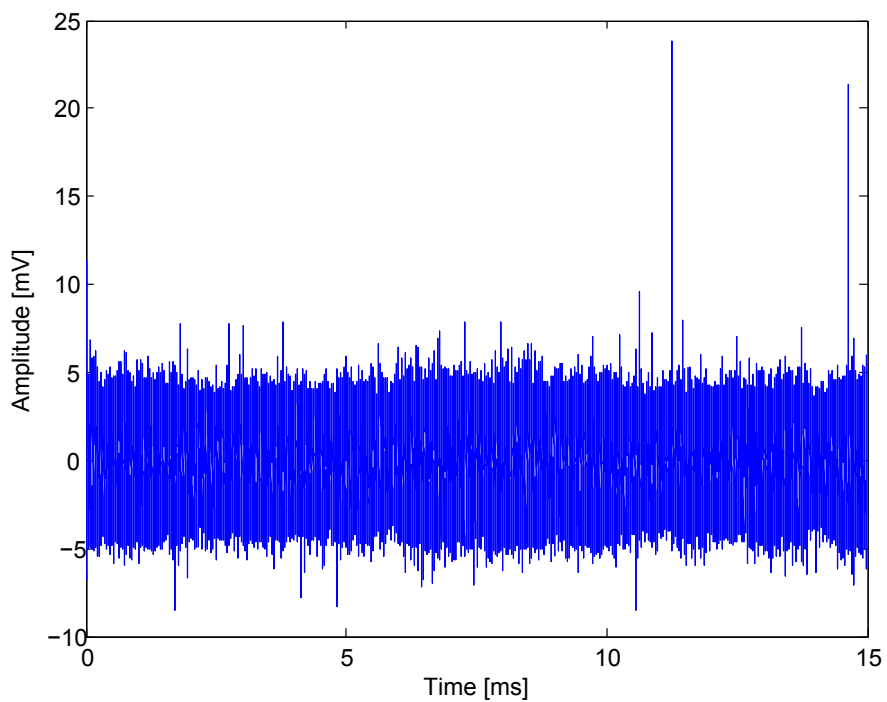
Figure 35: Sample of the measured noise.

3   COOPERATIVE POWER LINE COMMUNICATIONS APPROACH

The current knowledge and understanding of the EPG as data communication medium indicates that the direct link between the Source (S) and Destination (D) nodes can be unable to provide a reliable communication for both NB and BB applications for high data rate demands. Several contributions have clearly shown that the PLC channels have many undesired properties, such as time-varying behaviour, impedance mismatching at the connection and branching points, harmful additive noises, strong attenuations as the frequency and/or distance increases, and frequency selectivity. All of these characteristics make the EPG a challenging medium for data communication. To deal with these drawbacks, the use of cooperative communication strategies (HONG; HUANG; KUO, 2010), (LIU et al., 2009) have brought new opportunities because it can result in a PLC system with improved performance, reliability, and coverage. In fact, cooperative communication may allow two or more users work together to satisfy their data communication demands. Although, cooperative communication is being widely investigated for enhancing wireless communications, few contributions addressed it for the PLC case, such as in (LAMPE; VINCK, 2012), (KIM et al., 2012b), (SUNG; BOJANCZYK, 2010), and (KIM et al., 2012a). Among all kind of analysis that can be carried out, the ones relayed on measures are valuable to reveal advantages and drawbacks and give direction for devising cooperative communication schemes that really results in PLC systems gains.

In this regard, an analysis about the suitability of cooperation concepts for improving PLC system is done for the Brazilian IH-LV EPG. For this purpose, the performance of Amplify-and-Forward (AF) and Decode-and-Forward (DF) protocols, together with Equal-Gain Combining (EGC), Selection Combining (SC), and Maximal-Ratio Combining (MRC) techniques are analyzed. This analysis is carried out on measured PLC channels (obtained after a measurement campaign detailed in Sec. 2.2.1) addressing four different scenarios for possible locations of the Relay (R) node (R node in between the S and D nodes, R node far from S node and closer to D node, R node far from D node and closer to S node, and R node far from both the S and D nodes). The

attained results show that the AF is of limited applicability in the PLC context and the opposite is valid for the DF protocol, mainly if the error probability of detecting symbols at the relay node is zero. Additionally, it is shown that the EGC technique may in some cases reduce the system performance.

This chapter is organized as follows: The single relay model derived for cooperative communication in PLC systems is addressed in Sec. 3.2, followed by the typical relaying protocols and combining techniques used at the D node in Sec. 3.3 and Sec. 3.4, respectively. Finally, the analysis of the cooperative scheme results are presented in Sec. 3.5.

3.1   COOPERATIVE CHANNELS MEASUREMENT CAMPAIGN

In order to experimentally analyze the cooperative protocols and diversity techniques for the Brazilian IH-LV EPG we have used the measurement campaign procedure for P2P PLs described in Sec. 2.2.1. From these measurements, four different configurations were set as depicted in Fig. 36, and are denoted as

Case #1 The R node is in between the S and D nodes.

Case #2 The R node is closer to the D node and far from the S node.

Case #3 The R node is closer to the S node and far from the D node.

Case #4 The R node is far from both the S and D nodes.

These configurations were chosen in order to identify possible advantages of the cooperative scheme for one single R node, while varying the S-R and R-D distances. Therefore, all the individual measured channels were fit into one of the four cases, for further analysis.

Case # 1

Case # 2

Case # 3

Case # 4
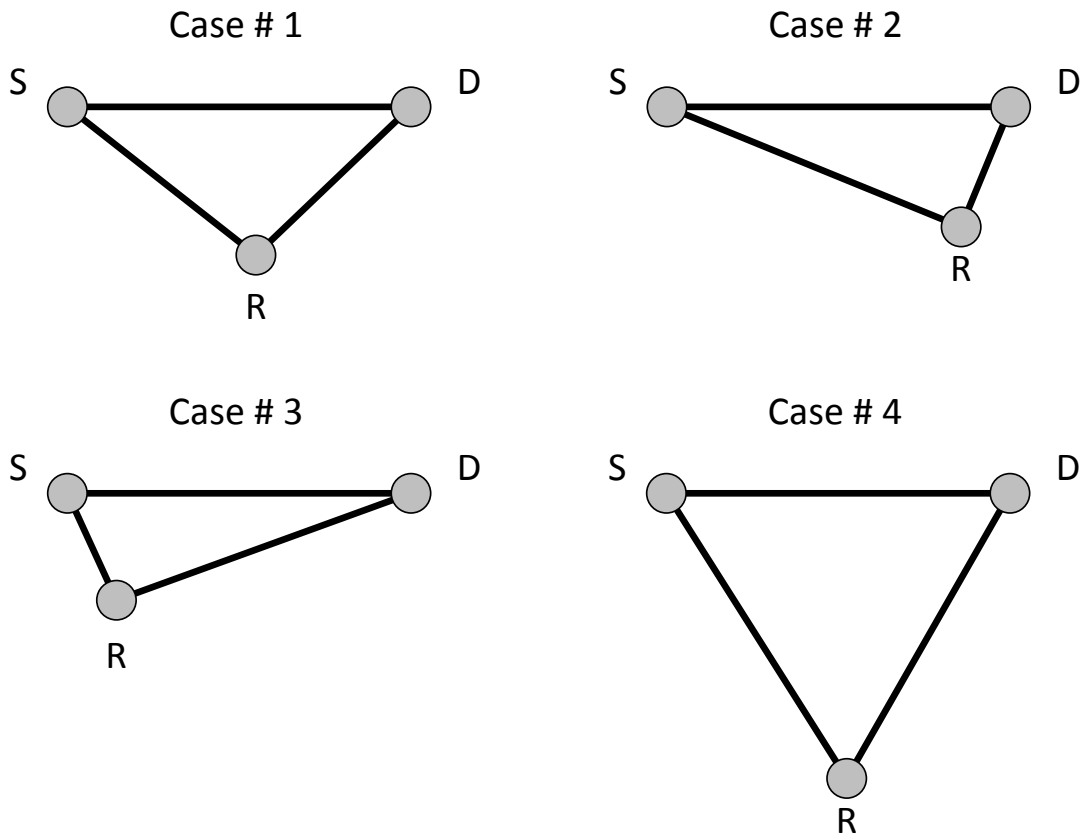
Figure 36: Relaying configurations.

3.2 SINGLE RELAY COOPERATIVE COMMUNICATIONS MODEL

The single relay model is a variation of the cooperation model, in which there is one S node, one R node and one D node. Thus, the relay channel works as an auxiliary channel for data transmission, in order to guarantee the reliability or enhance data rate at the destination node. This configuration is depicted in Fig. 37, where $h_{SD}[n]$, $h_{SR}[n]$, and $h_{RD}[n]$ denote the discrete time representation of the linear and time-invariant impulse responses for the Source-Destination (SD), Source-Relay (SR) and Relay-Destination (RD) links, respectively. Note that it is assumed that all channels are LTI during two time slots. Thus the equivalent channel Source-Relay-Destination (SRD) can be represented as $h_{SRD}[n] = h_{SR}[n]*h_{RD}[n]$, where $*$ denotes the convolution operator.
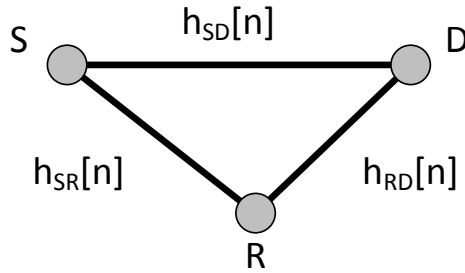
Figure 37: Single relaying channel model.

3.3 RELAYING PROTOCOLS

As it can be regarded in the previous section, the relaying channel topology with a single relay can be modeled with three independent channels, more specifically, three independent PLC channels. It is also important to mention, that the cooperation is carried out during two time slots, i.e., the S node transmits the information during the first time slot and the R node transmits the information during the second time slot, therefore two time slots are needed for data transmission from the S node to the D node. In order to take advantage of the cooperative communications, it is necessary the implementation of protocols. The most common protocols are the AF and the DF. On the one hand, by using the AF relaying protocol, the S node transmits an amplified version of the source signal to the R and D nodes with a power P_0 and then the information is re-transmitted from the R node to the D node with a power P_1. This protocol may have few advantages and drawbacks, since the information received at the R node is the result of the transmitted signal plus the additive noise in the SR link. Thus the R node would amplify both the transmitted signal and the noise. On the other hand, in the DF relaying protocol, the R node decodes the received signal from the S node, re-encodes it, and then re-transmits it with a power P_1 to the D node. For both protocols, the total transmission power is $P = P_0 + P_1$. It is worth mentioning that the DF protocol explored in this work, is considered to be an ideal DF protocol, in which the information received at the R node is perfectly detected and decoded.

From the previous definitions, it is possible to describe the output signal at the D node coming from the SD channel as

$$y_{SD}[n] = h_{SD}[n] * x[n] + v_{SD}[n], \tag{3.1}$$

where $v_{SD}[n]$ is the additive noise over the SD channel, and $x[n]$ is the transmitted signal. The signal at the output of the D node, if the SRD link is used and the AF

protocol is considered, is expressed by

$$
\begin{aligned}
y_{SRD}[n] &= (h_{SR}[n] * h_{RD}[n]) * x[n] + h_{RD}[n] * v_{SR}[n] + v_{RD}[n] \\
&= h_{SRD}[n] * x[n] + h_{RD}[n] * v_{SR}[n] + v_{RD}[n],
\end{aligned}
\tag{3.2}
$$

in which $v_{SR}[n]$ and $v_{RD}[n]$ denote the additive noises over the SR and RD channels, and $h_{SD}[n]$, $h_{SR}[n]$, $h_{RD}[n]$ and $h_{SRD}[n]$ denote the impulse responses of the linear and time-invariant PLC channels for the SD, SR, RD and SRD links. If the DF protocol is considered and the SRD link is used, the signal at the output of the D node is expressed as

$$
y_{SRD}[n] = h_{RD}[n] * \hat{x}[n] + v_{RD}[n],
\tag{3.3}
$$

where $\hat{x}[n]$ is an estimate of the transmitted signal.

Using the OFDM scheme to estimate the channel frequency responses (see Sec. 2.2.2) of the PLC channel impulse responses denoted by $\mathbf{h}_i = [h_i[0]\, h_i[1]\, ... \, h_i[L_i - 1]]^T$, where $i \in \{SD,\, SR,\, RD,\, SRD\}$, and L_i represent the i-th impulse response length, the frequency responses representation of these channels are given by

$$
\mathbf{H}_i = \frac{1}{\sqrt{2N}} \mathbf{W} \begin{bmatrix} \mathbf{h}_i \\ \mathbf{0}_{2N - L_i} \end{bmatrix},
\tag{3.4}
$$

where $\mathbf{0}_M$ denotes an M-length column vector constituted by zeros.

In this case, we assume that N is the number of sub-carriers and $L_{CP} \geq \max\{L_{SD}, L_{SR}, L_{RD}, L_{SRD}\}$. It is also assumed a perfect synchronization at the R and D nodes. Thus, in the frequency domain and considering only one OFDM symbol, the output of each possible channel in a single relay configuration can be defined as

$$
\mathbf{Y}_{SD} = \sqrt{\frac{P_0}{N}} \mathcal{H}_{SD} \mathbf{X} + \mathbf{V}_{SD},
\tag{3.5}
$$

$$
\mathbf{Y}_{SR} = \sqrt{\frac{P_0}{N}} \mathcal{H}_{SR} \mathbf{X} + \mathbf{V}_{SR},
\tag{3.6}
$$

$$
\mathbf{Y}_{RD,AF} = \sqrt{\frac{P_1}{N}} \mathcal{H}_{RD} \mathbf{Y}_{SR} + \mathbf{V}_{RD},
\tag{3.7}
$$

$$
\mathbf{Y}_{RD,DF} = \sqrt{\frac{P_1}{N}} \mathcal{H}_{RD} \hat{\mathbf{X}} + \mathbf{V}_{RD},
\tag{3.8}
$$

the output for the SRD link using the AF protocol is given by

$$
\mathbf{Y}_{SRD,AF} = \left(\sqrt{\frac{P_1 P_0}{N^2}} \mathcal{H}_{SRD} \right) \mathbf{X} + \left(\sqrt{\frac{P_1}{N}} \mathcal{H}_{RD} \mathbf{V}_{SR} + \mathbf{V}_{RD} \right),
\tag{3.9}
$$

and for the DF protocol

$$\mathbf{Y}_{SRD,DF} = \sqrt{\frac{P_1}{N}}\mathcal{H}_{RD}\hat{\mathbf{X}} + \mathbf{V}_{RD} \qquad (3.10)$$

where $\mathcal{H}_i = \text{diag}\{H_i[0]\,H_i[1]\,...\,H_i[N-1]\}$, and $H_i[k] = |H_i[k]|e^{j\phi_i[k]}$, is the k-th coefficient of the frequency response for the i-th channel. Due to the use of the OFDM scheme $\mathcal{H}_{SRD} = \mathcal{H}_{SR}\mathcal{H}_{RD}$, the vector $\hat{\mathbf{X}} = [\hat{X}[0]\,\hat{X}[1]\,...\,\hat{X}[N-1]]^T$ is an estimate of the frequency representation of an OFDM symbol at the R node, represented as $\mathbf{X} = [X[0]\,X[1]\,...\,X[N-1]]^T$, and $\mathbf{V}_l = [V_l[0]\,V_l[1]\,...\,V_l[N-1]]^T$ where $l \in \{SD, SR, RD\}$ denotes the frequency domain representation of the additive noise. It is worth to mention that in this work the DF protocol was considered ideal, which means that the estimated signal received at the R node is exactly the same as the transmitted signal from the D node. In other words, $\hat{\mathbf{X}} = \mathbf{X}$. Furthermore, it is also considered that $\mathbf{X} \in \mathbb{C}^{N \times 1}$ and $\mathbf{V} \in \mathbb{C}^{N \times 1}$ are independent and identically distributed (i.i.d) random vectors such that $E\{\mathbf{X}\} = \mathbf{0}$, $E\{\mathbf{V}_l\} = \mathbf{0}$, $E\{\mathbf{X} \odot \mathbf{V}_l\} = E\{\mathbf{X}\} \odot E\{\mathbf{V}_l\}$, $E\{\mathbf{V}_j \odot \mathbf{V}_l\} = 0$ $if\ j \neq l | j, l \in \{SD, SR, RD\}$. Also, $E\{\mathbf{X}\mathbf{X}^\dagger\} = \mathbf{\Lambda}_{\sigma_{\mathbf{X}}^2} = \text{diag}\{\sigma_{\mathbf{X}}^2[0]\,\sigma_{\mathbf{X}}^2[1]\,...\,\sigma_{\mathbf{X}}^2[N-1]\}$ and $E\{\mathbf{V}_l\mathbf{V}_l^\dagger\} = \mathbf{\Lambda}_{\sigma_{\mathbf{V}_l}^2} = \text{diag}\{\sigma_{\mathbf{V}_l}^2[0]\,\sigma_{\mathbf{V}_l}^2[1]\,...\,\sigma_{\mathbf{V}_l}^2[N-1]\}$, where $\odot$ and $E\{.\}$ denote the Hadamard product and stochastic expectation operators, respectively.

3.4 DIVERSITY COMBINING

In PLC systems, data communication is affected by strong channel attenuation and noises levels, that may result in communication errors. Therefore, in this work the spatial diversity concepts, explored in wireless systems, are taken for the PLC context. This type of diversity is exploited when the transmitter or the receiver have multiple antennas (HONG; HUANG; KUO, 2010), which makes it suitable for the adopted single-relay scheme in PLC systems, where two different links arrive to the destination (SD and SRD). This analogy can be regarded in Fig. 38.
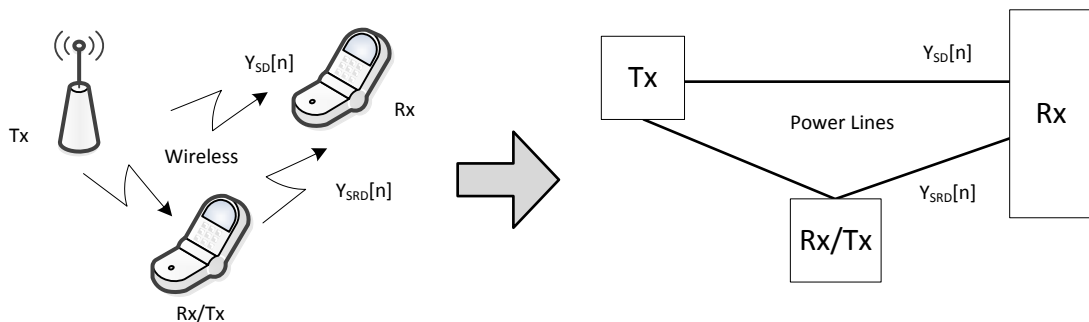
Figure 38: Wireless-PLC analogy.

To analyse the performance of the single-relay cooperative model in the IH PLC scenario, it was necessary an expression that quantifies the gain obtained from the signal combination at the D node. Taking into account (3.5), the resulting signal at the D node is expressed by

$$\hat{\mathbf{Y}} = (\mathbf{M}_\alpha \odot \mathbf{M}_y) \begin{bmatrix} 1 \\ 1 \end{bmatrix}, \tag{3.11}$$

and

$$\mathbf{M}_\alpha = \begin{bmatrix} \alpha_{SD}[0] & \alpha_{SRD}[0] \\ \alpha_{SD}[1] & \alpha_{SRD}[1] \\ \vdots & \vdots \\ \alpha_{SD}[N-1] & \alpha_{SRD}[N-1] \end{bmatrix} \quad \mathbf{M}_y = \begin{bmatrix} y_{SD}[0] & y_{SRD}[0] \\ y_{SD}[1] & y_{SRD}[1] \\ \vdots & \vdots \\ y_{SD}[N-1] & y_{SRD}[N-1] \end{bmatrix}$$

and α_w, where $w \in \{SD, SRD\}$, is the weighting coefficient for the SD and SRD links, respectively. The values of these coefficients are determined according to each combining technique. More precisely, three combining techniques were investigated: EGC, SC, and MRC.

3.4.1 EQUAL-GAIN COMBINING (EGC)

With this technique the received signals are compensated for the phase rotation introduced by the channel (HONG; HUANG; KUO, 2010). The combining coefficients, for the k-th subcarrier are defined as $\alpha_{SD}[k] = e^{-j\phi_{SD}[k]}$ and $\alpha_{SRD}[k] = e^{-j\phi_{SRD}[k]}$ for the SD and SRD links respectively, where $\phi_{SD}[k] = \arg\{H_{SD}[k]\}$ and $\phi_{SRD}[k] = \arg\{H_{SRD}[k]\}$, and it is assumed that the nodes R and D have a complete knowledge of the channel impulse responses. The derived expressions for the AF and DF protocols are described as follows.

EGC with AF: Let rewrite the expression in (3.11) as

$$
\begin{aligned}
\hat{\mathbf{Y}}_{EGC,AF} &= (\mathbf{M}_\alpha \odot \mathbf{M}_y) \begin{bmatrix} 1 \\ 1 \end{bmatrix} \\
&= \mathbf{D}_{\alpha_{SD}} \mathbf{Y}_{SD} + \mathbf{D}_{\alpha_{SRD}} \mathbf{Y}_{SRD,AF} \\
&= \mathbf{D}_{\alpha_{SD}} \left(\sqrt{\frac{P_0}{N}} \mathcal{H}_{SD} \mathbf{X} + \mathbf{V}_{SD} \right) + \\
&\quad + \mathbf{D}_{\alpha_{SRD}} \left(\sqrt{\frac{P_1 P_0}{N^2}} \mathcal{H}_{SRD} \mathbf{X} + \left(\sqrt{\frac{P_1}{N}} \mathcal{H}_{RD} \mathbf{V}_{SR} + \mathbf{V}_{RD} \right) \right) \\
&= \mathbf{D}_{\alpha_{SD}} \sqrt{\frac{P_0}{N}} \mathcal{H}_{SD} \mathbf{X} + \mathbf{D}_{\alpha_{SD}} \mathbf{V}_{SD} + \mathbf{D}_{\alpha_{SRD}} \sqrt{\frac{P_1 P_0}{N^2}} \mathcal{H}_{SRD} \mathbf{X} + \\
&\quad + \mathbf{D}_{\alpha_{SRD}} \left(\sqrt{\frac{P_1}{N}} \mathcal{H}_{RD} \mathbf{V}_{SR} + \mathbf{V}_{RD} \right) \\
&= \left(\mathbf{D}_{\alpha_{SD}} \sqrt{\frac{P_0}{N}} \mathcal{H}_{SD} + \mathbf{D}_{\alpha_{SRD}} \sqrt{\frac{P_1 P_0}{N^2}} \mathcal{H}_{SRD} \right) \mathbf{X} + \\
&\quad + \left(\mathbf{D}_{\alpha_{SD}} \mathbf{V}_{SD} + \mathbf{D}_{\alpha_{SRD}} \left(\sqrt{\frac{P_1}{N}} \mathcal{H}_{RD} \mathbf{V}_{SR} + \mathbf{V}_{RD} \right) \right) \\
&= \left(\sqrt{\frac{P_0}{N}} |\mathcal{H}_{SD}| + \sqrt{\frac{P_1 P_0}{N^2}} |\mathcal{H}_{SRD}| \right) \mathbf{X} + \\
&\quad + \left(\mathbf{D}_{\alpha_{SD}} \mathbf{V}_{SD} + \sqrt{\frac{P_1}{N}} \mathbf{D}_{\alpha_{SRD}} \mathcal{H}_{RD} \mathbf{V}_{SR} + \mathbf{D}_{\alpha_{SRD}} \mathbf{V}_{RD} \right) \quad (3.12)
\end{aligned}
$$

where

$$
\mathbf{D}_{\alpha_{SD}} = \operatorname{diag} \{ \alpha_{SD}[0] \, \alpha_{SD}[1] \, , ... \, , \alpha_{SD}[N-1] \}
$$

and

$$
\mathbf{D}_{\alpha_{SRD}} = \operatorname{diag} \{ \alpha_{SRD}[0] \, \alpha_{SRD}[1] \, ... \, \alpha_{SRD}[N-1] \}
$$

are the weighting coefficient matrices for the SD and SRD channels respectively.

Now, consider the resultant expression in (3.12) as $\hat{\mathbf{Y}}_{EGC,AF} = \mathbf{S}\mathbf{X} + \mathbf{Z}$, where

$$
\mathbf{S} = \left(\sqrt{\frac{P_0}{N}} |\mathcal{H}_{SD}| + \sqrt{\frac{P_1 P_0}{N^2}} |\mathcal{H}_{SRD}| \right),
$$

and

$$
\mathbf{Z} = \left(\mathbf{D}_{\alpha_{SD}} \mathbf{V}_{SD} + \sqrt{\frac{P_1}{N}} \mathbf{D}_{\alpha_{SRD}} \mathcal{H}_{RD} \mathbf{V}_{SR} + \mathbf{D}_{\alpha_{SRD}} \mathbf{V}_{RD} \right),
$$

in which $|\mathcal{H}_i| = \operatorname{diag} \{ |\mathcal{H}_i|[0] \, |\mathcal{H}_i|[1] \, ... \, |\mathcal{H}_i|[N-1] \}$. Then, the resulting SNR diagonal matrix at the output of the equal-gain combiner for the AF protocol is denoted by

$$\mathbf{\Lambda}_{EGC,AF} = \frac{E\left\{\mathbf{SS}^{\dagger}\right\}}{E\left\{\mathbf{ZZ}^{\dagger}\right\}}$$

$$= \frac{\left(\sqrt{\frac{P_0}{N}}|\mathcal{H}_{SD}| + \sqrt{\frac{P_1 P_0}{N^2}}|\mathcal{H}_{SRD}|\right)^2 \mathbf{\Lambda}_{\sigma_{\mathbf{x}}^2}}{\mathbf{\Lambda}_{\sigma_{SD}^2} + \frac{P_1}{N}|\mathcal{H}_{RD}|^2 \mathbf{\Lambda}_{\sigma_{SR}^2} + \mathbf{\Lambda}_{\sigma_{RD}^2}}, \qquad (3.13)$$

where

$$E\left\{\mathbf{SS}^{\dagger}\right\} = E\left\{\left[\left(\sqrt{\frac{P_0}{N}}|\mathcal{H}_{SD}| + \sqrt{\frac{P_1 P_0}{N^2}}|\mathcal{H}_{SRD}|\right)\mathbf{X}\right]\right.$$

$$\left.\left[\left(\sqrt{\frac{P_0}{N}}|\mathcal{H}_{SD}| + \sqrt{\frac{P_1 P_0}{N^2}}|\mathcal{H}_{SRD}|\right)\mathbf{X}\right]^{\dagger}\right\}$$

$$= \left(\sqrt{\frac{P_0}{N}}|\mathcal{H}_{SD}| + \sqrt{\frac{P_1 P_0}{N^2}}|\mathcal{H}_{SRD}|\right)E\left\{\mathbf{XX}^{\dagger}\right\}$$

$$\left(\sqrt{\frac{P_0}{N}}|\mathcal{H}_{SD}| + \sqrt{\frac{P_1 P_0}{N^2}}|\mathcal{H}_{SRD}|\right)^{\dagger}$$

$$= \left(\sqrt{\frac{P_0}{N}}|\mathcal{H}_{SD}| + \sqrt{\frac{P_1 P_0}{N^2}}|\mathcal{H}_{SRD}|\right)^2 \mathbf{\Lambda}_{\sigma_{\mathbf{x}}^2}, \qquad (3.14)$$

because

$$\left(\sqrt{\frac{P_0}{N}}|\mathcal{H}_{SD}| + \sqrt{\frac{P_1 P_0}{N^2}}|\mathcal{H}_{SRD}|\right) = \left(\sqrt{\frac{P_0}{N}}|\mathcal{H}_{SD}| + \sqrt{\frac{P_1 P_0}{N^2}}|\mathcal{H}_{SRD}|\right)^{\dagger}, \qquad (3.15)$$

and

$$
\begin{aligned}
E\left\{\mathbf{Z}\mathbf{Z}^{\dagger}\right\} &= E\left\{\left[\mathbf{D}_{\alpha_{SD}}\mathbf{V}_{SD} + \sqrt{\frac{P_1}{N}}\mathbf{D}_{\alpha_{SRD}}\mathcal{H}_{RD}\mathbf{V}_{SR} + \mathbf{D}_{\alpha_{SRD}}\mathbf{V}_{RD}\right]\right. \\
&\qquad \left.\left[\mathbf{D}_{\alpha_{SD}}\mathbf{V}_{SD} + \sqrt{\frac{P_1}{N}}\mathbf{D}_{\alpha_{SRD}}\mathcal{H}_{RD}\mathbf{V}_{SR} + \mathbf{D}_{\alpha_{SRD}}\mathbf{V}_{RD}\right]^{\dagger}\right\} \\
&= E\left\{\left(\mathbf{D}_{\alpha_{SD}}\mathbf{V}_{SD}\right)\left(\mathbf{D}_{\alpha_{SD}}\mathbf{V}_{SD}\right)^{\dagger} + \right. \\
&\qquad + \left(\sqrt{\frac{P_1}{N}}\mathbf{D}_{\alpha_{SRD}}\mathcal{H}_{RD}\mathbf{V}_{SR}\right)\left(\sqrt{\frac{P_1}{N}}\mathbf{D}_{\alpha_{SRD}}\mathcal{H}_{RD}\mathbf{V}_{SR}\right)^{\dagger} \\
&\qquad \left. + \left(\mathbf{D}_{\alpha_{SRD}}\mathbf{V}_{RD}\right)\left(\mathbf{D}_{\alpha_{SRD}}\mathbf{V}_{RD}\right)^{\dagger}\right\} \\
&= \mathbf{D}_{\alpha_{SD}}E\left\{\mathbf{V}_{SD}\mathbf{V}_{SD}^{\dagger}\right\}\mathbf{D}_{\alpha_{SD}}^{\dagger} + \\
&\qquad + \left(\sqrt{\frac{P_1}{N}}\mathbf{D}_{\alpha_{SRD}}\mathcal{H}_{RD}\right)E\left\{\mathbf{V}_{SR}\mathbf{V}_{SR}^{\dagger}\right\}\left(\sqrt{\frac{P_1}{N}}\mathbf{D}_{\alpha_{SRD}}\mathcal{H}_{RD}\right) + \\
&\qquad + \mathbf{D}_{\alpha_{SRD}}E\left\{\mathbf{V}_{RD}\mathbf{V}_{RD}^{\dagger}\right\}\mathbf{D}_{\alpha_{SRD}}^{\dagger} \\
&= E\left\{\mathbf{V}_{SD}\mathbf{V}_{SD}^{\dagger}\right\} + \frac{P_1}{N}|\mathcal{H}_{RD}|^2 E\left\{\mathbf{V}_{SR}\mathbf{V}_{SR}^{\dagger}\right\} + E\left\{\mathbf{V}_{RD}\mathbf{V}_{RD}^{\dagger}\right\} \\
&= \boldsymbol{\Lambda}_{\sigma_{SD}^2} + \frac{P_1}{N}|\mathcal{H}_{RD}|^2\boldsymbol{\Lambda}_{\sigma_{SR}^2} + \boldsymbol{\Lambda}_{\sigma_{RD}^2}, \qquad (3.16)
\end{aligned}
$$

because $\mathbf{D}_{\alpha_{SD}}\mathbf{D}_{\alpha_{SD}}^{\dagger} = \mathbf{I}$ and $\mathbf{D}_{\alpha_{SRD}}\mathbf{D}_{\alpha_{SRD}}^{\dagger} = \mathbf{I}$.

EGC with DF: As in the AF case, using the expression (3.12), one can arrive to the output signal at the D node for the DF protocol as follows

$$
\begin{aligned}
\hat{\mathbf{Y}}_{EGC,DF} &= \mathbf{D}_{\alpha_{SD}}\mathbf{Y}_{SD} + \mathbf{D}_{\alpha_{SRD}}\mathbf{Y}_{SRD,DF} \\
&= \mathbf{D}_{\alpha_{SD}}\left(\sqrt{\frac{P_0}{N}}\mathcal{H}_{SD}\mathbf{X} + \mathbf{V}_{SD}\right) + \mathbf{D}_{\alpha_{SRD}}\left(\sqrt{\frac{P_1}{N}}\mathcal{H}_{RD}\mathbf{X} + \mathbf{V}_{RD}\right) \\
&= \left(\sqrt{\frac{P_0}{N}}|\mathcal{H}_{SD}| + \sqrt{\frac{P_1}{N}}|\mathcal{H}_{SRD}|\right)\mathbf{X} + (\mathbf{D}_{\alpha_{SD}}\mathbf{V}_{SD} + \mathbf{D}_{\alpha_{SRD}}\mathbf{V}_{RD}) \quad (3.17)
\end{aligned}
$$

By considering $\hat{\mathbf{Y}}_{EGC,DF} = \mathbf{S}\mathbf{X} + \mathbf{Z}$, where

$$
\mathbf{S} = \left(\sqrt{\frac{P_0}{N}}|\mathcal{H}_{SD}| + \sqrt{\frac{P_1}{N}}|\mathcal{H}_{SRD}|\right),
$$

and

$$
\mathbf{Z} = \left(\mathbf{D}_{\alpha_{SD}}\mathbf{V}_{SD} + \mathbf{D}_{\alpha_{SRD}}\mathbf{V}_{RD}\right).
$$

Then, the resulting SNR diagonal matrix at the output of the equal-gain combiner for the DF protocol at the D node, is given by

$$\mathbf{\Lambda}_{EGC,DF} = \frac{E\left\{\mathbf{SS}^\dagger\right\}}{E\left\{\mathbf{ZZ}^\dagger\right\}}$$

$$= \frac{\left(\sqrt{\frac{P_0}{N}}|\mathcal{H}_{SD}| + \sqrt{\frac{P_1}{N}}|\mathcal{H}_{RD}|\right)^2 \mathbf{\Lambda}_{\sigma_{\mathbf{X}}^2}}{\mathbf{\Lambda}_{\sigma_{SD}^2} + \mathbf{\Lambda}_{\sigma_{RD}^2}}, \tag{3.18}$$

where

$$E\left\{\mathbf{SS}^\dagger\right\} = E\left\{\left[\left(\sqrt{\frac{P_0}{N}}|\mathcal{H}_{SD}| + \sqrt{\frac{P_1}{N}}|\mathcal{H}_{SRD}|\right)\mathbf{X}\right]\right.$$
$$\left.\left[\left(\sqrt{\frac{P_0}{N}}|\mathcal{H}_{SD}| + \sqrt{\frac{P_1}{N}}|\mathcal{H}_{SRD}|\right)\mathbf{X}\right]^\dagger\right\}$$
$$= \left(\sqrt{\frac{P_0}{N}}|\mathcal{H}_{SD}| + \sqrt{\frac{P_1}{N}}|\mathcal{H}_{SRD}|\right)E\left\{\mathbf{XX}^\dagger\right\}$$
$$\left(\sqrt{\frac{P_0}{N}}|\mathcal{H}_{SD}| + \sqrt{\frac{P_1}{N}}|\mathcal{H}_{SRD}|\right)^\dagger$$
$$= \left(\sqrt{\frac{P_0}{N}}|\mathcal{H}_{SD}| + \sqrt{\frac{P_1}{N}}|\mathcal{H}_{RD}|\right)^2 \mathbf{\Lambda}_{\sigma_{\mathbf{X}}^2}, \tag{3.19}$$

because

$$\left(\sqrt{\frac{P_0}{N}}|\mathcal{H}_{SD}| + \sqrt{\frac{P_1}{N}}|\mathcal{H}_{SRD}|\right) = \left(\sqrt{\frac{P_0}{N}}|\mathcal{H}_{SD}| + \sqrt{\frac{P_1}{N}}|\mathcal{H}_{SRD}|\right)^\dagger, \tag{3.20}$$

and

$$E\left\{\mathbf{ZZ}^\dagger\right\} = E\left\{[\mathbf{D}_{\alpha_{SD}}\mathbf{V}_{SD} + \mathbf{D}_{\alpha_{SRD}}\mathbf{V}_{RD}][\mathbf{D}_{\alpha_{SD}}\mathbf{V}_{SD} + \mathbf{D}_{\alpha_{SRD}}\mathbf{V}_{RD}]^\dagger\right\}$$
$$= E\left\{(\mathbf{D}_{\alpha_{SD}}\mathbf{V}_{SD})(\mathbf{D}_{\alpha_{SD}}\mathbf{V}_{SD})^\dagger + \right.$$
$$\left. + (\mathbf{D}_{\alpha_{SRD}}\mathbf{V}_{RD})(\mathbf{D}_{\alpha_{SRD}}\mathbf{V}_{RD})^\dagger\right\}$$
$$= \mathbf{D}_{\alpha_{SD}}E\left\{\mathbf{V}_{SD}\mathbf{V}_{SD}^\dagger\right\}\mathbf{D}_{\alpha_{SD}}^\dagger + \mathbf{D}_{\alpha_{SRD}}E\left\{\mathbf{V}_{RD}\mathbf{V}_{RD}^\dagger\right\}\mathbf{D}_{\alpha_{SRD}}^\dagger$$
$$= E\left\{\mathbf{V}_{SD}\mathbf{V}_{SD}^\dagger\right\} + E\left\{\mathbf{V}_{RD}\mathbf{V}_{RD}^\dagger\right\}$$
$$= \mathbf{\Lambda}_{\sigma_{SD}^2} + \mathbf{\Lambda}_{\sigma_{RD}^2}, \tag{3.21}$$

because $\mathbf{D}_{\alpha_{SD}}\mathbf{D}_{\alpha_{SD}}^\dagger = \mathbf{I}$ and $\mathbf{D}_{\alpha_{SRD}}\mathbf{D}_{\alpha_{SRD}}^\dagger = \mathbf{I}$.

3.4.2 SELECTION COMBINING (SC)

The main idea of this technique is to select the signal with the highest SNR among all the received signals. For this technique, the signal output for both the AF and DF protocols can be easily calculated as

$$\hat{\mathbf{Y}}_{SC_{AF,DF}} = \mathbf{D}_{\alpha_{SD}}\mathbf{Y}_{SD} + \mathbf{D}_{\alpha_{SRD}}\mathbf{Y}_{SRD_{AF,DF}}, \tag{3.22}$$

where the combining coefficients for the SD and SRD are calculated by using the following expressions

$$\alpha_{SD}[k] = \begin{cases} 1, & \text{if } \text{SNR}_{SD}[k] \geq \text{SNR}_{SRD}[k] \\ 0, & \text{otherwise} \end{cases} \tag{3.23}$$

and

$$\alpha_{SRD}[k] = \begin{cases} 1, & \text{if } \text{SNR}_{SRD}[k] \geq \text{SNR}_{SD}[k] \\ 0, & \text{otherwise} \end{cases}. \tag{3.24}$$

Then, the SNR diagonal matrix related to all subcarriers and for the SC technique is given by

$$\mathbf{\Lambda}_{SC} = \text{diag}\{\text{SNR}_{SC}[0], \text{SNR}_{SC}[1], ..., \text{SNR}_{SC}[N-1]\}, \tag{3.25}$$

in which,

$$\text{SNR}_{SC}[k] = \max\{\text{SNR}_{SD}[k], \text{SNR}_{SRD}[k]\}. \tag{3.26}$$

3.4.3 MAXIMAL-RATIO COMBINING (MRC)

The MRC technique maximizes the SNR at the D node by optimizing the weighting coefficients. The k-th coefficient can be expressed as

$$\alpha_{SD}[k] = \frac{|H_{SD}[k]|}{\sigma_{SD}^2[k]} e^{-j\phi_{SD}[k]} \tag{3.27}$$

and

$$\alpha_{SRD}[k] = \frac{|H_{SRD}[k]|}{\sigma_{SRD}^2[k]} e^{-j\phi_{SRD}[k]}, \tag{3.28}$$

for the SD and SRD links, respectively, where $\phi_{SD}[k] = \arg\{H_{SD}[k]\}$ and $\phi_{SRD}[k] = \arg\{H_{SRD}[k]\}$, and it is assumed that the nodes R and D have a complete knowledge

of the additive noises and channel impulse responses. Thus, the mathematical development to obtain the output of the MRC using the AF and DF protocol is described as follows:

MRC with AF: Based on the expression (3.12), the signal at the D node after the MRC combining technique, using the AF protocol is defined by

$$
\begin{aligned}
\hat{\mathbf{Y}}_{MRC_{AF}} &= \left(\mathbf{D}_{\alpha_{SD}} \sqrt{\frac{P_0}{N}} \mathcal{H}_{SD} + \mathbf{D}_{\alpha_{SRD}} \sqrt{\frac{P_1 P_0}{N^2}} \mathcal{H}_{SRD} \right) \mathbf{X} + \\
&\quad + \left(\mathbf{D}_{\alpha_{SD}} \mathbf{V}_{SD} + \mathbf{D}_{\alpha_{SRD}} \left(\sqrt{\frac{P_1}{N}} \mathcal{H}_{RD} \mathbf{V}_{SR} + \mathbf{V}_{RD} \right) \right) \\
&= \left(\sqrt{\frac{P_0}{N}} \frac{|\mathcal{H}_{SD}|^2}{\mathbf{\Lambda}_{\sigma_{SD}^2}} + \sqrt{\frac{P_1 P_0}{N^2}} \frac{|\mathcal{H}_{SRD}|^2}{\mathbf{\Lambda}_{\sigma_{SRD}^2}} \right) \mathbf{X} + \\
&\quad + \left(\mathbf{D}_{\alpha_{SD}} \mathbf{V}_{SD} + \sqrt{\frac{P_1}{N}} \mathbf{D}_{\alpha_{SRD}} \mathcal{H}_{RD} \mathbf{V}_{SR} + \mathbf{D}_{\alpha_{SRD}} \mathbf{V}_{RD} \right) \quad (3.29)
\end{aligned}
$$

where $\mathbf{\Lambda}_{\sigma_i^2} = \mathrm{diag}\left\{ \sigma_i^2[0]\ \sigma_i^2[1] \ldots \sigma_i^2[N-1] \right\}$ and $\sigma_i^2[k] = E\left\{ V_i[k] V_i^*[k] \right\}$.

The resulting SNR diagonal matrix at the output of the maximal-ratio combiner for the AF protocol is denoted by

$$
\begin{aligned}
\Lambda_{MRC,AF} &= \frac{E\left\{ \mathbf{S}\mathbf{S}^\dagger \right\}}{E\left\{ \mathbf{Z}\mathbf{Z}^\dagger \right\}} \\
&= \frac{\left(\sqrt{\frac{P_0}{N}} \frac{|\mathcal{H}_{SD}|^2}{\mathbf{\Lambda}_{\sigma_{SD}^2}} + \sqrt{\frac{P_1 P_0}{N^2}} \frac{|\mathcal{H}_{SRD}|^2}{\mathbf{\Lambda}_{\sigma_{SRD}^2}} \right)^2 \mathbf{\Lambda}_{\sigma_{\mathbf{X}}^2}}{\frac{|\mathcal{H}_{SD}|^2}{\mathbf{\Lambda}_{\sigma_{SD}^2}^2} + \frac{P_1}{N} \frac{|\mathcal{H}_{SRD}|^2 |\mathcal{H}_{RD}|^2}{\mathbf{\Lambda}_{\sigma_{SRD}^2}^2} \mathbf{\Lambda}_{\sigma_{SR}^2} + \frac{|\mathcal{H}_{SRD}|^2}{\mathbf{\Lambda}_{\sigma_{SRD}^2}^2} \mathbf{\Lambda}_{\sigma_{RD}^2}}, \quad (3.30)
\end{aligned}
$$

where

$$E\left\{\mathbf{S}\mathbf{S}^\dagger\right\} = E\left\{\left[\left(\sqrt{\frac{P_0}{N}}\frac{|\mathcal{H}_{SD}|^2}{\mathbf{\Lambda}_{\sigma_{SD}^2}} + \sqrt{\frac{P_1 P_0}{N^2}}\frac{|\mathcal{H}_{SRD}|^2}{\mathbf{\Lambda}_{\sigma_{SRD}^2}}\right)\mathbf{X}\right]\right.$$

$$\left.\left[\left(\sqrt{\frac{P_0}{N}}\frac{|\mathcal{H}_{SD}|^2}{\mathbf{\Lambda}_{\sigma_{SD}^2}} + \sqrt{\frac{P_1 P_0}{N^2}}\frac{|\mathcal{H}_{SRD}|^2}{\mathbf{\Lambda}_{\sigma_{SRD}^2}}\right)\mathbf{X}\right]^\dagger\right\}$$

$$= \left(\sqrt{\frac{P_0}{N}}\frac{|\mathcal{H}_{SD}|^2}{\mathbf{\Lambda}_{\sigma_{SD}^2}} + \sqrt{\frac{P_1 P_0}{N^2}}\frac{|\mathcal{H}_{SRD}|^2}{\mathbf{\Lambda}_{\sigma_{SRD}^2}}\right) E\left\{\mathbf{X}\mathbf{X}^\dagger\right\}$$

$$\left(\sqrt{\frac{P_0}{N}}\frac{|\mathcal{H}_{SD}|^2}{\mathbf{\Lambda}_{\sigma_{SD}^2}} + \sqrt{\frac{P_1 P_0}{N^2}}\frac{|\mathcal{H}_{SRD}|^2}{\mathbf{\Lambda}_{\sigma_{SRD}^2}}\right)^\dagger$$

$$= \left(\sqrt{\frac{P_0}{N}}\frac{|\mathcal{H}_{SD}|^2}{\mathbf{\Lambda}_{\sigma_{SD}^2}} + \sqrt{\frac{P_1 P_0}{N^2}}\frac{|\mathcal{H}_{SRD}|^2}{\mathbf{\Lambda}_{\sigma_{SRD}^2}}\right)^2 \mathbf{\Lambda}_{\sigma_{\mathbf{x}}^2}, \qquad (3.31)$$

because

$$\left(\sqrt{\frac{P_0}{N}}\frac{|\mathcal{H}_{SD}|^2}{\mathbf{\Lambda}_{\sigma_{SD}^2}} + \sqrt{\frac{P_1 P_0}{N^2}}\frac{|\mathcal{H}_{SRD}|^2}{\mathbf{\Lambda}_{\sigma_{SRD}^2}}\right) = \left(\sqrt{\frac{P_0}{N}}\frac{|\mathcal{H}_{SD}|^2}{\mathbf{\Lambda}_{\sigma_{SD}^2}} + \sqrt{\frac{P_1 P_0}{N^2}}\frac{|\mathcal{H}_{SRD}|^2}{\mathbf{\Lambda}_{\sigma_{SRD}^2}}\right)^\dagger, \quad (3.32)$$

and

$$
\begin{aligned}
E\left\{\mathbf{Z}\mathbf{Z}^{\dagger}\right\} &= E\left\{\left[\mathbf{D}_{\alpha_{SD}}\mathbf{V}_{SD} + \sqrt{\frac{P_1}{N}}\mathbf{D}_{\alpha_{SRD}}\mathcal{H}_{RD}\mathbf{V}_{SR} + \mathbf{D}_{\alpha_{SRD}}\mathbf{V}_{RD}\right]\right. \\
&\qquad \left.\left[\mathbf{D}_{\alpha_{SD}}\mathbf{V}_{SD} + \sqrt{\frac{P_1}{N}}\mathbf{D}_{\alpha_{SRD}}\mathcal{H}_{RD}\mathbf{V}_{SR} + \mathbf{D}_{\alpha_{SRD}}\mathbf{V}_{RD}\right]^{\dagger}\right\} \\
&= E\left\{\left(\mathbf{D}_{\alpha_{SD}}\mathbf{V}_{SD}\right)\left(\mathbf{D}_{\alpha_{SD}}\mathbf{V}_{SD}\right)^{\dagger} + \right. \\
&\qquad + \left(\sqrt{\frac{P_1}{N}}\mathbf{D}_{\alpha_{SRD}}\mathcal{H}_{RD}\mathbf{V}_{SR}\right)\left(\sqrt{\frac{P_1}{N}}\mathbf{D}_{\alpha_{SRD}}\mathcal{H}_{RD}\mathbf{V}_{SR}\right)^{\dagger} + \\
&\qquad \left. + \left(\mathbf{D}_{\alpha_{SRD}}\mathbf{V}_{RD}\right)\left(\mathbf{D}_{\alpha_{SRD}}\mathbf{V}_{RD}\right)^{\dagger}\right\} \\
&= \mathbf{D}_{\alpha_{SD}}E\left\{\mathbf{V}_{SD}\mathbf{V}_{SD}^{\dagger}\right\}\mathbf{D}_{\alpha_{SD}}^{\dagger} + \\
&\qquad \left(\sqrt{\frac{P_1}{N}}\mathbf{D}_{\alpha_{SRD}}\mathcal{H}_{RD}\right)E\left\{\mathbf{V}_{SR}\mathbf{V}_{SR}^{\dagger}\right\}\left(\sqrt{\frac{P_1}{N}}\mathbf{D}_{\alpha_{SRD}}\mathcal{H}_{RD}\right)^{\dagger} + \\
&\qquad + \mathbf{D}_{\alpha_{SRD}}E\left\{\mathbf{V}_{RD}\mathbf{V}_{RD}^{\dagger}\right\}\mathbf{D}_{\alpha_{SRD}}^{\dagger} \\
&= \left(\frac{|\mathcal{H}_{SD}|^2}{\mathbf{\Lambda}_{\sigma_{SD}^2}^2}\right)E\left\{\mathbf{V}_{SD}\mathbf{V}_{SD}^{\dagger}\right\} + \\
&\qquad + \left(\frac{P_1}{N}\frac{|\mathcal{H}_{SRD}|^2|\mathcal{H}_{RD}|^2}{\mathbf{\Lambda}_{\sigma_{SRD}^2}^2}\right)E\left\{\mathbf{V}_{SR}\mathbf{V}_{SR}^{\dagger}\right\} + \\
&\qquad + \left(\frac{|\mathcal{H}_{SRD}|^2}{\mathbf{\Lambda}_{\sigma_{SRD}^2}^2}\right)E\left\{\mathbf{V}_{RD}\mathbf{V}_{RD}^{\dagger}\right\} \\
&= \left(\frac{|\mathcal{H}_{SD}|^2}{\mathbf{\Lambda}_{\sigma_{SD}^2}^2}\mathbf{\Lambda}_{\sigma_{SD}^2}\right) + \left(\frac{P_1}{N}\frac{|\mathcal{H}_{SRD}|^2|\mathcal{H}_{RD}|^2}{\mathbf{\Lambda}_{\sigma_{SRD}^2}^2}\mathbf{\Lambda}_{\sigma_{SR}^2}\right) + \\
&\qquad + \left(\frac{|\mathcal{H}_{SRD}|^2}{\mathbf{\Lambda}_{\sigma_{SRD}^2}^2}\mathbf{\Lambda}_{\sigma_{RD}^2}\right) \\
&= \frac{|\mathcal{H}_{SD}|^2}{\mathbf{\Lambda}_{\sigma_{SD}^2}^2} + \frac{P_1}{N}\frac{|\mathcal{H}_{SRD}|^2|\mathcal{H}_{RD}|^2}{\mathbf{\Lambda}_{\sigma_{SRD}^2}^2}\mathbf{\Lambda}_{\sigma_{SR}^2} + \frac{|\mathcal{H}_{SRD}|^2}{\mathbf{\Lambda}_{\sigma_{SRD}^2}^2}\mathbf{\Lambda}_{\sigma_{RD}^2} \qquad (3.33)
\end{aligned}
$$

MRC with DF: In addition, the signal at the D node using the MRC technique

and the DF protocol is given by

$$
\begin{aligned}
\hat{\mathbf{Y}}_{MRC_{DF}} &= \left(\mathbf{D}_{\alpha_{SD}} \sqrt{\frac{P_0}{N}} \mathcal{H}_{SD} + \mathbf{D}_{\alpha_{SRD}} \sqrt{\frac{P_1}{N}} \mathcal{H}_{RD} \right) \mathbf{X} + \\
&\quad + \left(\mathbf{D}_{\alpha_{SD}} \mathbf{V}_{SD} + \mathbf{D}_{\alpha_{SRD}} \mathbf{V}_{RD} \right) \\
&= \left(\sqrt{\frac{P_0}{N}} \frac{|\mathcal{H}_{SD}|^2}{\mathbf{\Lambda}_{\sigma_{SD}^2}} + \sqrt{\frac{P_1}{N}} \frac{|\mathcal{H}_{RD}|^2}{\mathbf{\Lambda}_{\sigma_{RD}^2}} \right) \mathbf{X} + \\
&\quad \left(\mathbf{D}_{\alpha_{SD}} \mathbf{V}_{SD} + \mathbf{D}_{\alpha_{SRD}} \mathbf{V}_{RD} \right)
\end{aligned}
\tag{3.34}
$$

The resulting SNR diagonal matrix at the output of the maximal-ratio combiner for the DF protocol is given by

$$
\begin{aligned}
\mathbf{\Lambda}_{MRC,DF} &= \frac{E\left\{ \mathbf{S}\mathbf{S}^\dagger \right\}}{E\left\{ \mathbf{Z}\mathbf{Z}^\dagger \right\}} \\
&= \frac{\left(\sqrt{\frac{P_0}{N}} \frac{|\mathcal{H}_{SD}|^2}{\mathbf{\Lambda}_{\sigma_{SD}^2}} + \sqrt{\frac{P_1}{N}} \frac{|\mathcal{H}_{RD}|^2}{\mathbf{\Lambda}_{\sigma_{RD}^2}} \right)^2 \mathbf{\Lambda}_{\sigma_{\mathbf{X}}^2}}{\frac{|\mathcal{H}_{SD}|^2}{\mathbf{\Lambda}_{\sigma_{SD}^2}} + \frac{|\mathcal{H}_{RD}|^2}{\mathbf{\Lambda}_{\sigma_{RD}^2}}},
\end{aligned}
\tag{3.35}
$$

where

$$
\begin{aligned}
E\left\{ \mathbf{S}\mathbf{S}^\dagger \right\} &= E\left\{ \left[\left(\sqrt{\frac{P_0}{N}} \frac{|\mathcal{H}_{SD}|^2}{\mathbf{\Lambda}_{\sigma_{SD}^2}} + \sqrt{\frac{P_1}{N}} \frac{|\mathcal{H}_{RD}|^2}{\mathbf{\Lambda}_{\sigma_{RD}^2}} \right) \mathbf{X} \right] \right. \\
&\quad \left. \left[\left(\sqrt{\frac{P_0}{N}} \frac{|\mathcal{H}_{SD}|^2}{\mathbf{\Lambda}_{\sigma_{SD}^2}} + \sqrt{\frac{P_1}{N}} \frac{|\mathcal{H}_{RD}|^2}{\mathbf{\Lambda}_{\sigma_{RD}^2}} \right) \mathbf{X} \right]^\dagger \right\} \\
&= \left(\sqrt{\frac{P_0}{N}} \frac{|\mathcal{H}_{SD}|^2}{\mathbf{\Lambda}_{\sigma_{SD}^2}} + \sqrt{\frac{P_1}{N}} \frac{|\mathcal{H}_{RD}|^2}{\mathbf{\Lambda}_{\sigma_{RD}^2}} \right) E\left\{ \mathbf{X}\mathbf{X}^\dagger \right\} \\
&\quad \left(\sqrt{\frac{P_0}{N}} \frac{|\mathcal{H}_{SD}|^2}{\mathbf{\Lambda}_{\sigma_{SD}^2}} + \sqrt{\frac{P_1}{N}} \frac{|\mathcal{H}_{RD}|^2}{\mathbf{\Lambda}_{\sigma_{RD}^2}} \right)^\dagger \\
&= \left(\sqrt{\frac{P_0}{N}} \frac{|\mathcal{H}_{SD}|^2}{\mathbf{\Lambda}_{\sigma_{SD}^2}} + \sqrt{\frac{P_1}{N}} \frac{|\mathcal{H}_{RD}|^2}{\mathbf{\Lambda}_{\sigma_{RD}^2}} \right)^2 \mathbf{\Lambda}_{\sigma_{\mathbf{X}}^2},
\end{aligned}
\tag{3.36}
$$

because

$$
\left(\sqrt{\frac{P_0}{N}} \frac{|\mathcal{H}_{SD}|^2}{\mathbf{\Lambda}_{\sigma_{SD}^2}} + \sqrt{\frac{P_1}{N}} \frac{|\mathcal{H}_{RD}|^2}{\mathbf{\Lambda}_{\sigma_{RD}^2}} \right) = \left(\sqrt{\frac{P_0}{N}} \frac{|\mathcal{H}_{SD}|^2}{\mathbf{\Lambda}_{\sigma_{SD}^2}} + \sqrt{\frac{P_1}{N}} \frac{|\mathcal{H}_{RD}|^2}{\mathbf{\Lambda}_{\sigma_{RD}^2}} \right)^\dagger,
\tag{3.37}
$$

and

$$
\begin{aligned}
E\left\{\mathbf{Z}\mathbf{Z}^{\dagger}\right\} &= E\left\{[\mathbf{D}_{\alpha_{SD}}\mathbf{V}_{SD} + \mathbf{D}_{\alpha_{SRD}}\mathbf{V}_{RD}]\left[\mathbf{D}_{\alpha_{SD}}\mathbf{V}_{SD} + \mathbf{D}_{\alpha_{SRD}}\mathbf{V}_{RD}\right]^{\dagger}\right\} \\
&= E\left\{(\mathbf{D}_{\alpha_{SD}}\mathbf{V}_{SD})(\mathbf{D}_{\alpha_{SD}}\mathbf{V}_{SD})^{\dagger} + \right. \\
&\quad \left. + (\mathbf{D}_{\alpha_{SRD}}\mathbf{V}_{RD})(\mathbf{D}_{\alpha_{SRD}}\mathbf{V}_{RD})^{\dagger}\right\} \\
&= \mathbf{D}_{\alpha_{SD}}E\left\{\mathbf{V}_{SD}\mathbf{V}_{SD}^{\dagger}\right\}\mathbf{D}_{\alpha_{SD}}^{\dagger} + \mathbf{D}_{\alpha_{SRD}}E\left\{\mathbf{V}_{RD}\mathbf{V}_{RD}^{\dagger}\right\}\mathbf{D}_{\alpha_{SRD}}^{\dagger} \\
&= \left(\frac{|\mathcal{H}_{SD}|^2}{\mathbf{\Lambda}_{\sigma_{SD}^2}^2}\right)E\left\{\mathbf{V}_{SD}\mathbf{V}_{SD}^{\dagger}\right\} + \left(\frac{|\mathcal{H}_{RD}|^2}{\mathbf{\Lambda}_{\sigma_{RD}^2}^2}\right)E\left\{\mathbf{V}_{RD}\mathbf{V}_{RD}^{\dagger}\right\} \\
&= \frac{|\mathcal{H}_{SD}|^2}{\mathbf{\Lambda}_{\sigma_{SD}^2}} + \frac{|\mathcal{H}_{RD}|^2}{\mathbf{\Lambda}_{\sigma_{RD}^2}},
\end{aligned}
\tag{3.38}
$$

because $\mathbf{D}_{\alpha_{SD}}\mathbf{D}_{\alpha_{SD}}^{\dagger} = \mathbf{I}$ and $\mathbf{D}_{\alpha_{SRD}}\mathbf{D}_{\alpha_{SRD}}^{\dagger} = \mathbf{I}$.

3.5 COOPERATIVE EXPERIMENTAL ANALYSIS

To experimentally analyse the advantage of the cooperative communication model, the data obtained from the measurement campaign, explained in Sec. 2.2.1, was taken into consideration. In addition, to understand the single-relaying behaviour in IH-LV PLC channels, four different configurations for the S, R and D nodes were considered. In these configurations, the relative position of the relay can be: in the middle between the source and the destination (case #1); closer to the destination but far away from the source (case #2); closer to the source but far away from the destination (case #3); and in the worst case, the relay might be far from both the source an the destination (case #4).

In Figs. 39, 40, 41, 42, 43, 44, 45, and 46, are presented the channel frequency responses and the noise PSDs of one realization of the configurations Cases #1, #2, #3, and #4, respectively. It is possible to distinguish the strong attenuation in the equivalent SRD link, and the similarity of the additive noise PSDs behaviour in the SD, SR an RD links. Note that the PLC channels are frequency selective, but they also present increasing attenuation as the frequency increases. As a result, the attenuation of the $h_{SRD}[n]$ is strong, even though the attenuations in $h_{SR}[n]$ and $h_{RD}[n]$ are low, if the AF protocol is considered at the R node.
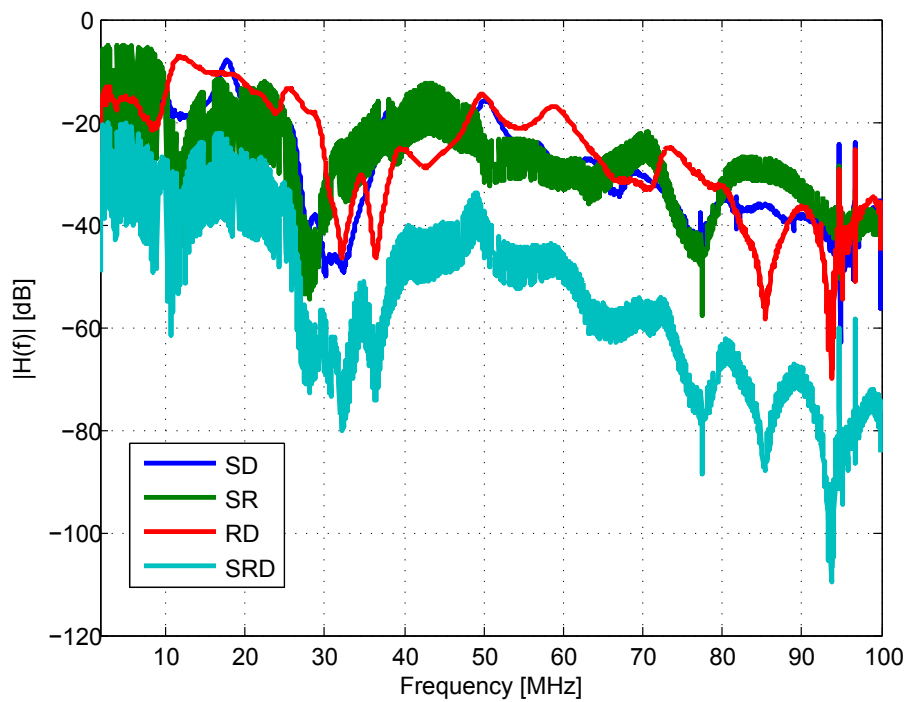
Figure 39: Measured magnitude frequency response for the Case #1.
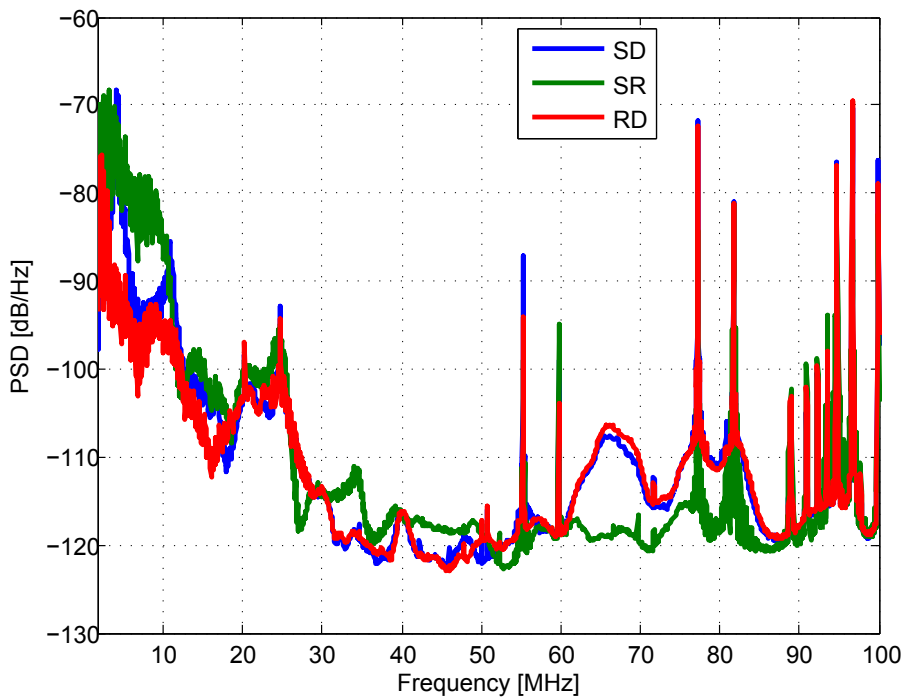
Figure 40: PSD estimation of the additive noises for the Case #1.
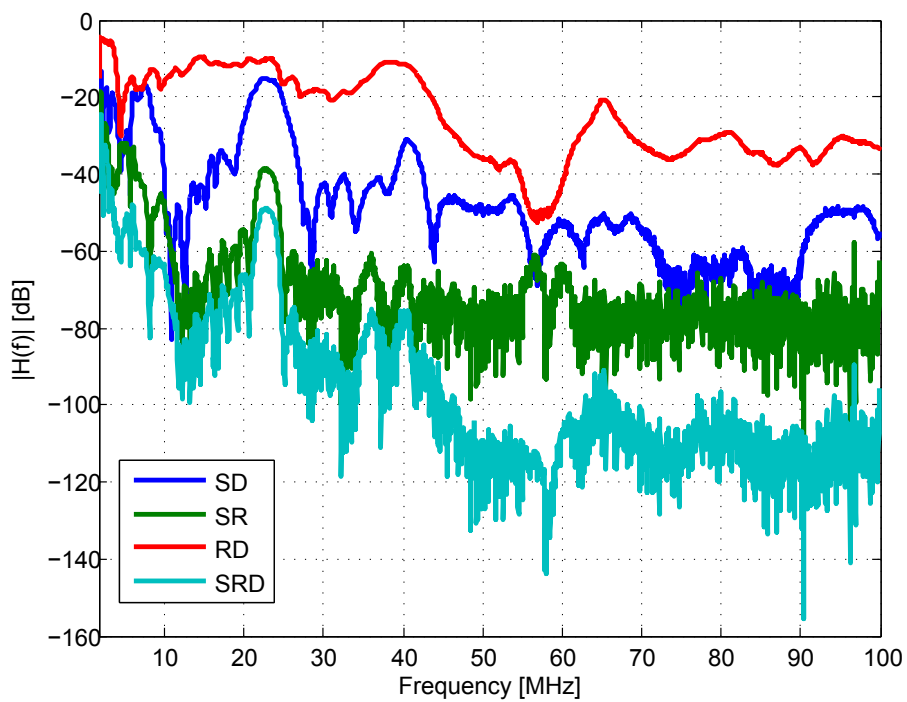
Figure 41: Measured magnitude frequency response for the Case #2.
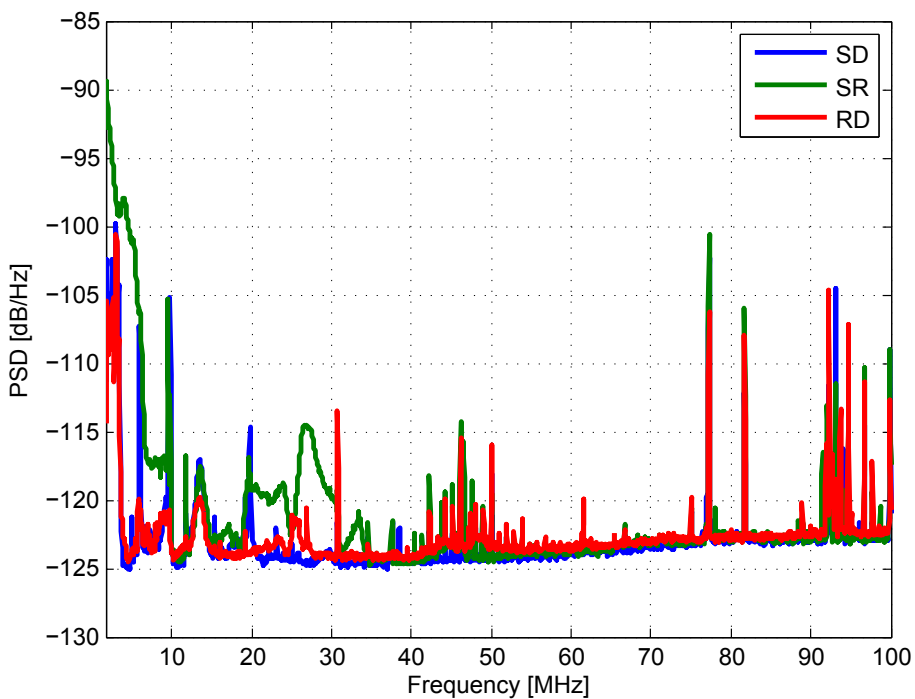
Figure 42: PSD estimation of the additive noises for the Case #2.
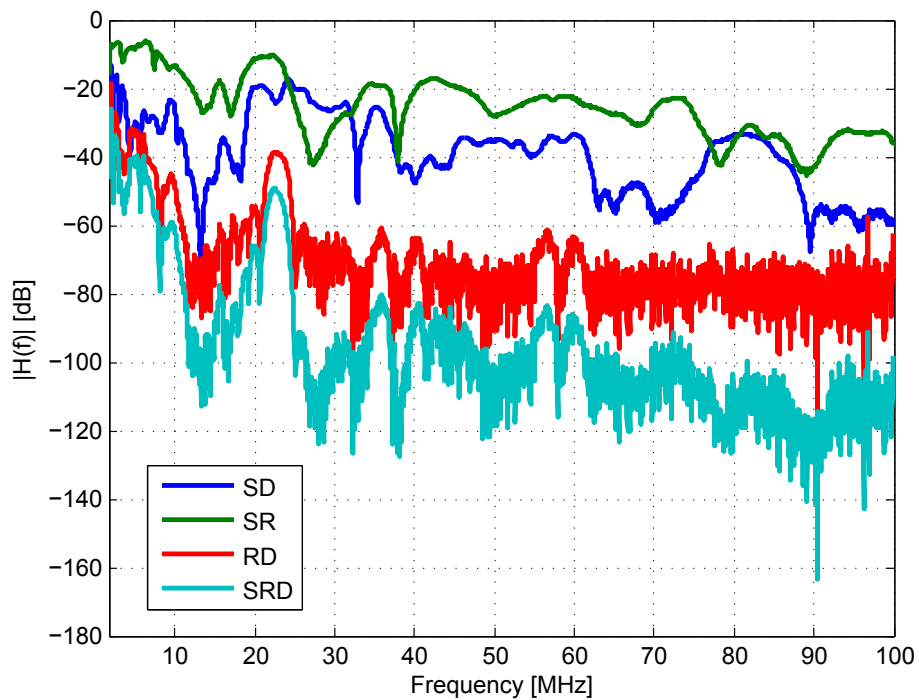
Figure 43: Measured magnitude frequency response for the Case #3.
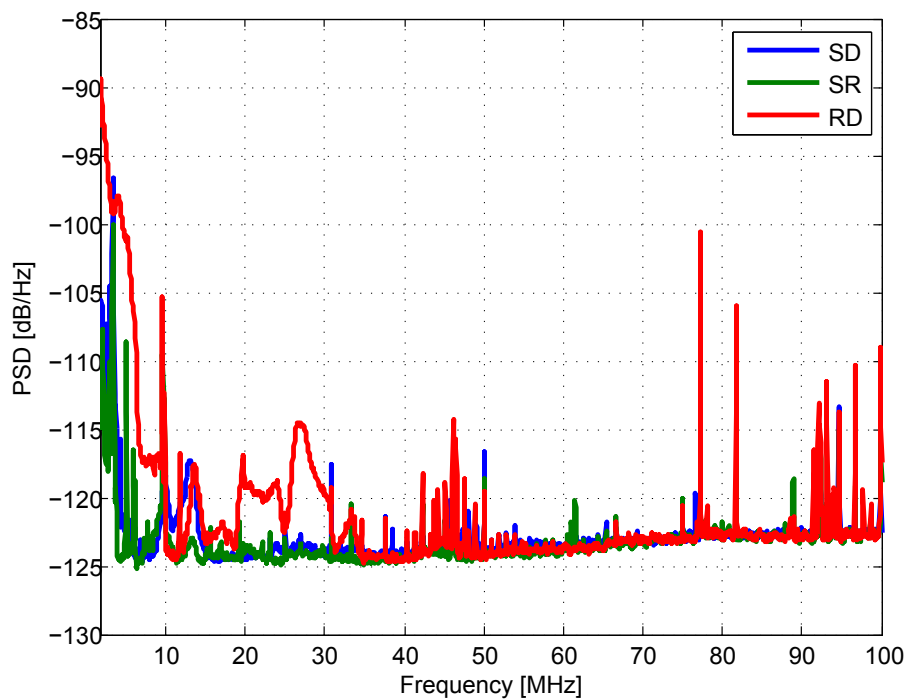
Figure 44: PSD estimation of the additive noises for the Case #3.
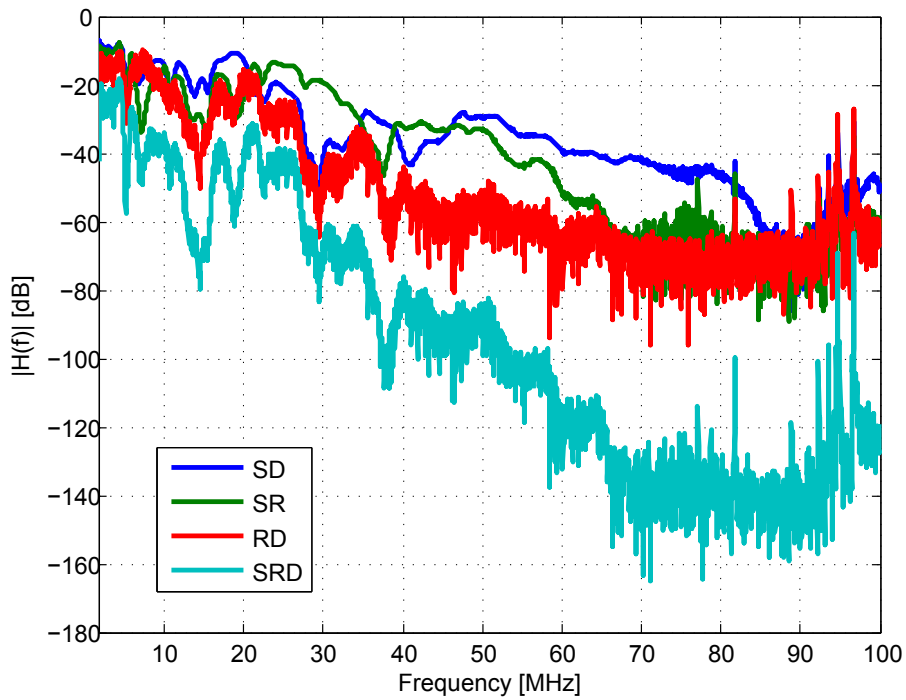
Figure 45: Measured magnitude frequency response for the Case #4.
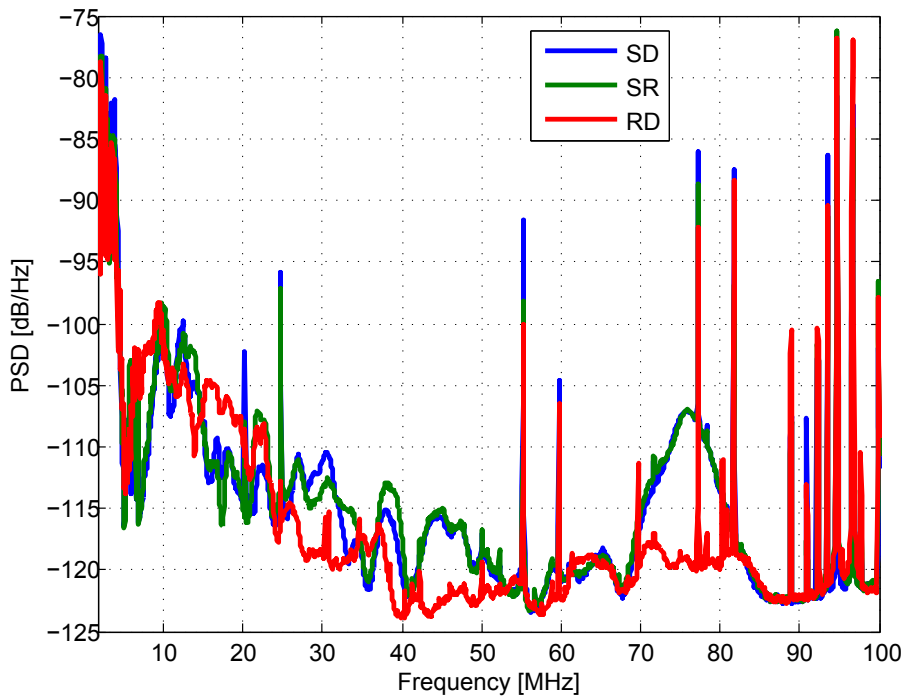
Figure 46: PSD estimation of the additive noises for the Case #4.

In addition, to analyze the influence of the power allocation P_0 and P_1, the capacity was estimated for a particular set of channels, considering the combining techniques explained in Sec. 3.4, for the AF and DF protocols, and assuming the total power $P = 1$ W and $P_0 \geq \frac{1}{2}$. The constraint in P_0 means that no more than a half of the

total power is allocated to P_1 and an ideal (error-free) DF protocol is applied at the R node.
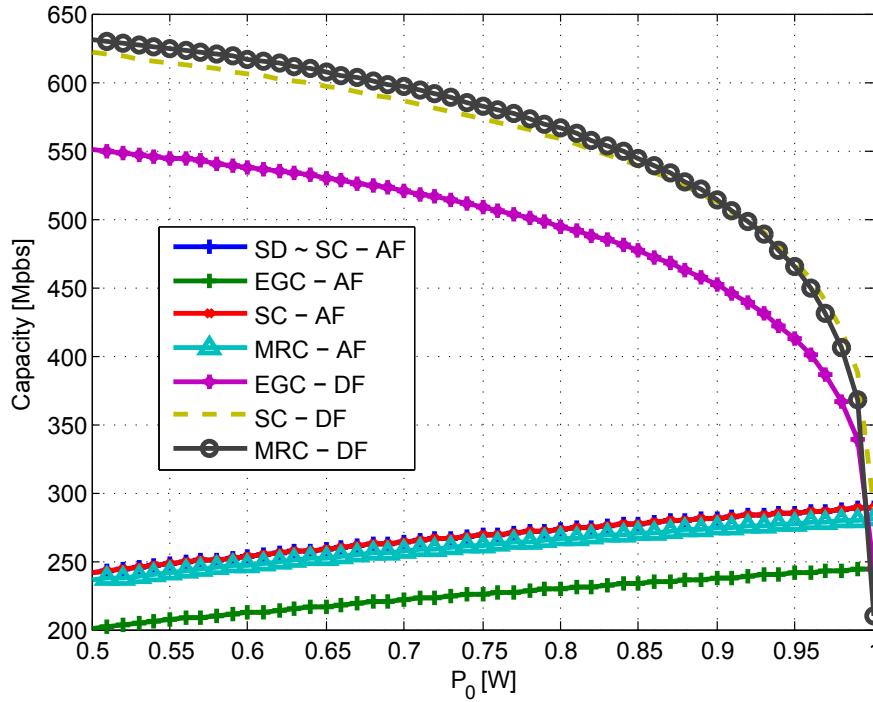
Figure 47: AF and DF simulation in terms of power allocation at source.

In Fig. 47 are highlighted the results of simulating AF and DF protocols in terms of power allocation at source. From these results it is possible to note that the use of the AF protocol result in an increasing performance while the power P_0 is being increased. On the contrary, the DF cases show a decreasing capacity while the P_0 increases, which is expected since the power at the R node is being decreased. The AF protocol results in negligible capacity gain because the $h_{SRD}[n]$ channel presents a strong attenuation profile. Regarding the DF protocol, one note that it can potentially offer an interesting capacity gain if the R node is capable of detecting the received signal with an error probability equal to zero.

From Fig. 48 to 55, the channel capacity for the measured PLC channels are shown for the four cases stated previously. It is also considered the relative position of the relay regarding the S and D nodes, and the AF and DF protocols. Regarding the AF protocol results from Figs. 48, 50, 52 and 54; it is possible to observe that the R node does not offer any advantage over the SD link, in order to improve the signal reception at the D node. For instance, if the EGC technique is applied and the AF protocol is used, then the channel capacity is lower than the capacity when other combination techniques are used. Additionally, it can be seen that the SRD link presents a very low

channel capacity, which is due to the strong attenuation profile in this link. Regarding the DF protocol in Fig. 49, 51, 53 and 55; two scenarios were found. In the first scenario, it can be noted from Fig. 49 that the combination at the D node delivers high capacity over the single SD link, for any SRD link attenuation. This is due to the distance from the R node to the D node, because the R node is in between the S and D nodes, which results in low path loss. However, in the second scenario, it can be seen from Figs. 51, 53 and 55, that the combination does not offer any significant capacity improvement over the SD link performance.
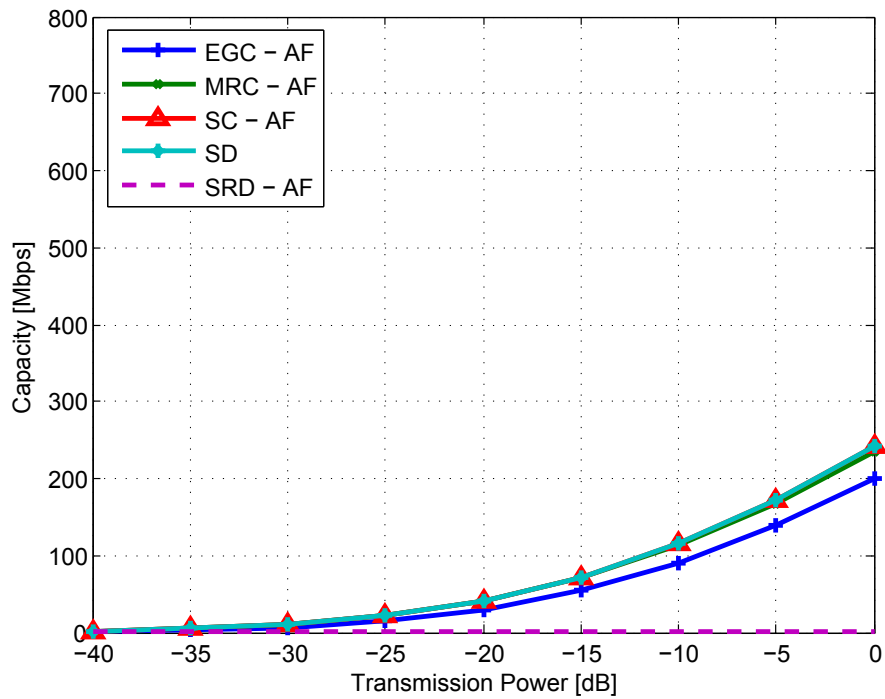
Figure 48: Relaying capacities for Case #1: Relay in the middle using AF.
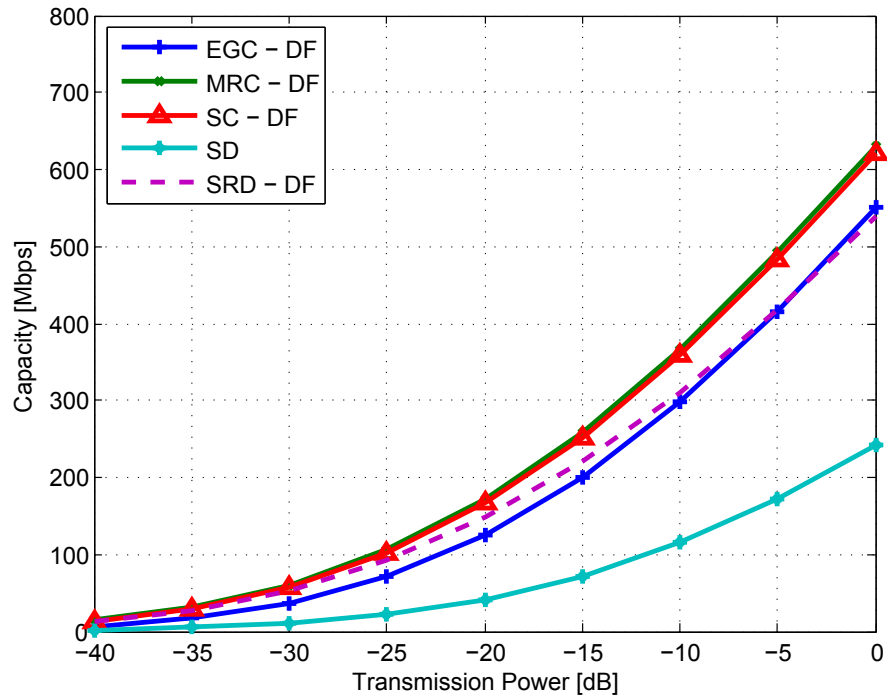
Figure 49: Relaying capacities for Case #1: Relay in the middle using DF.
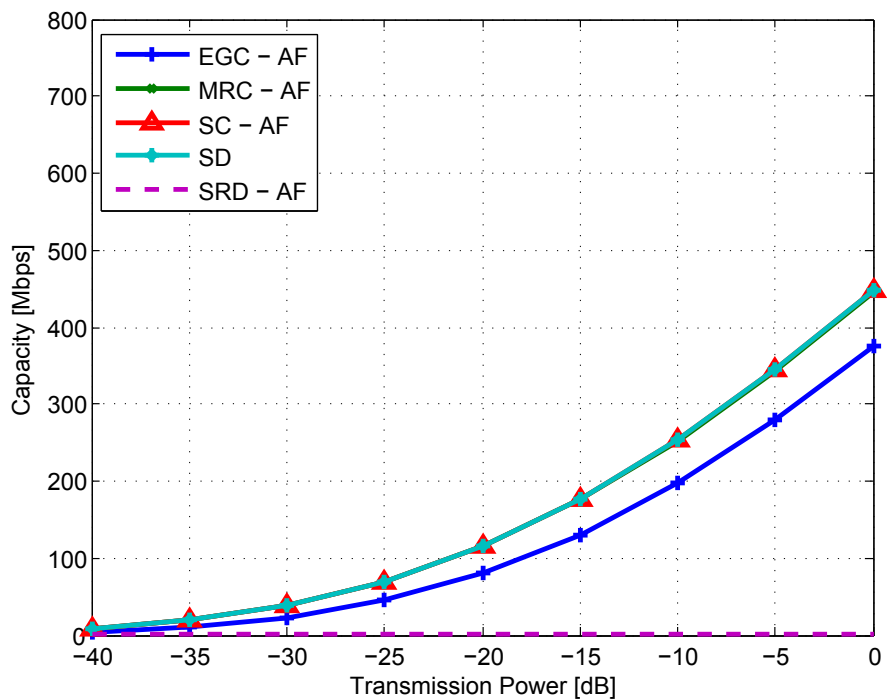
Figure 50: Relaying capacities for Case #2: Relay far from the S node, closer to D node using AF.
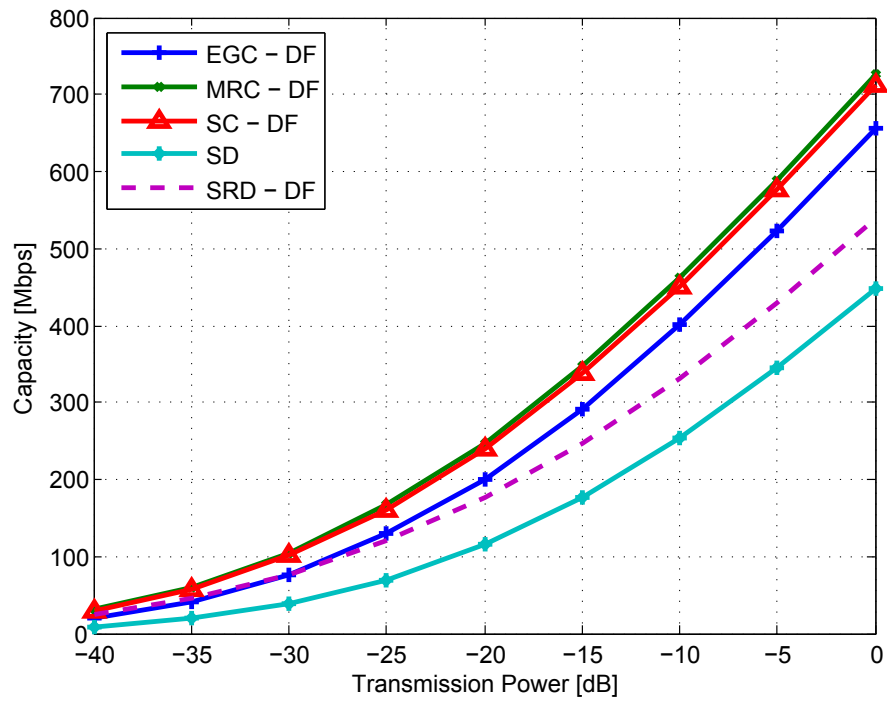
Figure 51: Relaying capacities for Case #2: Relay far from the S node, closer to D node using DF.
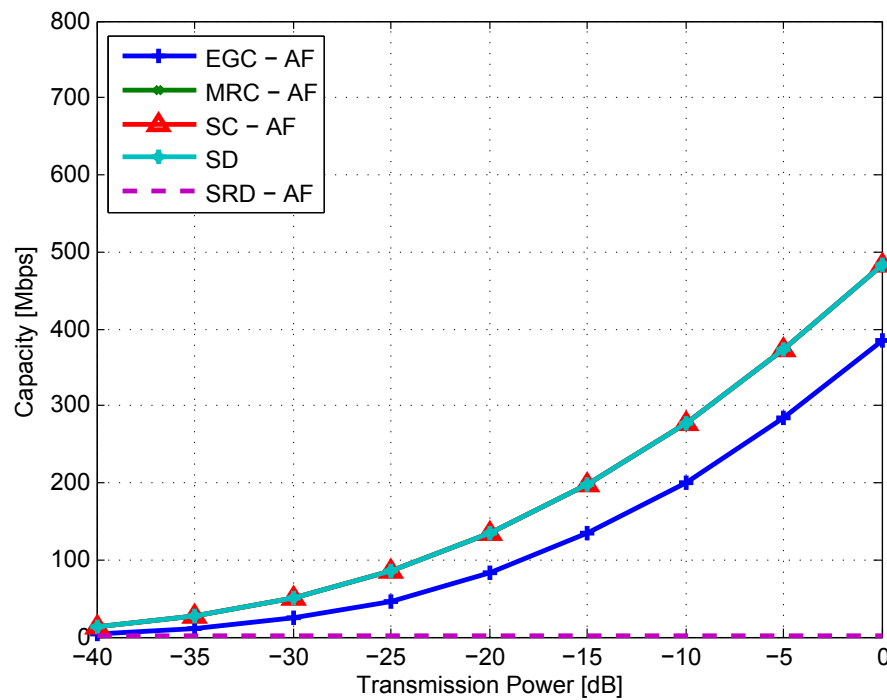
Figure 52: Relaying capacities for Case #3: Relay far from the D node, closer to the S node using AF.
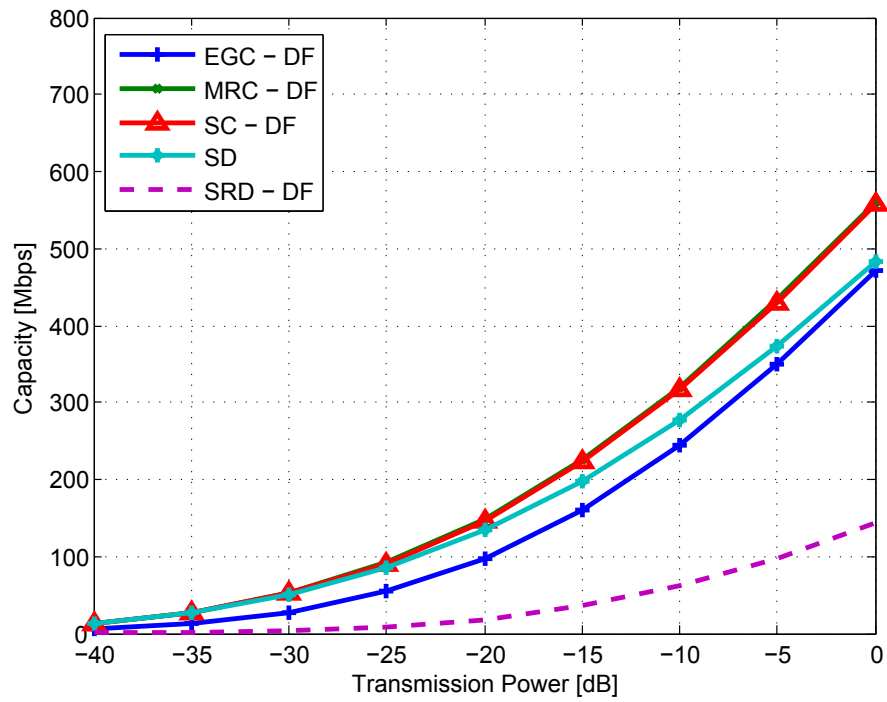
Figure 53: Relaying capacities for Case #3: Relay far from the D node, closer to the S node using DF.
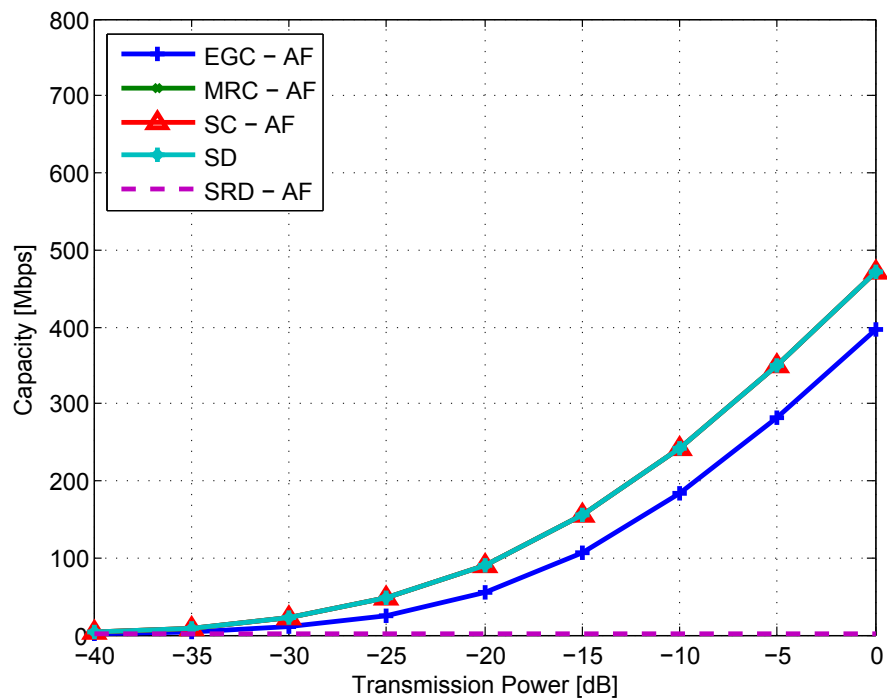
Figure 54: Relaying capacities for Case #4: Relay far from the D and S nodes using AF.
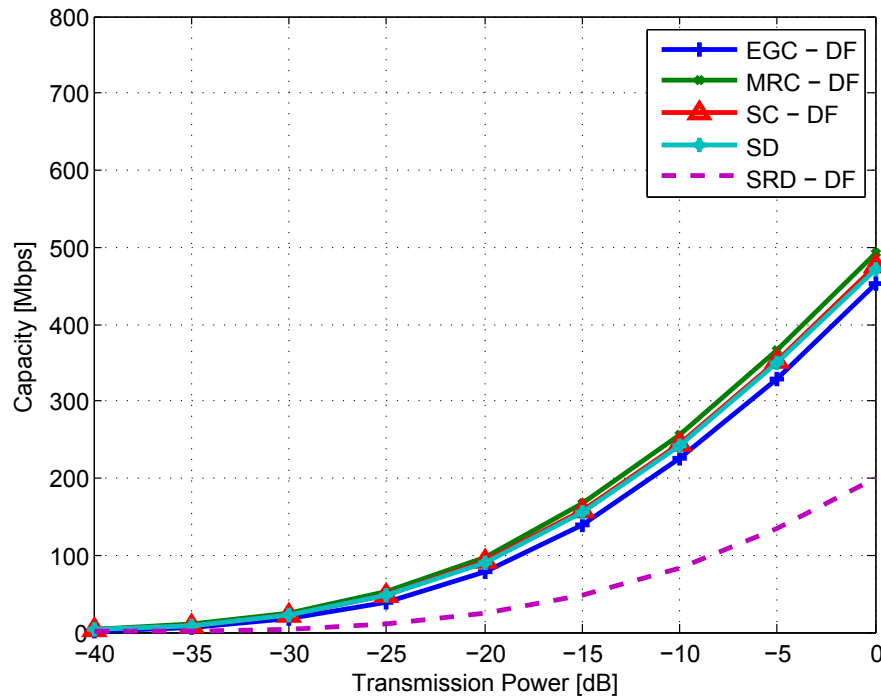
Figure 55: Relaying capacities for Case #4: Relay far from the D and S nodes using DF.

In Tab. 3 are summarized the channel capacity gains (calculated by $\rho = \frac{C_{protocol}}{C_{SD}}$, where $C_{protocol}$ is the channel capacity obtained by using one of the protocols and C_{SD} is the channel capacity in the SD link) observed when the EGC, SC and MRC techniques are considered together with the AF and DF protocols. It is possible to see that the AF protocol does not yield any channel capacity gain. Additionally, for the the DF protocol, only the Case #1 results in gains ($\rho > 2$) for all the combination techniques. One can finally note, that the channel capacity improvement offered by an ideal DF protocol can be as high as 30.91% of the achieved channel capacity in the SD link, considering the EGC, SC, and MRC combining techniques.

Case	EGC		SC		MRC	
	AF	DF	AF	DF	AF	DF
#1	0.83	2.28	1	2.57	0.97	2.61
#2	0.83	1.46	1	1.59	0.99	1.62
#3	0.79	0.97	1	1.15	0.99	1.15
#4	0.84	0.95	1	1.00	0.99	1.04

Table 3: Summary of the cooperative channel capacity gains.

4   CONCLUSIONS

In this thesis were discussed the main results after an initial analysis of the Brazilian IH-LV PLC channels. The statistical analysis for log-normality and channel capacity; qualitative analysis of access impedance; and cooperative model analysis have yielded different conclusions, that might remark the importance of the channel characterization, in order to confirm the suitability of the PLC channel for data communication, as well as, for what kind of improvement might be expected if cooperative protocols are taken into account.

In only 33.33% of the IH-LV PLC channels measured in Brazil, the log-normality was confirmed for the RMS-DS, and in 100% of the channels the log-normality was rejected for the average channel gain. Therefore, it cast doubt with the conclusions found in (GALLI, 2011), where the log-normality for the average channel gain and the RMS-DS is confirmed. However, the negative log-normality relation between the channel gain and the RMS-DS was confirmed and agrees to the results found in (GALLI, 2011). Moreover, it could be noted that the RMS-DS statistics of IH-LV PLC channels measured in Brazil are close to US PLC channels analysed in (GALLI, 2011), and the average channel gain statistics show a variation in the Brazilian scenario. This information can be used in order to design more robust PLC systems that might be available in both regions.

Additionally, it is possible to conclude that due to the similarity in the impedance values for different houses (see Sec. 2.2.5), it will be of great advantage to implement couplers with impedance matching. This will reduce the attenuation that the transmitted and received signals suffer during data transmission.

In this thesis cooperative protocols for IH-LV PLC channels were also analyzed. The analysis was based on channels, that were obtained in a measurement campaign carried out in medium size apartments (size between 50 and 90 square meters). The attained performance, in terms of channel capacity, by applying AF and ideal DF (error-free) protocols, at the R node together with EGC, SC, and MRC techniques

were presented. The reported results paid attention to four scenarios and limited power for transmission. Based on measured data, this contribution showed that the AF protocol cannot offer improvements because the link SRD results in a strong signal attenuation, even though the links SR and RD present lower attenuation than the SD link. On the other hand, the DF protocol can result in improved performance if the received signal at the R node is correctly detected. This improvement is reduced if the error probability of detecting the received signal at the D node increases. Finally, it is possible to conclude that among the EGC, SC and MRC techniques, the EGC offers the worst results.

4.1 FUTURE WORK

As a future work, it is necessary to carry out more measurements in different scenarios, such as, homes and apartments belonging to people with high and low incomes. Based on the literature, the differences in PLC channels will be evident by having it. Also, it is important to come up with channel and noise models for IH-LV PLC channels to provide theoretical analysis regarding non-cooperative and cooperative communications in Brazil. It is also highly important to analyze other protocols and more relaying models. This will broaden the cooperative communications perspective for PLC systems. Finally, adaptable impedance couplers must be developed to improve the PLC system performance. These couplers must take into consideration both the real and imaginary part variations in the frequency domain.

REFERENCES

ANATEL. *REGULAMENTO SOBRE CONDIÇÕES DE USO DE RADIOFRE-QÜÊNCIAS POR SISTEMAS DE BANDA LARGA POR MEIO DE REDES DE ENERGIA ELÉTRICA. RESOLUÇÃO N° 527, DE 8 DE ABRIL DE 2009.* Apr. 2009.

ANATORY, J.; THEETHAYI, N.; THOTTAPPILLIL, R. Power-line communication channel model for interconnected networks part i: Two-conductor system. *IEEE Transactions on Power Delivery*, v. 24, n. 1, p. 118–123, Jan. 2009.

ANATORY, J.; THEETHAYI, N.; THOTTAPPILLIL, R. Power-line communication channel model for interconnected networks part ii: Multiconductor system. *IEEE Transactions on Power Delivery*, v. 24, n. 1, p. 124–128, Jan. 2009.

ARANEO, R.; CELOZZI, S.; LOVAT, G. Design of impedance matching couplers for power line communications. In: *IEEE International Symposium on Electromagnetic Compatibility.* 2009. p. 64–69.

BAKHOUM, E. S -parameters model for data communications over 3-phase transmission lines. *IEEE Transactions on Smart Grid*, v. 2, n. 4, p. 615–623, Dec. 2011.

BANWELL, T.; GALLI, S. A novel approach to the modeling of the indoor power line channel part i: circuit analysis and companion model. *IEEE Transactions on Power Delivery*, v. 20, n. 2, p. 655–663, Apr. 2005.

BERT, L. D. et al. On noise modeling for power line communications. In: *Proc. IEEE International Symposium on Power Line Communications and Its Applications (ISPLC).* 2011. p. 283–288.

CANETE, F. et al. Modeling and evaluation of the indoor power line transmission medium. *IEEE Communications Magazine*, v. 41, n. 4, p. 41–47, Apr. 2003.

COLEN, G. R. et al. Measurement setup for characterizing low-voltage and outdoor electric distribution grids for [plc] systems. In: *Proc. IEEE PES Conference On Innovative Smart Grid Technologies Latin America.* 2013. p. 1–5.

CORRIPIO, F. et al. Analysis of the cyclic short-term variation of indoor power line channels. *IEEE Journal on Selected Areas in Communications*, v. 24, n. 7, p. 1327–1338, Jul. 2006.

DOHLER, M.; LI, Y. *Cooperative Communications: Hardware, Channel and PHY.* First. Wiley, 2010. ISBN 0470997680.

FERREIRA, H. C. et al. (Ed.). *Power Line Communications: Theory and Applications for Narrowband and Broadband Communications over Power Lines.* First. Wiley, 2010. ISBN 0470740302.

GAGE. *CompuGen 4300/4302 Data-Sheet. High-speed arbitrary waveform generator card.* Disponível em: <http://www.gage-applied.com/products/PDF/CG4300-4302.pdf>.

GAGE. *Razor CompuScope 16XX Data-Sheet. 16-Bit Family of Multi-channel Digitizers for the PCI Express and PCI Bus.* Disponível em: <http://www.gage-applied.com/digitizers/GaGe-Digitizer-RazorCS16XX-PCI-PCIe-Data-Sheet.pdf>.

GALLI, S. A simplified model for the indoor power line channel. In: *Proc. IEEE International Symposium on Power Line Communications and Its Applications*. 2009. p. 13–19.

GALLI, S. A simple two-tap statistical model for the power line channel. In: *Proc. IEEE International Symposium on Power Line Communications and Its Applications (ISPLC)*. 2010. p. 242–248.

GALLI, S. A novel approach to the statistical modeling of wireline channels. *IEEE Transactions on Communications*, v. 59, n. 5, p. 1332–1345, May. 2011.

GALLI, S.; BANWELL, T. A novel approach to the modeling of the indoor power line channel-part ii: transfer function and its properties. *IEEE Transactions on Power Delivery*, v. 20, n. 3, p. 1869–1878, Jul. 2005.

GALLI, S.; BANWELL, T. A deterministic frequency-domain model for the indoor power line transfer function. *IEEE Journal on Selected Areas in Communications*, v. 24, n. 7, p. 1304–1316, Jul. 2006.

HASHMAT, R. et al. A channel model for multiple input multiple output in-home power line networks. In: *Proc. IEEE International Symposium on Power Line Communications and Its Applications (ISPLC)*. 2011. p. 35–41.

HONG, Y. W. P.; HUANG, W.-J.; KUO, C. C. J. *Cooperative Communications and Networking: Technologies and System Design*. First. Springer, 2010.

KIM, K. et al. Capacity analysis of relay channels for medium voltage powerline access network. In: *International Conference on Computing, Networking and Communications (ICNC)*. 2012. p. 917–921.

KIM, K. et al. Cooperative multihop af relay protocol for medium-voltage power-line-access network. *IEEE Transactions on Power Delivery*, v. 27, n. 1, p. 195–204, Jan. 2012.

LAMPE, L.; VINCK, A. J. H. Cooperative multihop power line communications. In: *Proc. IEEE International Symposium on Power Line Communications and Its Applications*. 2012. p. 1–6.

LI, H. et al. Channel order and RMS delay spread estimation for AC power line communications. In: *Proc. IEEE Workshop on Statistical Signal and Array Processing*. 2000. p. 229–233.

LIU, E. et al. Broadband powerline channel and capacity analysis. In: *Proc. IEEE International Symposium on Power Line Communications and Its Applications*. 2005. p. 7–11.

LIU, K. J. R. et al. *Cooperative Communications and Networking*. First. Cambridge University Press, 2009.

MOHAMED, T.; GAUTIER, A.; AHMED, Z. Coherence bandwidth and its relationship with the RMS delay spread for PLC channels using measurements up to 100 MHz. In: AGHA, K.; CARCELLE, X.; PUJOLLE, G. (Ed.). *Home Networking*. Springer US, 2008, (IFIP International Federation for Information Processing, v. 256). p. 129–142. ISBN 978-0-387-77215-8.

OLIVEIRA, T. *Caracterização de Redes de Energia Elétrica como Meio de Transmissão de Dados*. Dissertação (Mestrado) — Universidade Federal de Juiz de Fora, 2010.

OLIVEIRA, T.; FINAMORE, W.; RIBEIRO, M. A sounding method based on ofdm modulation for plc channel measurement. In: *Proc. IEEE International Symposium on Power Line Communications and Its Applications (ISPLC)*. 2013. p. 185–190.

O'MAHONY, B. Field testing of high-speed power line communications in north american homes. In: *IEEE International Symposium on Power Line Communications and Its Applications*. 2006. p. 155–159.

PENG, L.; HÉRALD, M.; HAESE, S. Optimization of multi-band DFT-spread DMT system for polymer optical fiber communications. In: *Proc. IEEE International Conference on Communications*. 2013. p. 3862–3867.

SARTENAER, T.; DELOGNE, P. Deterministic modeling of the (shielded) outdoor power line channel based on the multiconductor transmission line equations. *IEEE Journal on Selected Areas in Communications*, v. 24, n. 7, p. 1277–1291, Jul. 2006.

SCHMID, H. *How to use the FFT and MATLAB's pwelch function for signal and noise simulations and measurements*. Aug. 2012.

SUNG, T.; BOJANCZYK, A. Optimal power control and relay capacity for plc-embedded cooperative systems. In: *7th IEEE Consumer Communications and Networking Conference (CCNC)*. 2010. p. 1–5.

TAHERINEJAD, N. et al. A study on access impedance for vehicular power line communications. In: *IEEE International Symposium on Power Line Communications and Its Applications (ISPLC)*. 2011. p. 440–445.

TONELLO, A.; VERSOLATTO, F. Bottom-up statistical plc channel modeling-part ii: Inferring the statistics. *IEEE Transactions on Power Delivery*, v. 25, n. 4, p. 2356–2363, Oct. 2010.

TONELLO, A.; VERSOLATTO, F. Bottom-up statistical plc channel modeling-part i: Random topology model and efficient transfer function computation. *IEEE Transactions on Power Delivery*, v. 26, n. 2, p. 891–898, Apr. 2011. ISSN 0885-8977.

TONELLO, A. et al. A fitting algorithm for random modeling the plc channel. *IEEE Transactions on Power Delivery*, v. 27, n. 3, p. 1477–1484, Jul. 2012.

TONELLO, A.; ZHENG, T. Bottom-up transfer function generator for broadband plc statistical channel modeling. In: *Proc. IEEE International Symposium on Power Line Communications and Its Applications*. 2009. p. 7–12.

VERONESI, D. et al. Characterization of in-home mimo power line channels. In: *IEEE International Symposium on Power Line Communications and Its Applications (ISPLC)*. 2011. p. 42–47.

VERSOLATTO, F.; TONELLO, A. An mtl theory approach for the simulation of mimo power-line communication channels. *IEEE Transactions on Power Delivery*, v. 26, n. 3, p. 1710–1717, Jul. 2011.

ZHU, W. et al. State-of-art power line communications channel modelling. *Procedia Computer Science*, v. 17, n. 0, p. 563 – 570, 2013.

ZIMMERMANN, M.; DOSTERT, K. Analysis and modeling of impulsive noise in broad-band powerline communications. *IEEE Transactions on Electromagnetic Compatibility*, v. 44, n. 1, p. 249–258, Feb. 2002.

ZIMMERMANN, M.; DOSTERT, K. A multipath model for the powerline channel. *IEEE Transactions on Communications*, v. 50, n. 4, p. 553–559, Apr. 2002.

APPENDIX A – MEASUREMENT CAMPAIGN

The measurement campaign details are presented in this appendix. It basically consists of the frequency response and channel capacity values that were found in each house, together with the electrical plan for each house. Additionally, a table summarizing the measurement campaign details and configurations is presented in Tab. 4. In this table TX and RX make reference to the transmitter and and the receiver computers, MSs stands for Mega samples per second, TX device channel is the corresponding channel number in the TX device, and the RX device channel includes the corresponding channel numbers used in the RX device (1/3 means channels 1 and 3, respectively).

House ID	House A	House B	House C	House D
Approx. size [m^2]	54	93	62	54
Year built	2012	2009	2004	2004
Location (city)	JF	JF	JF	JF
Neighborhood	Vale do Ipe	Sao Mateus	Sao Pedro	Sao Pedro
Service type	Aerial	Aerial	Aerial	Aerial
Approx. Transformer distance [m]	25	5	15	15
House type	Apartment	Apartment	Apartment	Apartment
Distance meter-central panel [m]	12	16	15	20
Total evaluated outlets	12	18	11	7
Frequency band MHz	100	100	100	100
TX sampling frequency MSs	200	200	200	200
RX sampling frequency MSs	200	200	200	200
Measurement samples MS	3	3	3	3
TX device	GAGE 501	GAGE 501	GAGE 501	GAGE 501
TX device channel	2	2	2	2
RX device	PC-AUX	PC-AUX	PC-AUX	PC-AUX
RX device channel	1/3	1/3	1/3	1/3

Table 4: Summary of the measurement campaign details.

A.1 HOUSE A

In Fig. 56 the electrical plan for the House A is presented. Twelve different outlets were used for the measurements, in which the $C01$ and $C04$ nodes, were chosen for transmission. Thus, eleven channels were measured from $C01$ and, other eleven channels from $C04$. Note that the position of the $C01$ node was chosen because it is located in a kind of external position within the apartment. The $C04$ node was chosen in a central position instead. These positions, were highly important for the evaluation of the single-relay configuration for cooperative PLC communications.
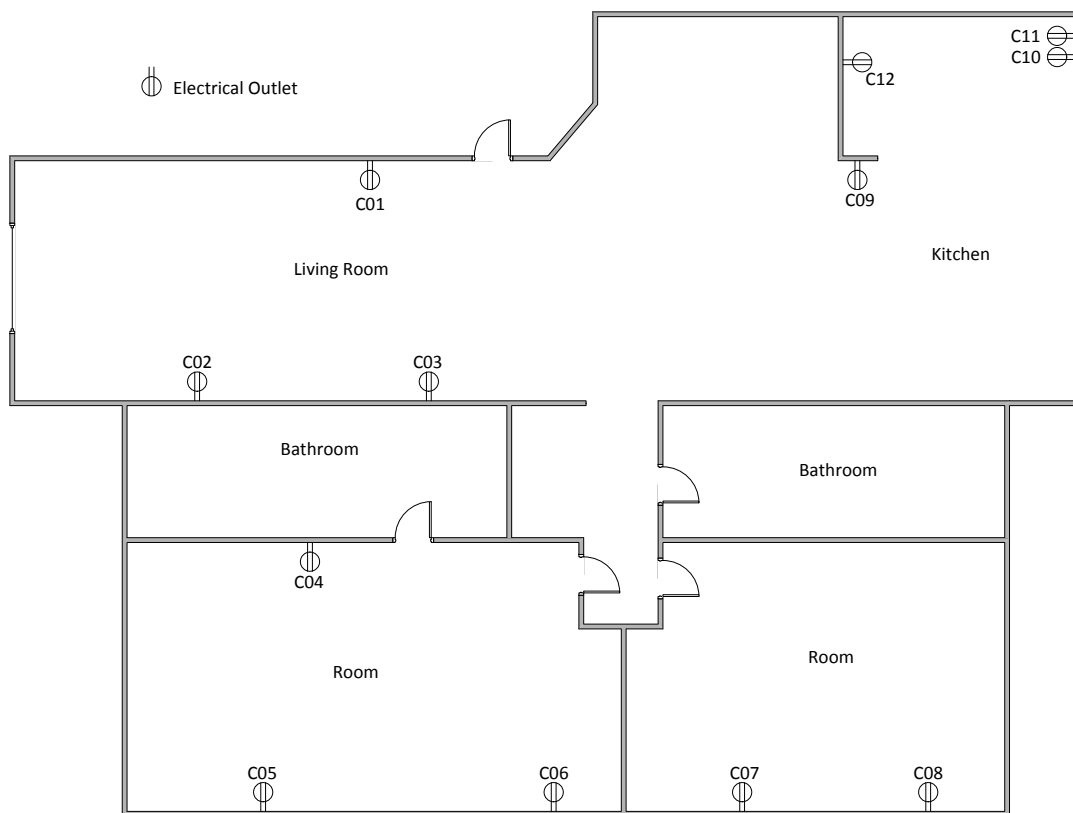
Figure 56: Electrical outlet plan of House A.

The characteristic frequency response magnitude and channel capacity for this house are depicted in Fig. 57 and Fig. 58, respectively.
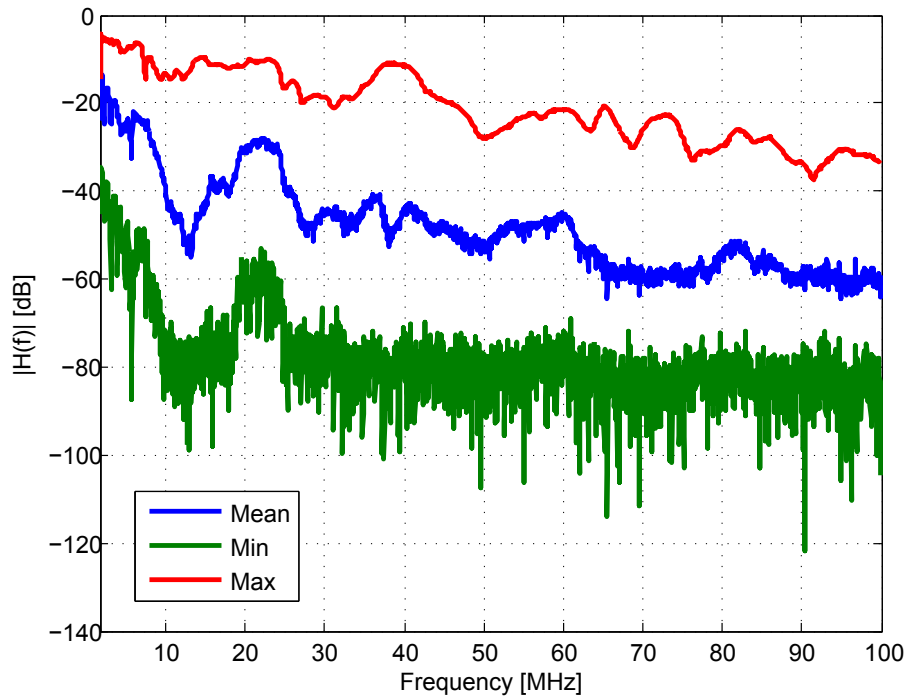
Figure 57: Frequency response magnitude in House A.
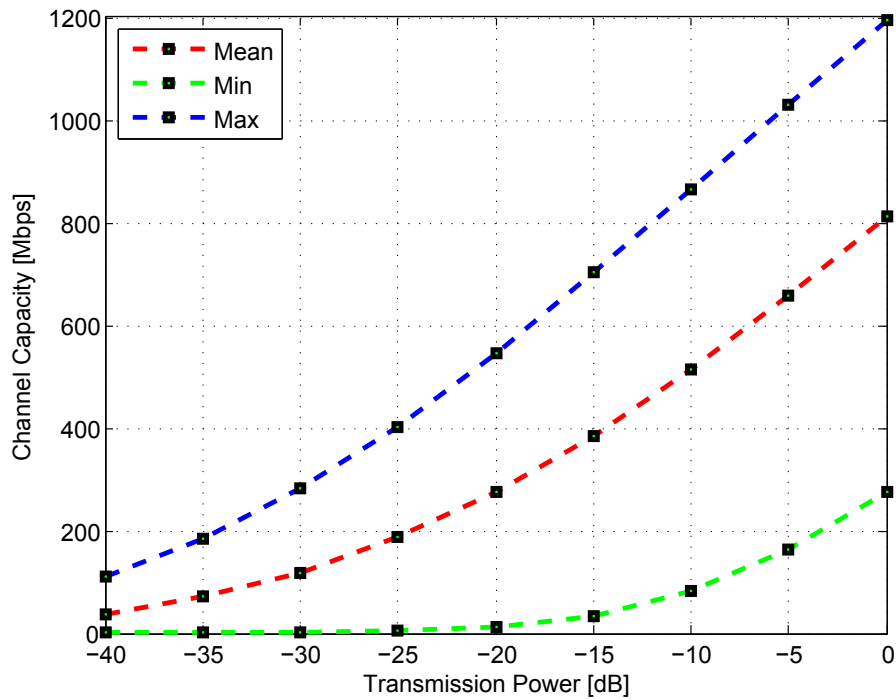
Figure 58: Channel capacity in House A.

A.2   HOUSE B

The electrical plan for House B is shown in Fig. 59. In this house a total of 18 outlets were used. The nodes $C01$ and $C07$ were chosen for data transmission, for

the same reasons of cooperative analysis explained above. Then a total of 34 channels were measured. In this house, we have experienced problems we did not in House A. For instance, only 3 of the 17 channels, measured when the transmitter was located at the $C01$ node, were useful for further analysis. Similarly, only 4 of the 17 channels, measured when the transmitter was located at the $C07$ node, were useful for further analysis. The main problem with these measurements, was that different circuits inside the house belonged to different phases. Also, when measuring using the same phase, the data were not useful due to strong attenuation profiles (long paths). Therefore, for this very first IH-LV measurement campaign, it was decided to measure only the possible channels that belong to the same circuit, following the distribution board.
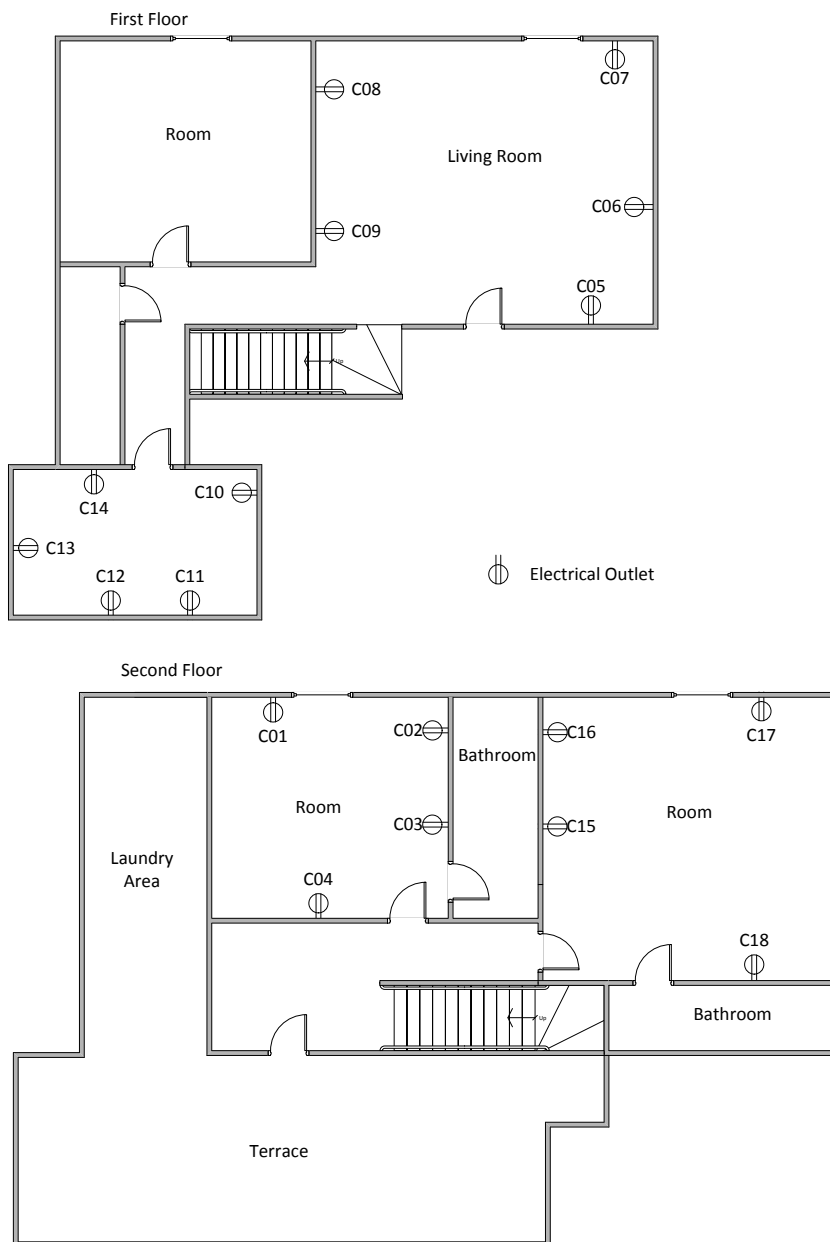
Figure 59: Electrical outlet plan of House B.

The characteristic frequency response magnitude and channel capacity for House B are presented in Fig. 60 and Fig. 61, respectively.
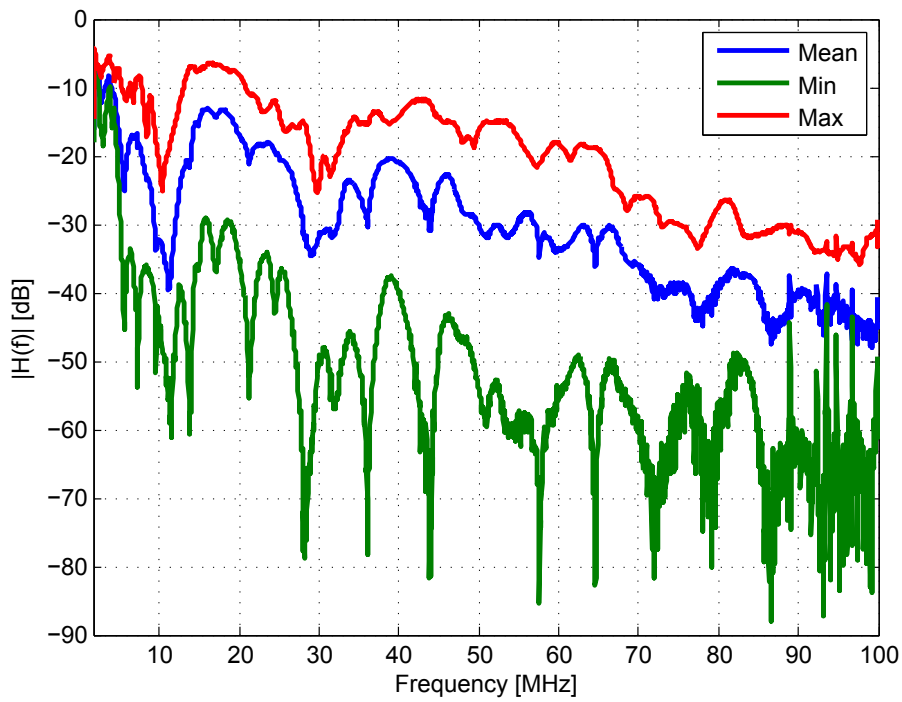
Figure 60: Frequency response magnitude in House B.
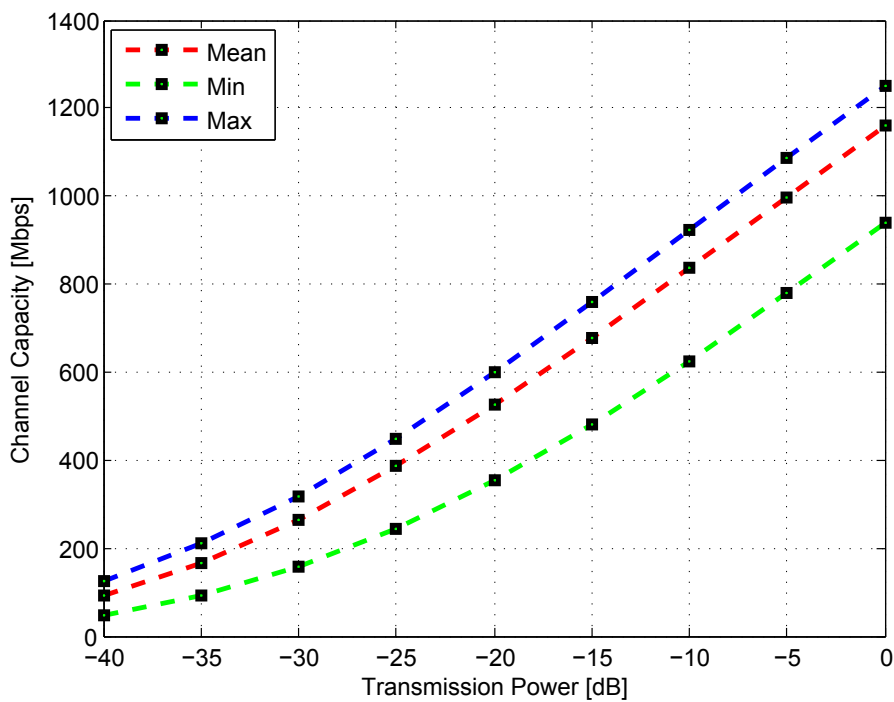
Figure 61: Channel capacity in House B.

A.3 HOUSE C

In Fig. 62 can be regarded the electrical plan of House C. Only 11 outlets were considered, and in this case 4 transmission nodes were chosen: $C02$, $C03$, $C05$ and $C11$. Also, the measurements were made only within the same circuit of a circuit breaker from the distribution board. Therefore, we have guaranteed that the channels were useful for analysis. Two circuits were measured using 2 transmission nodes in each one. For the first circuit and from node $C02$ were measured 5 different channels to the nodes $C02$, $C08$, $C09$, $C10$ and $C11$, and from node $C11$ were also measured 5 different channels to the nodes $C01$, $C02$, $C08$, $C09$ and $C10$. For the second circuit and from node $C03$ were measured 4 different channels to the nodes $C04$, $C05$, $C06$ and $C07$, similarly from node $C05$ were measured 4 different channels to the nodes $C03$, $C04$, $C06$ and $C07$.
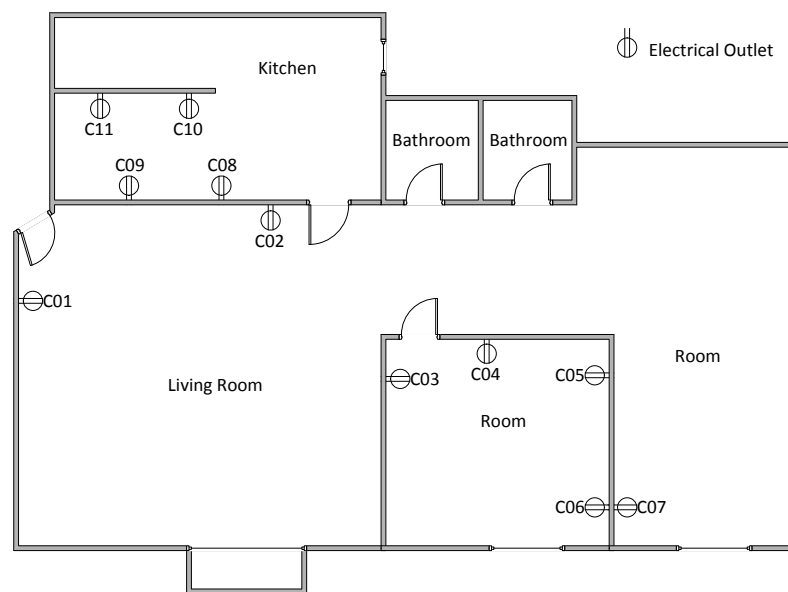
Figure 62: Electrical outlet plan of House C.

The characteristic frequency response magnitude and channel capacity for House C are presented in Fig. 63 and Fig. 64, respectively.
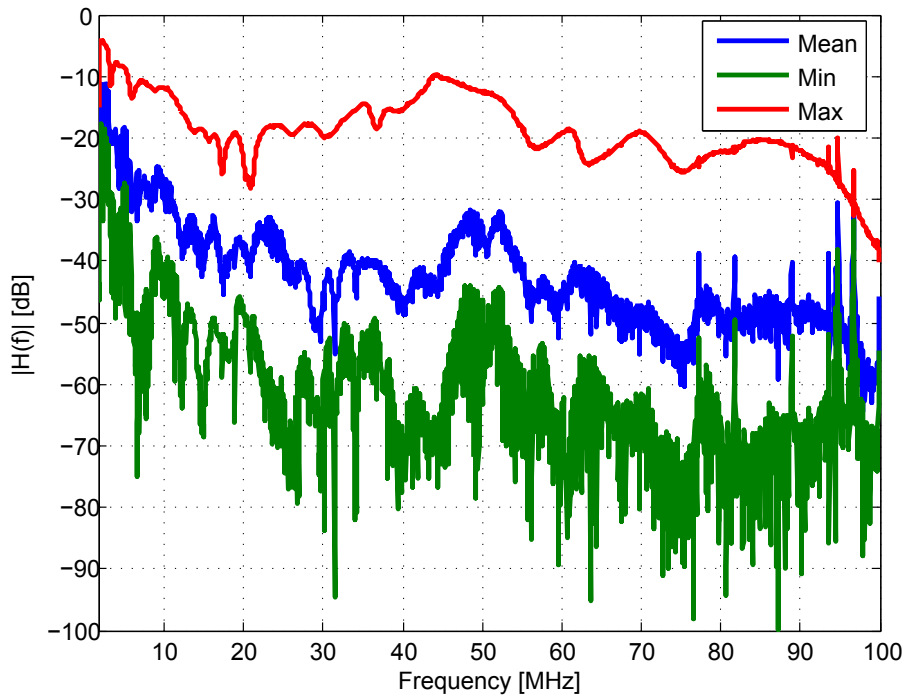
Figure 63: Frequency response magnitude of House C.
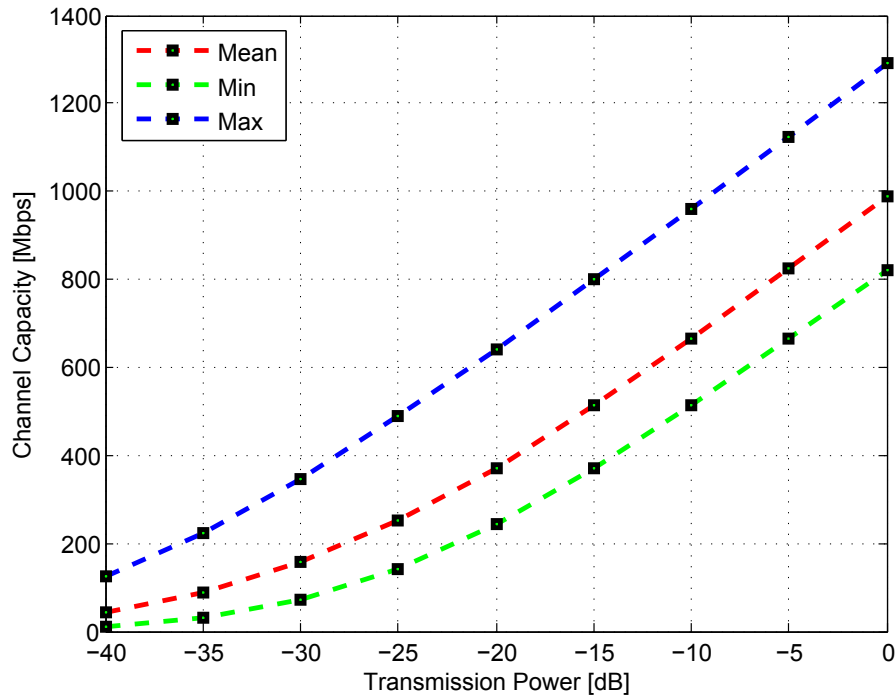
Figure 64: Channel capacity in House C.

A.4   HOUSE D

House D is a small apartment with an electrical plan pictured in Fig. 65. Two circuits were identified for the nodes $C03$, $C04$, $C05$ and $C02$, $C07$, $C06$, respectively,

and discarding the node $C01$. In addition, 4 nodes were chosen for data transmission: $C02$, $C04$, $C05$, and $C07$. Then a total of 8 channels were measured.
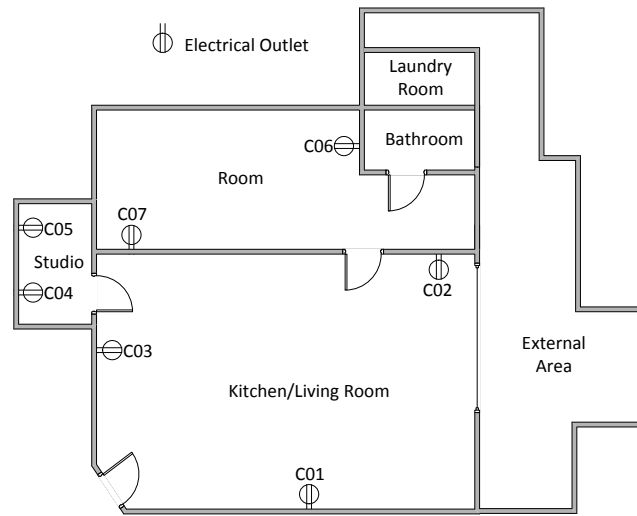
Figure 65: Electrical outlet plan of House D.

The characteristic frequency response magnitude and channel capacity for House D are presented in Fig. 66 and Fig. 67, respectively.
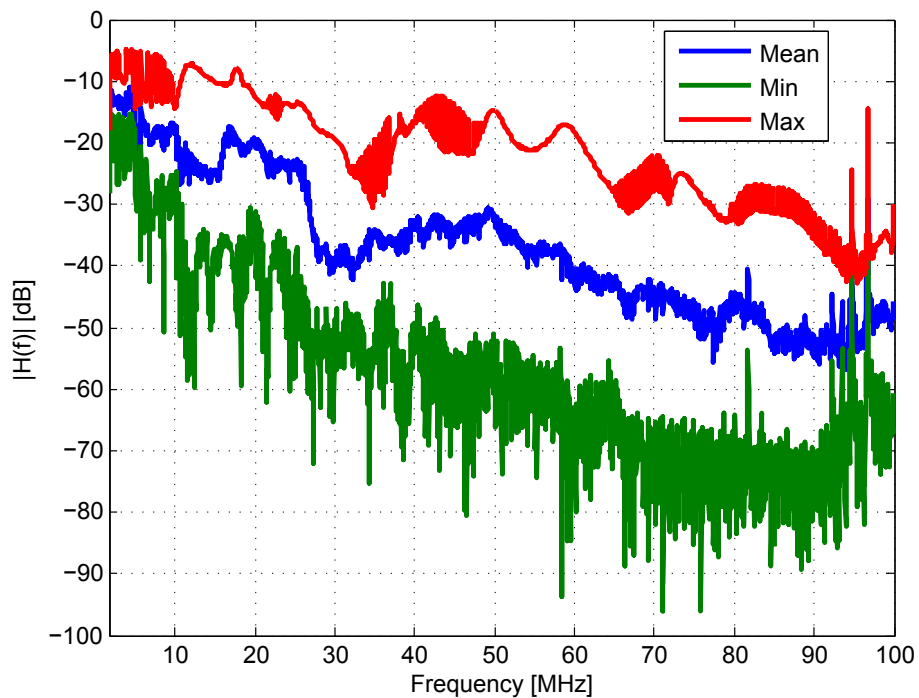
Figure 66: Frequency response magnitude in House D.
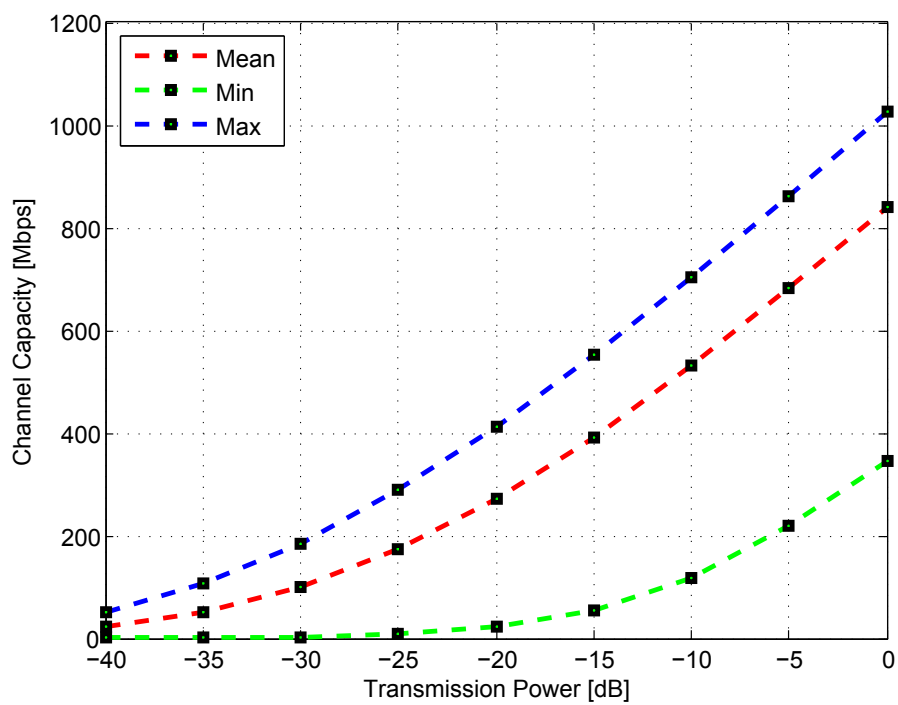
Figure 67: Channel capacity in House D.